KANSAS GEOLOGICAL SURVEY
OPEN-FILE REPORT 88-29

The Effects of Near-Surface Geology on Shallow,
High-Resolution Seismic Reflection Data Quality in Northeastern Kansas

by

Andrew J. Kalik

KANSAS GEOLOGICAL SURVEY
1930 Constant Avenue
University of Kansas
Lawrence, KS 66047

The effects of near-surface geology on shallow, high-resolution seismic reflection data quality in northeastern, Kansas

Andrew J. Kalik

Kansas Geological Survey
The University of Kansas
Lawrence, Kansas 66046

August 5, 1988

Open-file Report No. 88-29

Abstract

Two important deleterious effects found on shallow high-resolution seismic data are caused by near-surface geology in northeastern Kansas. Transmission losses result in extremely low signal-to-noise content on seismic sections. Reverberating energy, in the form of ringing refractions, obscures early arriving reflection energy. These problems do not hamper the use of conventional seismic reflection methods because of the inherent lower-frequency, higher-energy input and deeper targets.

A zone of chaotic data is observable on seismic records obtained in localities with near-surface limestone units. On data from a site near Lyndon, Kansas, this chaotic zone extends beyond the outcrop area of a limestone unit in two directions. To the south, the limestone unit is truncated by alluvium. The presence of chaotic energy on data from beneath the alluvium is suggestive of subcropping limestone. The existence of this limestone was confirmed by drilling. Thus near-surface geology may be predicted on the basis of data quality.

To the north of the outcrop area, reflection energy returns to the seismic section. The only obvious difference between the area of the chaotic zone and the area to the north is the depth to the limestone unit.

One possible mechanism for the observed chaotic zone is a profusion of wide-angle reflection energy in areas of insufficient overburden. In this scenario, transmission losses result because most energy approaches the near-surface limestone bed at greater than the critical angle. Other possible causes of the chaotic zone include opacity, Fresnel effects, channel waves, and severe structural disturbance.

Since the severity of reverberation noise varies from site to site, it is apparently a function of near-surface geology, and in particular the first refracting interface. Frequency filtering has resulted in limited success in removing reverberation noise. At a site near Clinton, Kansas, frequency filtering reduced 130 ms of reverberating noise to just 20 ms. Although deconvolution was largely unsuccessful, this remaining 20 ms evidently represents the convolved source wavelet. Also noteworthy, is that regardless of shot location or pre-emphasis filters, walkaway noise test data from near Lyndon, Kansas exhibit disruption of the reverberating wave train directly beneath an outcropping limestone unit. Future research should be directed towards determining the effects of altering the source wavelet in areas exhibiting severe reverberation noise.

Table of Contents

List of Figures

List of Tables

Acknowledgements

I severely underestimated the difficulty associated with earning a graduate degree. Admittedly, if I had to do it all over, at the very least, I would do many things differently. I must first thank Rick Miller for seeing me through this ordeal. On several occasions, I came dangerously close to quitting. Without his patience and guidance, I know I would not have stayed in school. I think I will appreciate this even more fully in the years to come. I would especially like to thank Rick for sharing his knowledge of the acquisition and processing of shallow, high-resolution seismic reflection data. I could not have learned this anywhere else.

I would also like to thank Don Steeples for giving me the opportunity to study at the University of Kansas, and for advising me on this thesis. To Don Sprowl and Tony Walton, the two other advisors on my committee, I would like to extend my appreciation for their helpful suggestions and timely review of the text. I am also indebted to Ralph Knapp for never being to busy to answer a question.

I would like to thank the Kansas Geological Survey for financial support and facility accessibility. I would like to thank Brad Birkelo for recommending me for the program, and Jeff Treadway for help and advice, early on. I would like to thank the field crew which

helped me collect this compelling data. Rick Miller and Paul Myers were present and invaluable during each field excursion. Randie Grantham, George Coyle, Chong Chung, and Mary Anne Markezich were also extremely helpful on several trips. Lastly, I would like to thank Pam Chaffee for help on the geology of the Lyndon site, Mary Anne Markezich for reviewing the text, Yi Yang Song for his Zoeppritz modeling program, and Krzysztof Wojcik for being a filter for many of my ideas and conclusions.

Introduction

Since 1980, the seismic reflection method has been used to discern relatively shallow subsurface features. "Shallow" refers to strata imaged with a two-way arrival time of less than one-quarter second, typically less than 250 m deep. Though the method used for shallow study is theoretically identical to the conventional methods of seismic reflection, there are inherent practical differences.

The differences between the shallow reflection method and conventional reflection methods are primarily a function of scale. The shallow reflection method is performed on a much smaller scale, both spatially and temporally. Higher frequencies are also used, permitting better resolving power in shallow work. These differences allow the detection of shallow structure, bedrock, voids, and even the water-table. However, the inherent differences also create problems which are only observable at the smaller scale used for shallow work.

Any phenomenon that results in a decrease of signal quality on a seismic record is detrimental. Reverberations and transmission losses are two such phenomena. These sources of noise are important because they may limit the effectiveness of the shallow reflection method.

Purpose

The purpose of this study is to exhibit and explain the decrease in signal quality associated with geologic units near the surface. A relationship between near-surface geology, reverberating seismic energy, and transmission losses would represent a significant advance in determining potential applications and limitations of the shallow reflection method. In this thesis, I present the occurrence of reverberating seismic energy and transmission losses related to near-surface geology, and possible causal mechanisms. In addition, I attempt to show why these problems are unique to the shallow reflection method, and to develop acquisition and processing procedures to remove the resulting noise from seismic data.

Geographic and Geologic Setting

The study areas are in northeastern Kansas, at sites similar to where reverberation noise and transmission losses have been observed during previous seismic work by the Kansas Geological Survey (KGS)(Fig. 1). The near-surface geology of northeastern Kansas consists generally of alternating limestone and shale units of Pennsylvanian age, in places occasionally dissected by streams that have deposited Quaternary alluvium (O'Connor, 1955; Zeller, 1968). This simple setting greatly reduces the number of possible geologic causes of

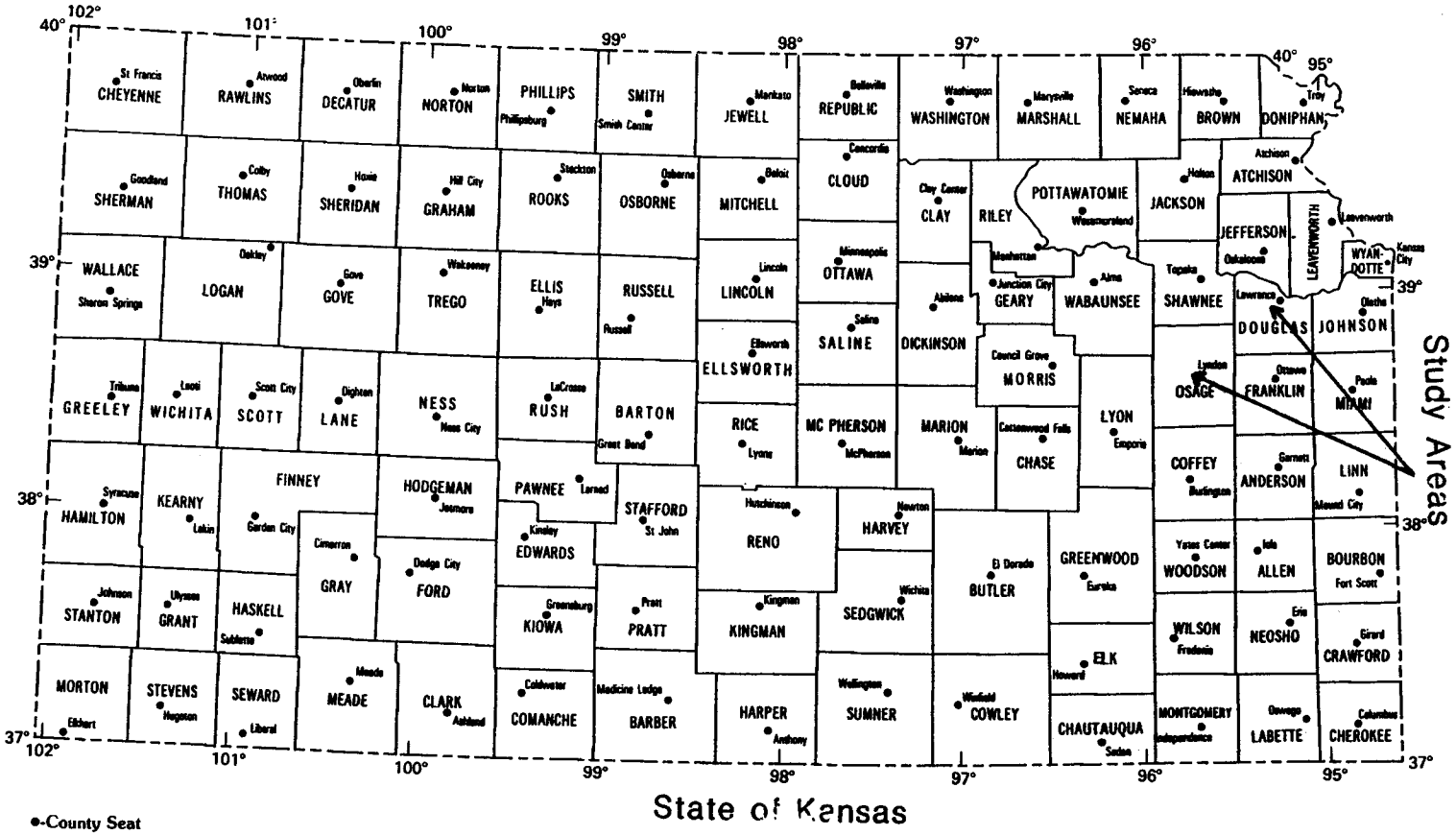

Figure 1. County map of Kansas, showing study areas.

the observed noise. To determine if the reverberations and transmission losses do indeed have a definable geologic cause, the study includes sites with varying near-surface lithologies. For experimental purposes, it is the near-surface geology that is varied since the reverberations occur early in the seismic record. Two sites which proved suitable for study are near Lyndon, Kansas (Fig. 2) and near Clinton, Kansas (Fig. 6).

Site Near Lyndon, Kansas

The site near Lyndon, Kansas (Station 137 at lat: 38° 36′ 18″ N; lon: 95° 43′ 43″ W) was chosen because of the varied near-surface geology, close to the site of a previous survey by the KGS for the proposed Superconducting Super-Collider (SSC) facility (Miller, et al, 1988). The site is located 2 miles west and .2 miles south of Lyndon, Kansas, partly in the Salt Creek alluvial valley (Fig. 2). Several surveys were performed on the surface of a light-duty, north-south trending road (Fig. 2).

The local near-surface geology of the site consists of an alluvial valley truncating formerly continuous interbedded Pennsylvanian limestone and shale units (O'Connor, 1955). Subcropping directly beneath the road are Quaternary alluvium to the south and the truncated Deer Creek Limestone to the north. Slightly contrary to the map of O'Connor (1955), the Tecumseh Shale is not

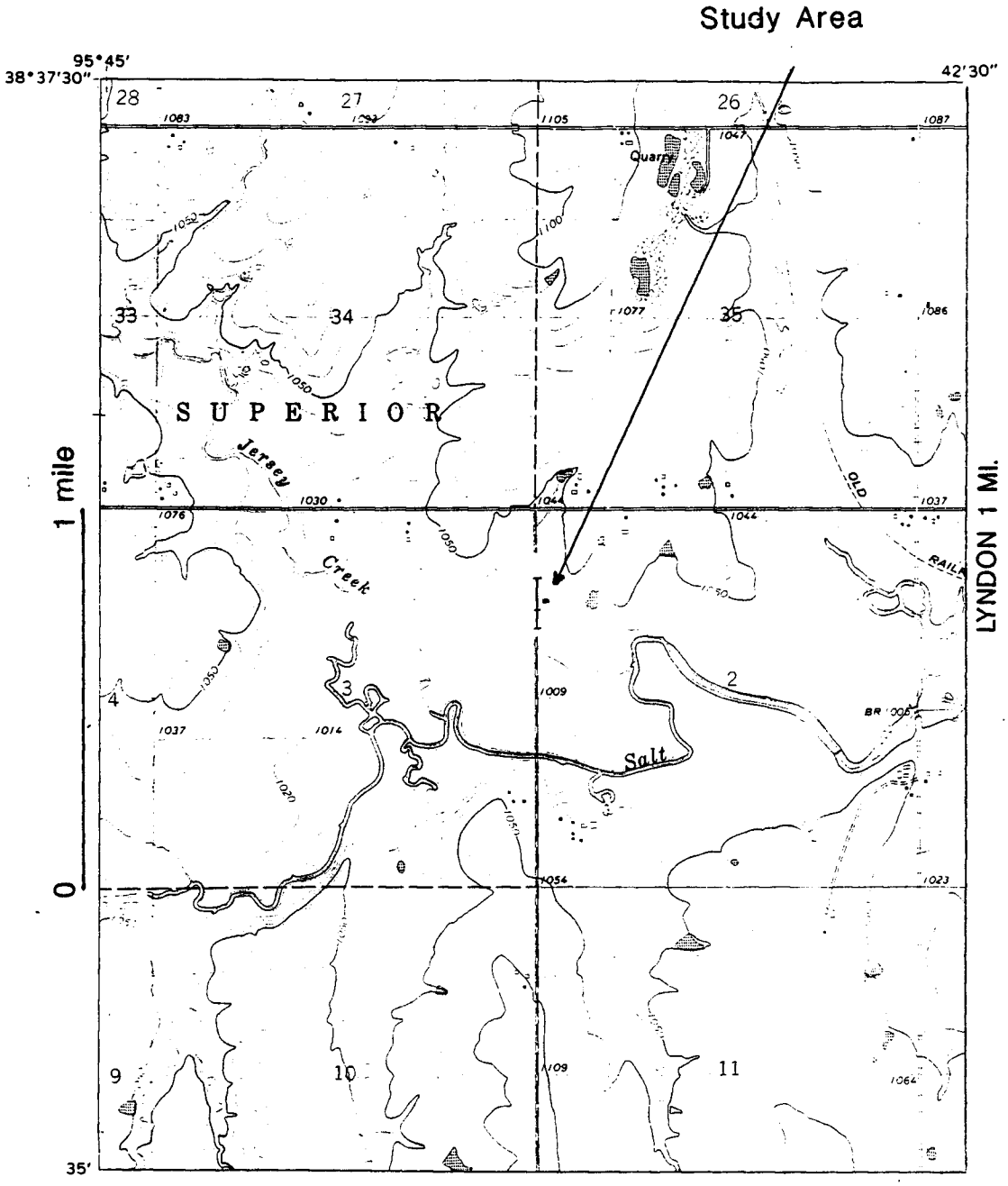

Figure 2. Topographic map of area near Lyndon, Kansas.

evident in outcrop (Fig. 3). The lowermost limestone unit of the Ozawkie Limestone Member of the Deer Creek Limestone discontinuously crops out for about 3 m parallel to the road. The effective outcrop area of this limestone unit occurs between Stations 134 and 142. This includes the outcrop area, and area to the north where the lowermost unit of the Ozawkie Limestone Member is less than 1 ft below land surface (Fig. 7a). Stratigraphically above, and further to the north, are a thin shale and another limestone unit which comprise the upper part of the Ozawkie Limestone Member (Fig. 4) (O'Connor, 1955).

Site near Clinton, Kansas

The site near Clinton, Kansas (Station 70 at lat: 38° 56′ 24″ N; lon: 95° 19′ 42″ W) was chosen because of the existence of an adjacent exposure excavated for the Clinton Lake Spillway (Fig. 5). The exposure was desirable because it permits direct study of the near-surface geology and it affords a unique setting for geophysical experimentation. The site is located 4 miles west of Lawrence, Kansas, just off of Clinton Parkway at the Clinton Spillway (Fig. 6). Walkaway noise tests were performed on both sides of the spillway, very close to the upper edge of the cliff.

The local near-surface geology of the site consists of Pennsylvanian system rocks of the Shawnee and Douglas

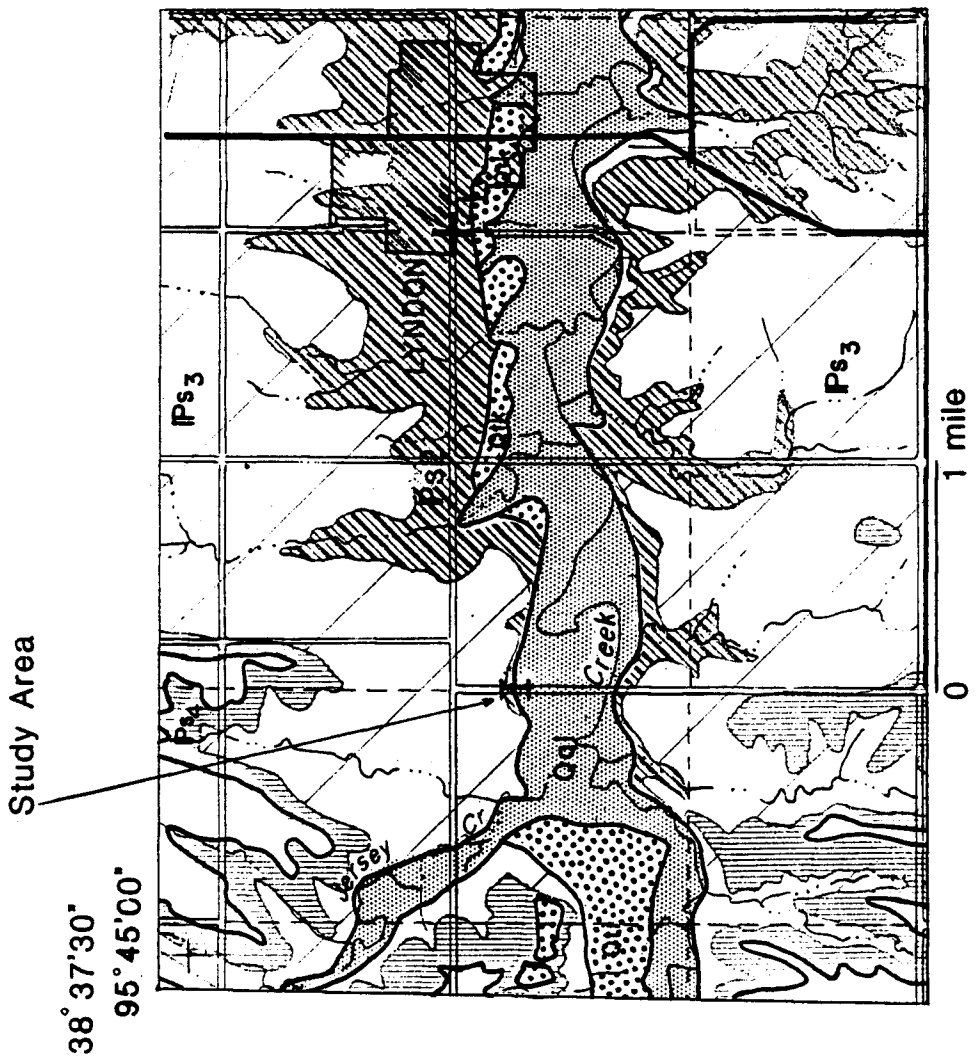

Figure 3. Geologic map of area near Lyndon, Kansas.

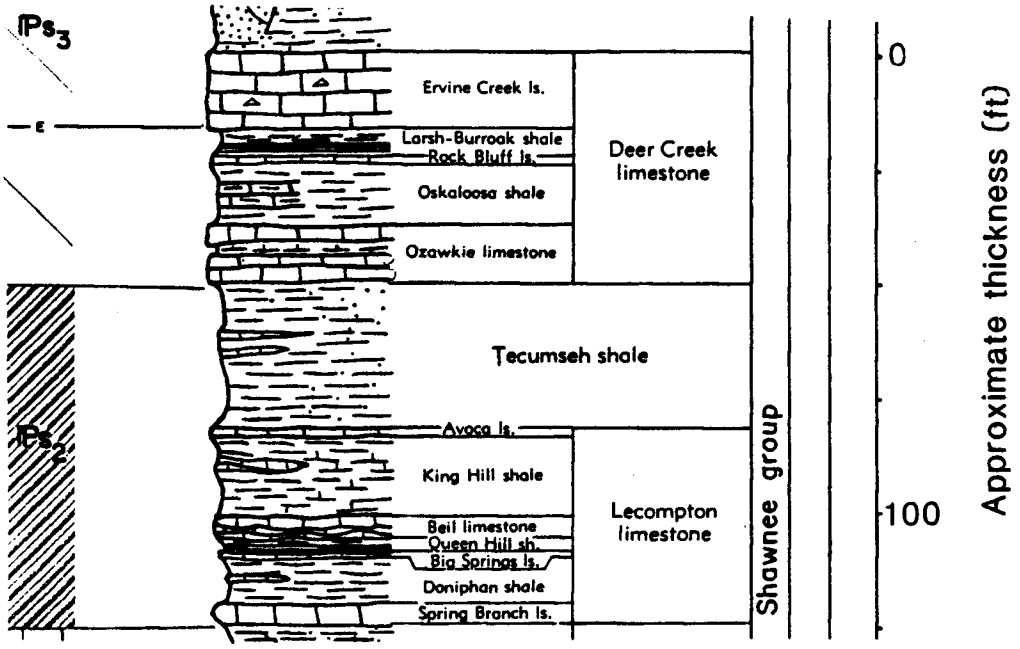

Figure 4. Stratigraphic column of area near Lyndon, Kansas.

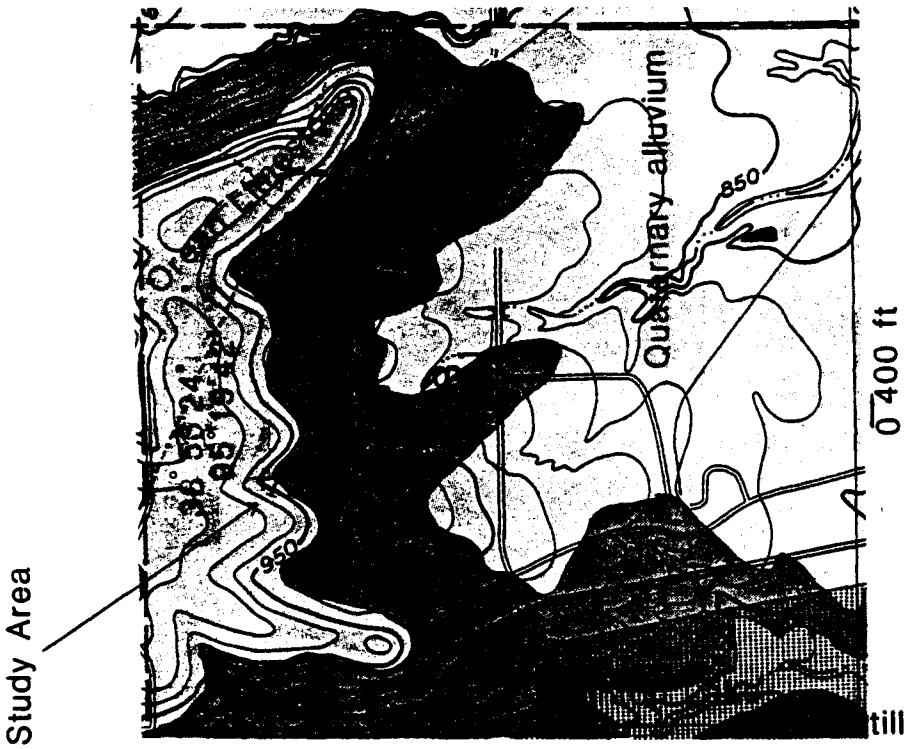

Figure 5. Geologic map of area near Clinton, Kansas.

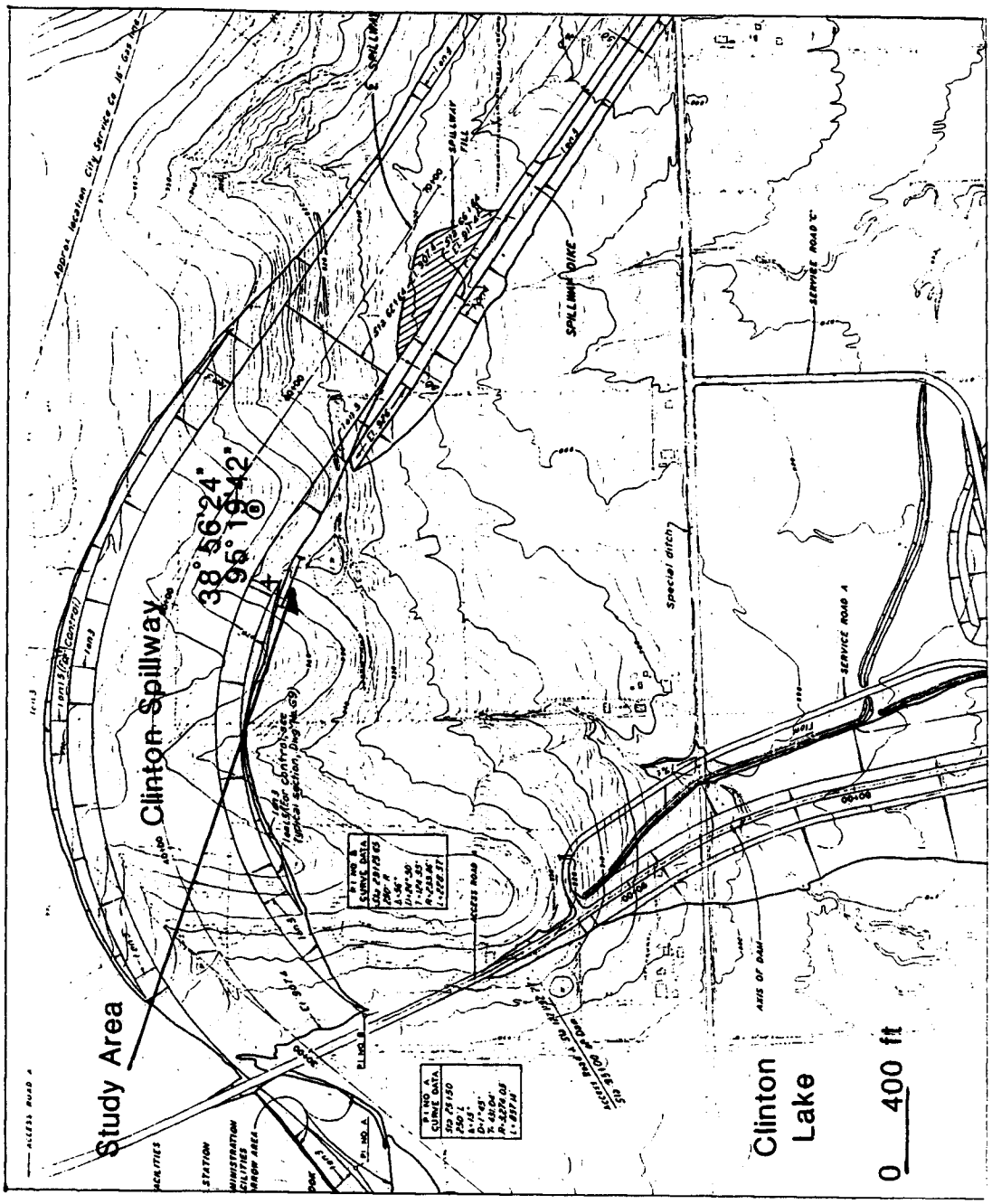

Figure 6. Topographic map of area near Clinton, Kansas. Note the location of the Clinton spillway.

Groups (McClain, 1979). Along the exposure, the Lawrence Formation is overlain by the Oread Limestone (O'Connor, 1960). Subcropping at the site on the south side, from east (Station 1) to west (Station 72), are the Snyderville Shale Member, the Leavenworth Limestone Member, and the Heebner Shale Member. These units are overlain by 2 to 4 ft of regolith. Exposed in the spillway and beneath the Plattsmouth Limestone Member on the north side are the Heebner Shale Member (6.5 ft), the Leavenworth Limestone Member (2 ft), the Snyderville Shale Member (10 ft), the Toronto Limestone Member (10 ft), and the uppermost shale units of the Lawrence Formation (30 to 40 ft), respectively (Fig. 52; Clinton Lake, 1976).

Geophysical Background

Of the many geophysical techniques available, the seismic reflection method is the most useful for petroleum exploration. It is relatively reliable for imaging the subsurface under various geologic conditions. Before 1980, seismic reflection methods were not ordinarily applied to the shallow subsurface, primarily because of the expense associated with instrumentation and processing. An additional remaining problem is that near-surface reflectors are often obscured on seismic records by acquisition-generated noise. Because of the occurrence of this noise early in seismic records, it is

not uncommon for researchers to apply a first-arrival mute which eliminates both the noise and the shallow reflection signal. Wavelet processing may then be applied to the remaining, relatively noise-free data. The occurrence of acquisition-generated noise may also have hampered the efforts of early researchers to acquire shallow seismic reflection data.

After 1980, a new generation of seismographs combined with the need for shallow subsurface imaging, resulted in pioneering efforts to obtain shallow, high-resolution seismic data (Steeples and Knapp, 1982). This high-resolution technique has been successfully used for bedrock mapping, void detection, and thin-bed resolution (Steeples and Miller, 1988). Its potential applicability to engineering and environmental problems is vast. The procedures for obtaining shallow reflection data are generally similar in concept to those of more conventional methods. However, in order to obtain the necessary high-frequency information, the procedures differ in detail.

Theoretical Background

Seismic reflections occur at interfaces at which there are contrasts in acoustic impedance. Acoustic impedance is the product of seismic velocity and density. Interfaces must also be smooth and large relative to the wavelength of the impinging seismic

energy (Halliday and Resnick, 1978). Unconformities are the surfaces most often imaged with conventional reflection methods (Mitchum, et al, 1977a). The shallow reflection method has been shown to be able to image intra-alluvial features, and thus, abrupt facies changes (Steeples and Miller, 1988). This is because of the characteristic short-wavelength energy used. However, even facies changes and unconformities will not act as reflecting surfaces if there are no acoustic impedance contrasts across the interface. Seismic reflections appear as coherent temporal events on seismic records, corresponding to acoustic impedance contrasts at depth. The approximate depth to these interfaces may be computed by multiplying the seismic velocity by half the two-way traveltime.

Summary of the Shallow Reflection Method

In general, the seismic reflection method involves seismic data acquisition, processing, and interpretation. The primary differences between shallow reflection and conventional reflection techniques occur in the acquisition phase. These differences are primarily a function of scale, both spatially and temporally (Table 1). The spatial differences involve both target location and the resulting spread geometry. Target depth is shallower; target thickness is often thinner; source-receiver offsets, receiver (group) spacing, and source

Table 1

Parameter	Conventional Reflection	Shallow Reflection
Energy Source.	Vibroseis	.50 caliber rifle
Fold	24	12
Number of Recording Channels	48	24
Group Spacing (ft)	100	9.84
Minimum Offset Distance (ft)	300	49.21
Maximum Offset Distance (ft)	2600	167.32
100 % Passband (Hz)	30-90	120-250
Target Depth (ft)	3500	30

(Bally, 1983)

spacing are all smaller. In fact, the target location is often less than 100 m deep, and the bed thickness may be as small as 1 m (Steeples and Miller, 1988).

In order to image such small targets, the resolution of the shallow reflection method must be considerably greater than that attained by conventional methods. Since resolution is directly proportional to frequency content, a source capable of producing high frequencies is required (Knapp and Steeples, 1986b). High frequency receivers are also desirable. Other temporal considerations include relatively low seismic velocities, a relatively short record length, and a relatively high sample rate.

The three components needed to acquire seismic data are the seismograph, the source, and the receiver. Relevant parameters of importance include pre-emphasis filters, sample rate, record length, natural geophone frequency, field geometry, and source characteristics. Pre-emphasis filters are used to increase the dynamic range of the seismograph in the domain of the high-frequency signal (Knapp, et al, 1988). These filters enable the recording of relatively high frequencies which the Earth tends to suppress because of its low-pass nature. The sample rate must be kept high to eliminate the risk of temporally aliasing the desired high-frequency information. Aliasing is a frequency ambiguity

resulting from the sampling process (Sheriff, 1984). The record length is normally kept short to reduce the total number of samples and because shallow reflection information generally occurs within the first quarter second of record.

Natural geophone frequency should be relatively high for shallow reflection data acquisition in order to take advantage of the geophone's low-cut nature. Operating characteristics of high-frequency geophones are better than those of low-frequency geophones for high-frequency information. In addition, low-frequency geophones may have parasitic resonant frequencies within the passband of shallow reflection data (Knapp and Steeples, 1986a).

In shallow seismic surveys there are usually two competing goals: velocity control and spatial resolution. Velocity control is desirable in order to yield reliable depth determinations. Sufficient velocity control may be attained with relatively large offsets. Spatial resolution is the competing goal, in which it is desirable to image the subsurface with as many closely spaced receivers as possible. Since engineering seismographs typically have a limited number of available recording channels (usually 12 or 24), these competing goals must be carefully considered before a survey is begun. In seismic reflection work, the field geometry is

usually split-spread or end-on. The geometry used is dependent upon the goals of the survey and the capacity of the seismograph. The end-on geometry is preferable for velocity control, due to the resulting larger offsets; while the split-spread geometry is preferable for spatial coverage.

The source must be of a high-frequency, impulsive nature for shallow reflection work. An impulsive source is desirable in order to produce a flat amplitude response over a broad range of frequencies. The source should contain a relatively large amount of high-frequency energy because of the Earth's low-pass nature, and because of the limited dynamic range of the typical engineering seismograph. A high-frequency source boosts high frequencies relative to low, permitting the reception of high-frequency signal (Knapp and Steeples, 1986b).

In general, there are few differences in the seismic data processing procedure between shallow reflection and conventional methods. One difference involves the muting of the air-coupled wave. This noise often has nearly the same frequency content as the desired signal and is therefore muted prior to stack (Knapp, 1987). Ground-roll sometimes presents a problem, but it is generally of lower frequency content than the desired signal, and may often be frequency-filtered. The first-arrival mute is

critical because desired targets often occur extremely early on seismic records. For this reason, caution must be exercised in distinguishing between reflected and refracted energy. Other problems unique to shallow reflection include wide-angle reflection phenomena, poor velocity control due to small offsets, and transmission-related signal losses.

Interpretation procedures used for conventional methods may be extended to the shallow reflection method; however, scale must be carefully considered. This is because with shallow methods, units the size of stratigraphic members a few meters thick may be resolved. In conventional methods stratigraphic group (10's to 100's of meters thick) resolution is the norm. The possibility of spatial aliasing must also be taken into account (Steeples and Miller, 1988).

Pitfalls Related to Near-surface Geology

The greatest benefits afforded by the shallow reflection method are due to the frequency content of the signal. These high frequencies permit high resolution (Widess, 1973). Unfortunately, in certain situations, these same high frequencies may cause deleterious effects. It has been observed that the near-surface geology may have adverse effects on the transmission of high-frequency seismic energy. In particular, it will be shown that near-surface limestone units inhibit the

transmission of high-frequency energy under certain circumstances (Fig. 25). This is in contrast to conventional seismic methods in which data are routinely acquired despite such conditions. The reason for this apparent paradox will be investigated more fully in the section entitled "Discussion".

Another deleterious phenomenon associated with shallow seismic reflection is the occurrence of high-amplitude reverberations immediately following the first refraction on seismic records (Fig. 7b). This noise obscures reflection energy and limits the effective use of the shallow reflection method on extremely shallow reflectors. Early arrivals are often the target of shallow reflection studies, and for this reason, these reverberations are insidious. On the following pages, near-surface geology will be shown to have an effect on these reverberations and on the transmission of seismic energy.

Methods of Study

Acquisition

At any new acquisition site, it is suggested procedure to conduct a series of walkaway noise tests (Steeples and Miller, 1988). These tests enable seismologists to identify the various coherent waveforms on a seismogram (Fig. 7b). They also help determine the optimum window for common-depth-point (CDP) data

acquisition at a given site, for a specific target (Hunter, et al, 1984). In this study, the walkaway noise tests also helped to determine the conditions under which changes occur in the reverberating wave train. The actual acquisition parameters used on the walkaway noise tests are listed in Tables 2, 3, and 4. The more important variable parameters are discussed in the section entitled "Analysis of Data".

For the CDP lines, high resolution was desired spatially as well as temporally. For this reason, a split-spread geometry with 3 m station spacing was employed. The maximum offset of any of the CDP lines was 51 m. This corresponds to within the first seventeen stations on the walkaway noise test data shown on Figure 7b. Few reflections are visible on the walkaway data within this window. Obscuring the reflection information are the air-coupled wave and ground roll. Both can usually be readily removed during processing. Data were not acquired at greater offsets, because of problems associated with wide-angle reflections (Pullen and Hunter, 1985). Wide-angle reflections simply disrupt the expected partitioning of energy according to the Zoeppritz equations (Sheriff, 1984).

Pre-emphasis filters were the primary acquisition variable for the CDP lines. In this thesis, the stated frequency value of the analog, pre-emphasis low-cut

filter refers to the point at which the amplitude has already been reduced by 3 dB. The filter then decreases the amplitude of lower frequencies at a rate of 24 dB per octave. The term "open filters" indicates that filters were not applied. Data were collected with three different pre-emphasis filter settings, over many of the same stations, to determine if the observed phenomena were frequency related. Also varied, in order to optimize the filter settings, were the minimum offset and the natural receiver frequency (Table 3).

General Processing Procedure

All the seismic data included in this paper were processed on the Data General MV-20000 computer at the KGS. The Seismic Processing Executive software (SPEX) marketed by Sytech Corporation was used extensively, along with some application programs developed in-house.

Walkaway noise test data generally require very little processing. Adjacent field files with similar acquisition parameters were merged to show the resulting waveform from the same shot-point over a large number of offsets (Fig. 7b). First-break based static corrections were applied to Walkaways 1 through 3 in order to improve the coherency of refraction events (Fig's. 7b, 8, and 10). Walkaways 4 and 7 were digitally filtered (Fig's. 12 and 17). Walkaway 4 was also deconvolved (Fig. 13). This is the extent of seismic processing applied to the

Table 2

Constant Acquisition Parameters:	
Seismograph	Input/Output DHR 2400
Amplifiers	IA 5
Sample Interval	0.250 ms
Record Length	250 ms
Notch Filter	60 Hz
Anti-Alias	3,000 Hz
Group Spacing	3 m
Source	.50 Caliber Rifle

Key

DH = Downhole
EO = End-on
f = frequency
S = Surface
SS = Split Spread
WW = Walkaways

Table 3

Variable Acquisition Parameters:	Line 0	Line 1 Low	Line 1 High	Line 1 WW	Line 2	Line 3	Line 4	Line 5
Source Type	DH	DH			DH	DH	DH&S	DH
Source Spacing	6 m	3 m			3 m	3 m	3 m	3 m
Spread Geometry	EO	SS		EO	SS	SS	SS	SS
# of Stations	48	48	47	72	72	72	72	67
Minimum Offset	6 m	6 m		3 m	12 m	3 m	12 m	12 m
Resonant f (Hz)	100	100			100	100	40	40
# of Phones	2	1			2	2	3	3
Low-cut Filter (Hz)	340	220	220&Open		220	600	20	220
High-cut Filter (Hz)	1000	1000			1000	Open	Open	1000
Soil Conditions	Dry	Dry			Wet	Wet	Dry	Dry
Amp. Scan Delay					75 ms			0 ms
Acquisition Date	5/87	6/87			11/87	11/87	4/88	4/88

Table 4

Walkaway Noise Test #	Source Type	Low-cut Filter	Soil Conditions	Shot #
4	DH .50 Cal.	Open	Dry	1
5	DH .50 Cal.	Open	Dry	2
6	DH .50 Cal.	Open	Wet	1
7	Sledge	Open	Dry	1
8	DH .50 Cal.	220 Hz	Dry	1
9	DH .50 Cal.	110 Hz	Dry	1

Key
DH = Downhole
Cal. = Caliber rifle

walkaway noise test data.

For CDP data, the standard processing procedure was much more extensive (Table 5). In general, the procedure involved sorting, editing, static correcting, normal-moveout correcting, filtering, and stacking. Each of the CDP lines was processed for the purpose of maximizing the signal-to-noise ratio. To achieve this goal, each line required a slightly different processing procedure (Table 5). In addition, certain processes were attempted on specific lines only, because of applicability or experimental failure.

In order to facilitate interpretation, and to increase the signal-to-noise ratio, a few specialized processes were utilized. These include: deconvolution (Fig's. 13 and 22), signal-to-noise determinations based on the semblance statistic (Fig. 30), spatially and temporally-varying frequency filtering (Fig. 25b), and velocity filtering (Fig. 28). These specialized processes yielded some surprising, yet insightful results (refer to the section entitled "Conclusions").

Deconvolution is a wavelet processing procedure designed to restore a seismic waveform to the shape it had prior to being filtered by the Earth (Sheriff, 1984). Predictive deconvolution is typically used in an attempt to attenuate multiples which involve near-surface reflectors. For this reason, I applied predictive

Table 5

Process	Line 1A	Line 1B	Line 2	Line 3	Line 4	Line 6
Sort	*	*	*	*	*	*
Mute	*	*	*	*	*	*
Edit	*		*	*	*	*
Frequency Scan	@	@	@	@	@	
Velocity Scan	@		@			
Velocity Spectra			@			
Trace Mixing					x	
Edit			x			*
Automatic Statics	*		*	*	*	*
Deconvolution	x	x				
Normal Moveout	*	*	*	*	*	*
Residual Statics	x	x	x	*	*	*
Velocity Filter					x	
Filter	*	*	*	*	*	*
Signal-to-noise			@			@
Stack	*	*	*	*	*	*

Key
@ = Analytical procedure
x = Procedure not included in final stacked section
* = Procedure included in final stacked section

deconvolution to the reverberating energy of CDP Line 1A. A number of filter-operator lengths were used, and the one that produced the highest signal-to-noise ratio is shown in Figure 22. Spiking deconvolution is a wavelet processing procedure designed to compress a non-impulsive wavelet to an impulse or spike. I applied it to the data of Walkaway 4 in an attempt to discern early reflection energy (Fig. 13). Deconvolution is not a new process, it is included here with special processes because the results were less than encouraging. For this reason it was not universally applied.

The signal-to-noise ratio is used to assess the relative data quality of a seismic record. It may be determined by dividing the integrated signal of a trace by its integrated noise (Sheriff, 1984; Sheriff and Geldart, 1982). The above procedure is heavily subjective. This is undesirable since we are then attempting to quantify something which has been interpreted. When we look at a seismic section and attempt to distinguish between signal and noise, our first criterion is coherence. This is because coherence is typically indicative of reflection events. Of course, incoherent signal and coherent noise also exist on seismic records.

Incoherent reflection signal is often diagnostic of static problems or structural disturbances, such as fault

zones and salt diapirs. It may also have seismic stratigraphic significance (Mitchum, et al, 1977b). Incoherent signal is effectively worthless without corresponding coherent signal. Coherent noise is insidious and must be correctly identified to avoid gross misinterpretation. It may result from an incorrect velocity function, insufficient velocity control, static problems, spatial aliasing, or over-processing. Both coherent noise and incoherent signal degrade any attempt to determine the signal-to-noise ratio based on coherency alone. However, if coherent noise, such as multiples and refractions are correctly identified, a signal-to-noise ratio based only upon coherence is a conservative estimate of the true signal-to-noise ratio.

Given the above, what we would like as a useful basis for comparison, is a ratio of coherent signal to incoherent noise. Such a ratio is available through the use of coherency statistics (Douze, 1979). For signal-to-noise comparisons in this study, I developed a coherency program based on the semblance statistic (Kalik, 1988) (Appendices B, C, and D). The program computes the signal-to-noise ratio based on the coherence of seismic traces summed over n samples and m+1 CDP's (Fig. 30). To test the program, I also applied it to random data (App. D) (Fig's. 54 through 60). The program may be used successfully on either stacked or unstacked

data. As stated previously, accounting for the possibility of both coherent noise and incoherent signal, a coherency plot of the semblance statistic is an instructive measure of signal-to-noise on a seismic record.

Spatially and temporally varying frequency filtering is simply a format to present a seismic record with the highest attainable overall signal-to-noise ratio. If, for some reason, the frequency content of the signal is variable in both space and time, such a filter is ideally suited to enhance signal relative to noise. The disadvantage of this procedure, is the loss of resolution under the relatively low-frequency signal areas (Fig. 25). However, the ability to correlate across areas that would otherwise exhibit no signal whatsoever, is clearly beneficial.

Velocity filtering is a procedure, utilizing the tau - p transform, to isolate seismic events for the purpose of enhancing data quality (Tatham, et al, 1983). In this study, it was used in an attempt to separate low-frequency reflection signal from ground roll. Theoretically, ground roll transforms to a point at time zero in tau - p space. Reflection hyperbolas transform to ellipses. These ellipses can then be isolated prior to transforming back to x-t (seismic record) space. To test the technique, it was also applied to random data

(Fig's. 61 and 62; and refer to the section entitled "Analysis of Data, Line 4").

Instrumentation and Acquisition Parameters

Site near Lyndon, Kansas

Seismic data have been collected by the KGS at a site near Lyndon, Kansas on four separate occasions. Eight CDP lines and three walkaway noise tests were processed from the collected data. The first CDP line (Line 0) was collected and processed for the proposed SSC facility (Miller, et al, 1987). The remaining seven CDP lines and the walkaway noise tests were acquired during three subsequent surveys and processed specifically for this study. The last CDP line (Line 6) is composed of Line 2 and Line 5 combined.

Common instrumentation and acquisition parameters used for all CDP lines and walkaway noise tests acquired at both sites are listed in Table 2. The common parameters include the seismograph, amplifiers, sample interval, record length, notch filters, and anti-alias filters having a 60 dB per octave roll-off with a 60 dB point of 3,000 Hz. In addition, a 3 m receiver group spacing was also kept constant at the site near Lyndon, Kansas. A modified (downhole) .50 caliber rifle lowered approximately .50 m into augured holes was used as a source for all the CDP lines.

The instrumentation and acquisition parameters

unique to each line are listed in Table 3. Variable parameters include the following: source type, source spacing, spread geometry, number of receiver stations, minimum source-receiver offset, natural geophone frequency, number of geophones per group, filters, and soil conditions.

Site near Clinton, Kansas

A series of walkaway noise tests was run at a site near Clinton, Kansas (Fig. 6). In addition to the parameters listed in Table 2, common instrumentation and acquisition parameters used at the site near Clinton, Kansas include: 4 ft minimum offsets, 4 ft group spacing, and 100 Hz geophones in groups of two. To identify all the events on the noise tests and to determine possible causes of the reverberating energy, several acquisition parameters were varied. These parameters include the following: source type, number of shots, low-cut filters, and soil conditions (Table 4).

Analysis of Data

Walkaway Noise Test Data

The objectives of the walkaway noise tests performed at sites near Lyndon, Kansas and near Clinton, Kansas were to determine the character of the reverberating wave train, the effects of near-surface geology on the reverberating wave train, and the optimum window for CDP data acquisition.

Ground roll, the air-coupled wave, reflections, and refractions can all be identified on the walkaway record acquired near Lyndon, Kansas (Figure 7b). The first arrival on this walkaway data is refracted energy. First-break based static corrections were applied to Walkaways 1 through 3 in order to make the refracted energy more coherent.

The high-amplitude events which are parallel to the first arrival exhibit linear rather than hyperbolic moveout (Fig. 7b). They are therefore not composed of primary reflected energy and are herein referred to as reverberation noise. On Walkaway 1 (Fig. 7b), the reverberation noise occupies an interval of approximately 45 to 50 ms in duration. Any reflection information occurring in the first 50 ms is therefore obscured by this noise. Thus, reverberation noise severely limits the effective use of the shallow reflection method on depths shallower than that corresponding to 50 ms, at this site.

In order to image the subsurface to arbitrarily shallow depths, reverberation noise must somehow be eliminated. In order to eliminate it, while also maintaining the integrity of any obscured signal, it is desirable to determine the cause of the noise. Several experiments were performed in an attempt to determine the cause of the reverberation noise.

Walkaway 1

Walkaway 1 (Fig. 7b) was acquired using open low-cut filters. As stated previously, this means that no low-cut filters were applied. The shotpoint was at station 100 over Quaternary alluvium. Note the conspicuous change in wavelet character of the reverberation noise between stations 137 and 147, and between 95 ms and 135 ms. This corresponds well with the effective outcrop area of the lowermost limestone unit of the Ozawkie Limestone Member (Stations 134 through 142). To determine if this phenomenon was indeed dependent on the near-surface geology beneath the shotpoint, a reversed profile (Walkaway 2) was performed.

Walkaway 2

On Walkaway 2, also acquired with open low-cut filters, the shotpoint was at Station 172 and there were 71 live receivers (Fig. 8). Here the shotpoint was over a thin shale within the Ozawkie Limestone Member. The amplifier-gain settings were not ideal for this comparison, but disruption of the fourth arrival (in time) is evident from the walkaway record. This occurs beneath Stations 139 to 151 on Figure 8. Note that the width of the reverberation noise is still approximately 50 ms, although it is more difficult to distinguish from the reflected energy on this profile.

Figure 7. **a.** Near-surface geologic cross-section of site near Lyndon, Kansas. Note the effective outcrop area. **b.** Walkaway 1 from site near Lyndon, Kansas. Note the change in wavelet character of the reverberating noise between Stations 137 and 147, and between 95 ms and 135 ms. This corresponds fairly well with the effective outcrop area of the Ozawkie Limestone Member. Acquired with open low-cut filters.

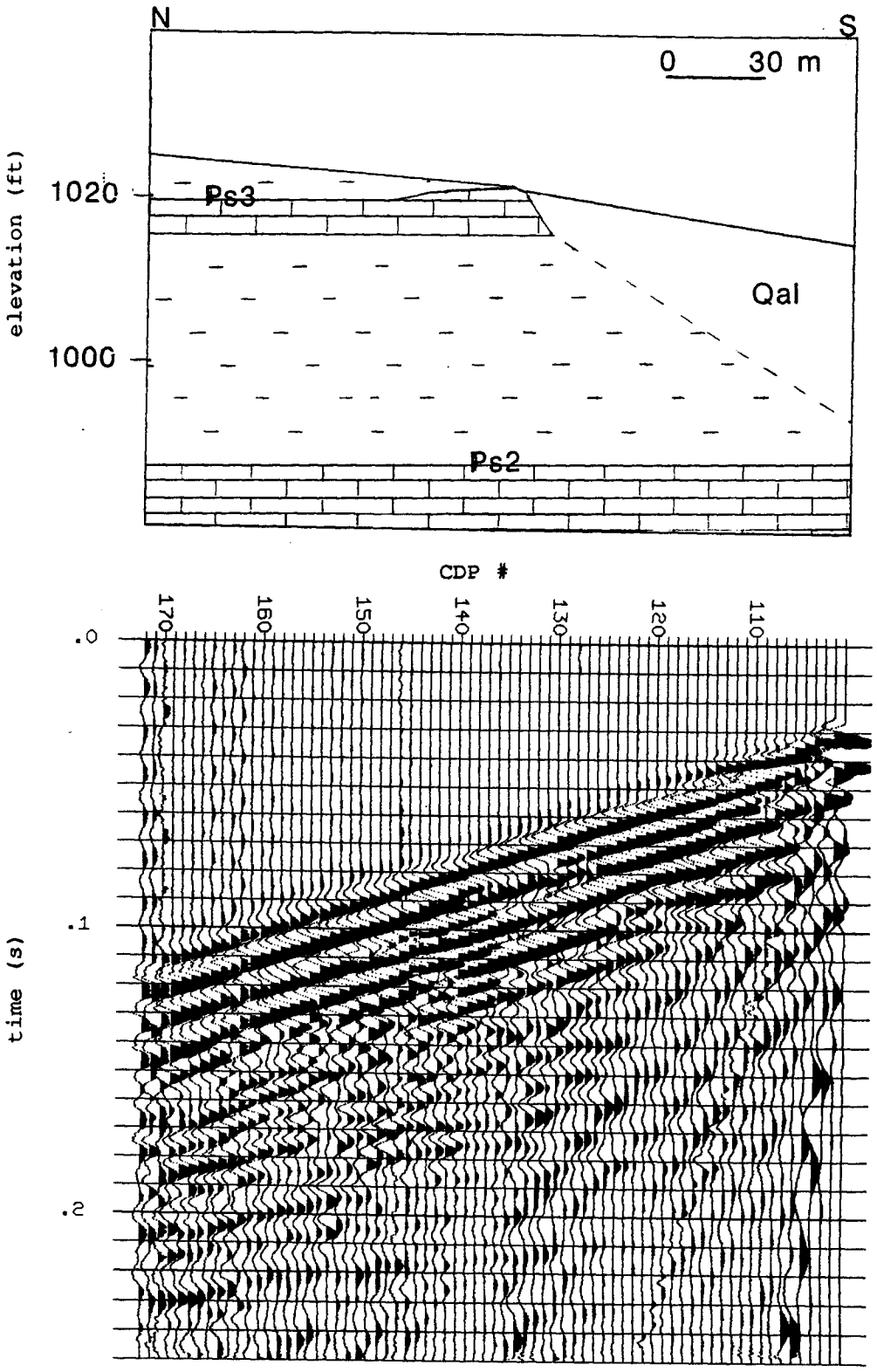
N
S
0 30 m
elevation (ft)
1020
1000
Ps3
Qal
Ps2
CDP #
170
160
150
140
130
120
110
.0
.1
.2
time (s)

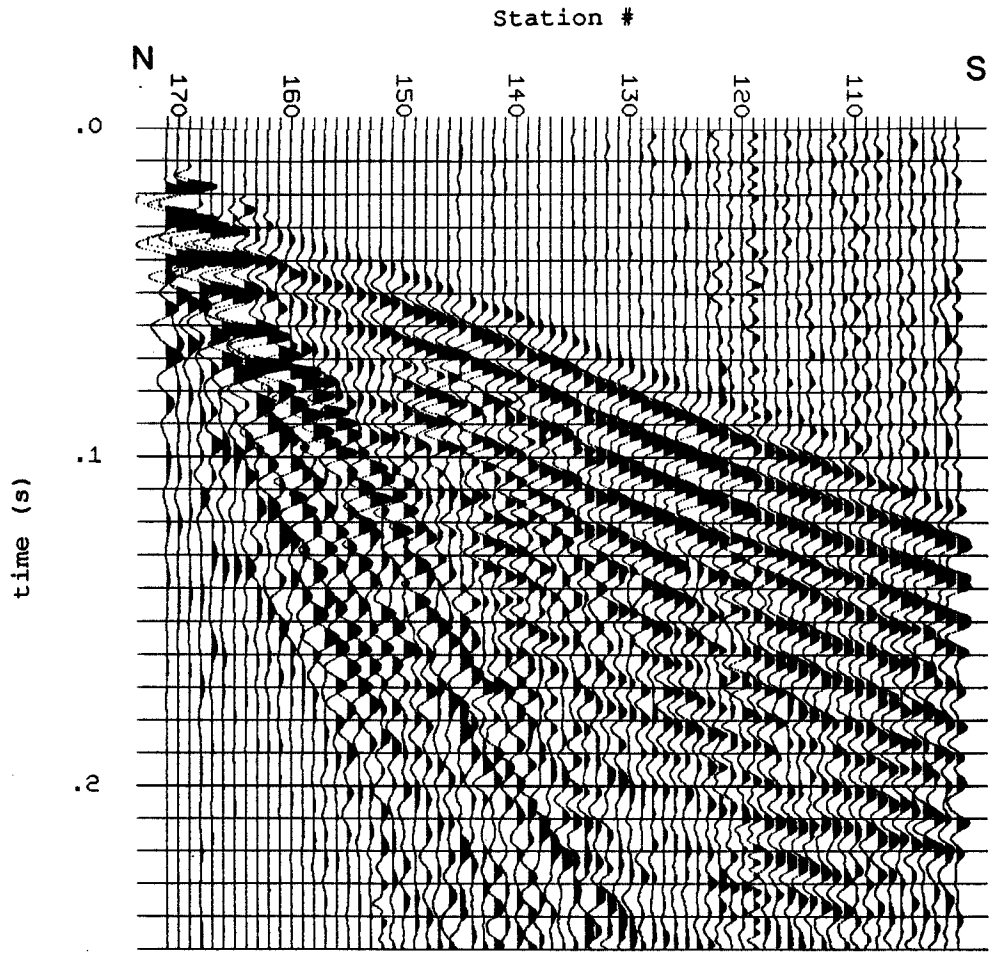

Figure 8. Walkaway 2 from site near Lyndon, Kansas. This is the reverse profile of Walkaway 1. Acquired with open low-cut filters.

Walkaways 1 and 2 Combined

In an attempt to isolate the differences due to the near-surface geology of the shotpoint, I combined the data from Walkaways 1 and 2 using a differencing scheme. To do this, it was necessary to reverse the polarity of one of the data sets, and add traces of like offset (Fig. 9). It was hoped that this would amplify any differences between the two data sets. Evident on the combined section (Fig. 9) are the ground roll from Walkaway 2, and the air-coupled wave from Walkaway 1. Unfortunately, however, no conclusions could be reached with respect to the reverberating energy. The failure of the above procedure was probably due to the dissimilar amplifier-gain settings between the two noise tests.

Walkaway 3

To determine the effect of signal frequency on the reverberating energy at the site near Lyndon, Kansas, a comparison can be made between Walkaways 2 and 3. Like Walkaway 2, Walkaway 3 was shot over the Pennsylvanian system rocks situated on the northern half of the line. However, 220 Hz low-cut filters were used for Walkaway 3. The change in character of the reverberating energy is evident on the third arrival (in time) between Stations 137 and 146 (Fig. 10). This is essentially the same area of disruption occurring on Walkaways 1 and 2, and corresponds fairly well with the outcrop of the lowermost

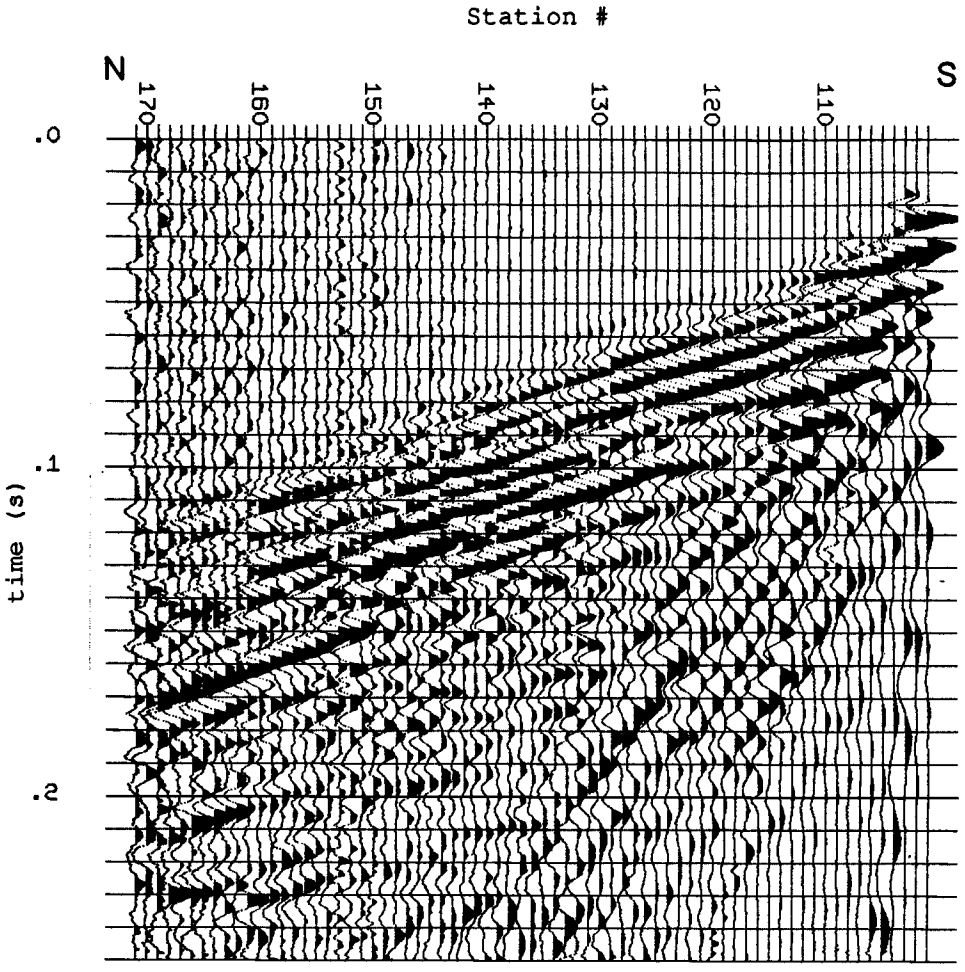

Figure 9. Combined data from Walkaways 1 and 2.

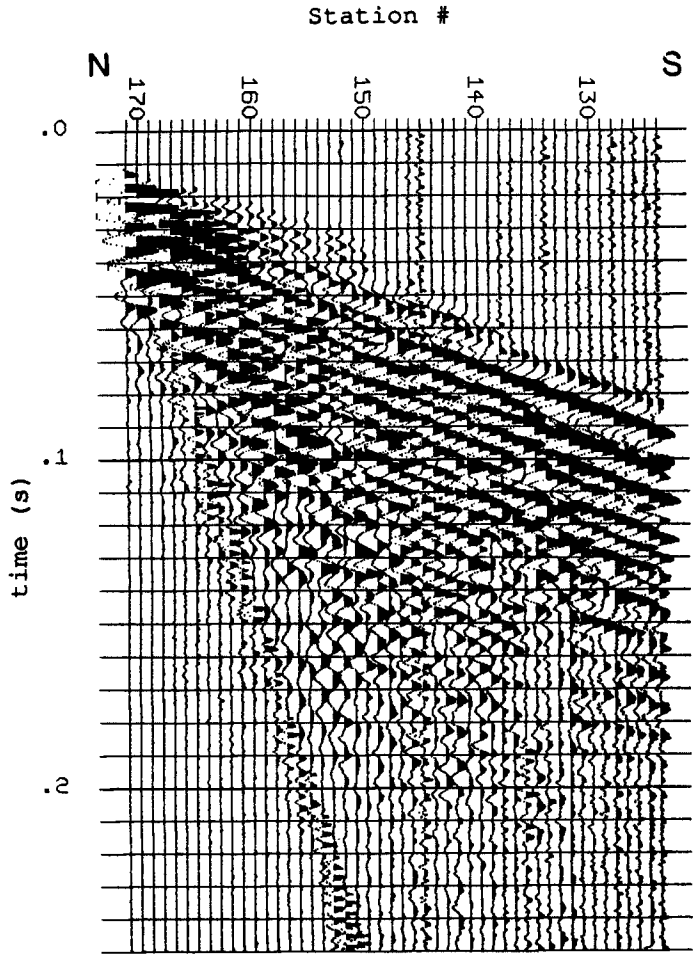

Figure 10. Walkaway 3 from site near Lyndon, Kansas. Note the change in character of the reverberating noise on the third arrival (in time) between Stations 137 and 146. Acquired with 220 Hz low-cut filters.

limestone unit of the Ozawkie Limestone Member. Thus, the data sets from the above three walkaway noise tests exhibit disruption of the reverberating wave train beneath an outcropping limestone unit.

Walkaway 4

In an attempt to determine the effect of local geology on the occurrence of reverberations, several walkaway noise tests were performed at a site near Clinton, Kansas. Walkaway 4 was acquired with open low-cut filters (Table 4). The reverberation phenomenon is readily apparent and occupies at least 130 ms on Figure 11. Upon the application of a low-cut digital filter, Walkaway 4 exhibits strong, high-frequency reflection energy (Fig. 12). Refraction energy is still visible on Figure 12, but it is now restricted to about 20 ms. This could very well be the convolved source wavelet. If so, the wavelet is a doublet or triplet, and does not contain reverberating energy. To compress a wavelet to a spike, spiking deconvolution is often applied. Ideally, this procedure would yield reflection energy which was previously obscured by the wavelet. Unfortunately, spiking deconvolution applied to Walkaway 4 failed to significantly compress the wavelet (Fig. 13). However, this process does seem to enable the distinction between reflected energy and reverberation noise.

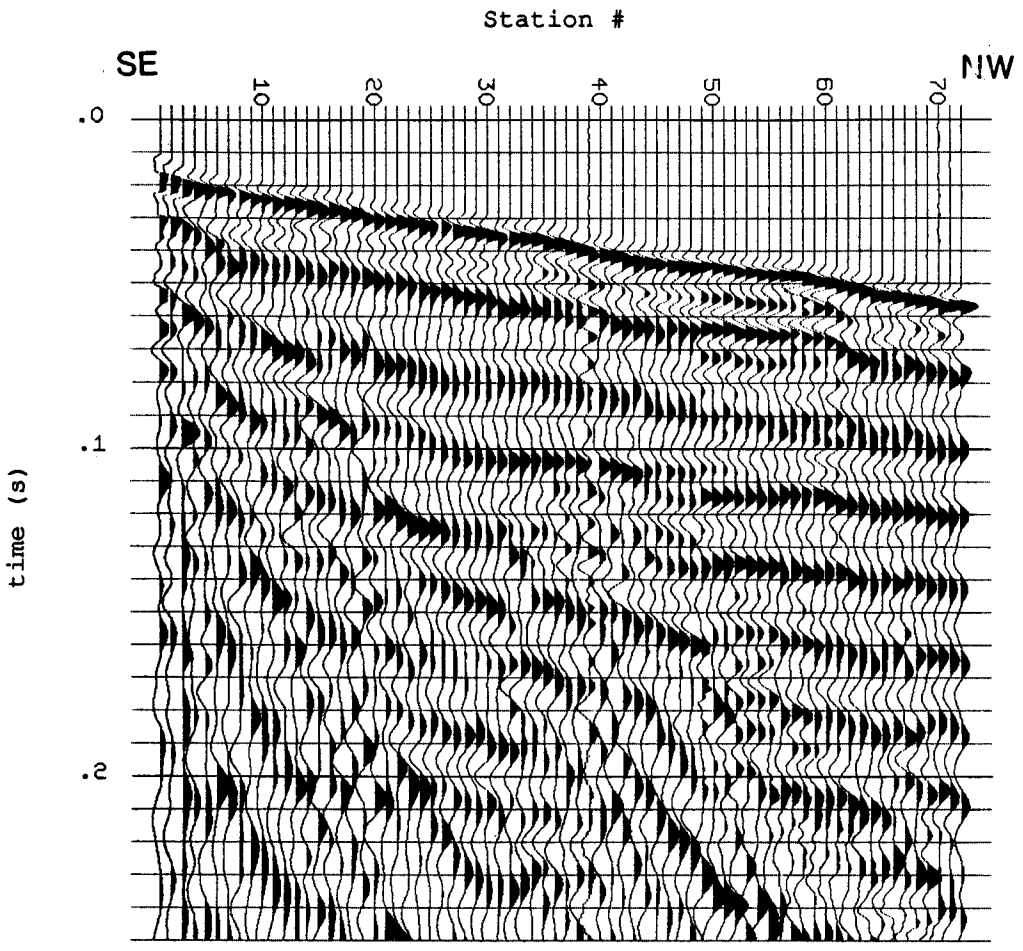

Figure 11. Walkaway 4 from site near Clinton, Kansas. Note the pervasive reverberating energy. Acquired with open low-cut filters.

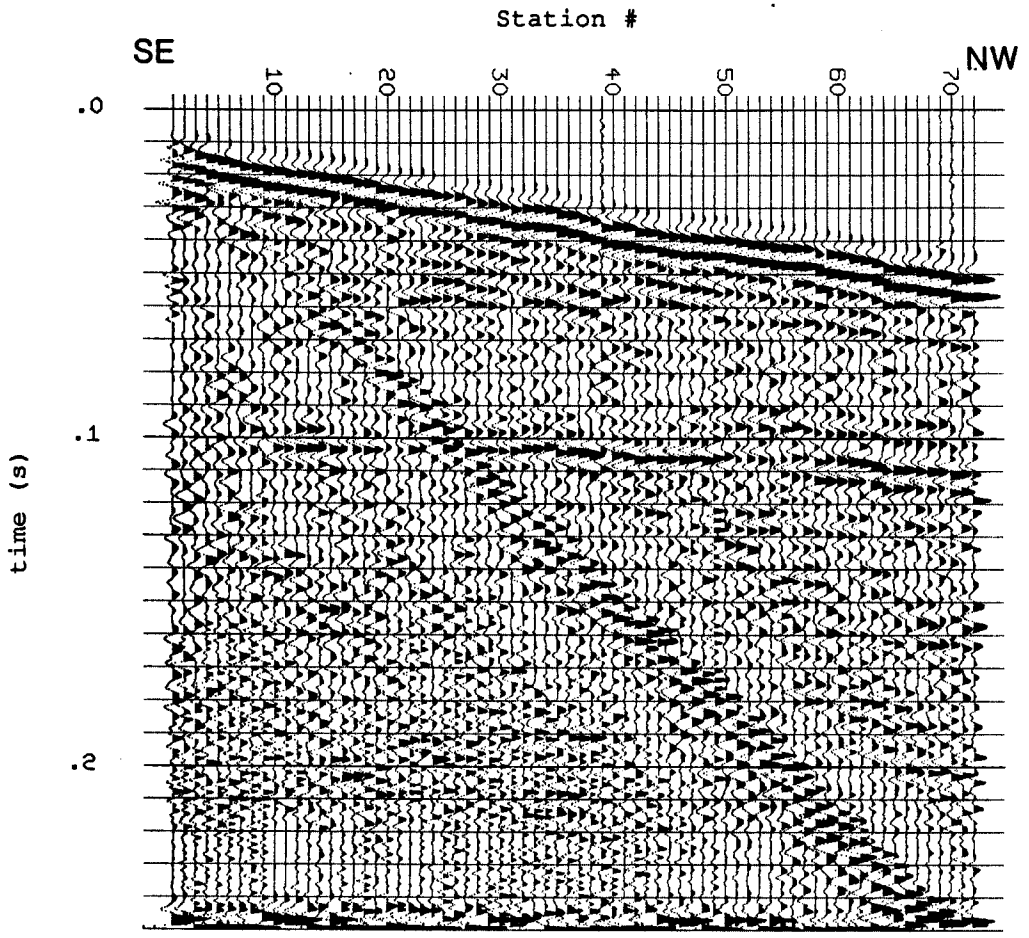

Figure 12. Digitally filtered plot of Walkaway 4 from site near Clinton, Kansas. Note the appearance of high-frequency reflection energy (Station 70 at 111 ms). Acquired with open low-cut filters.

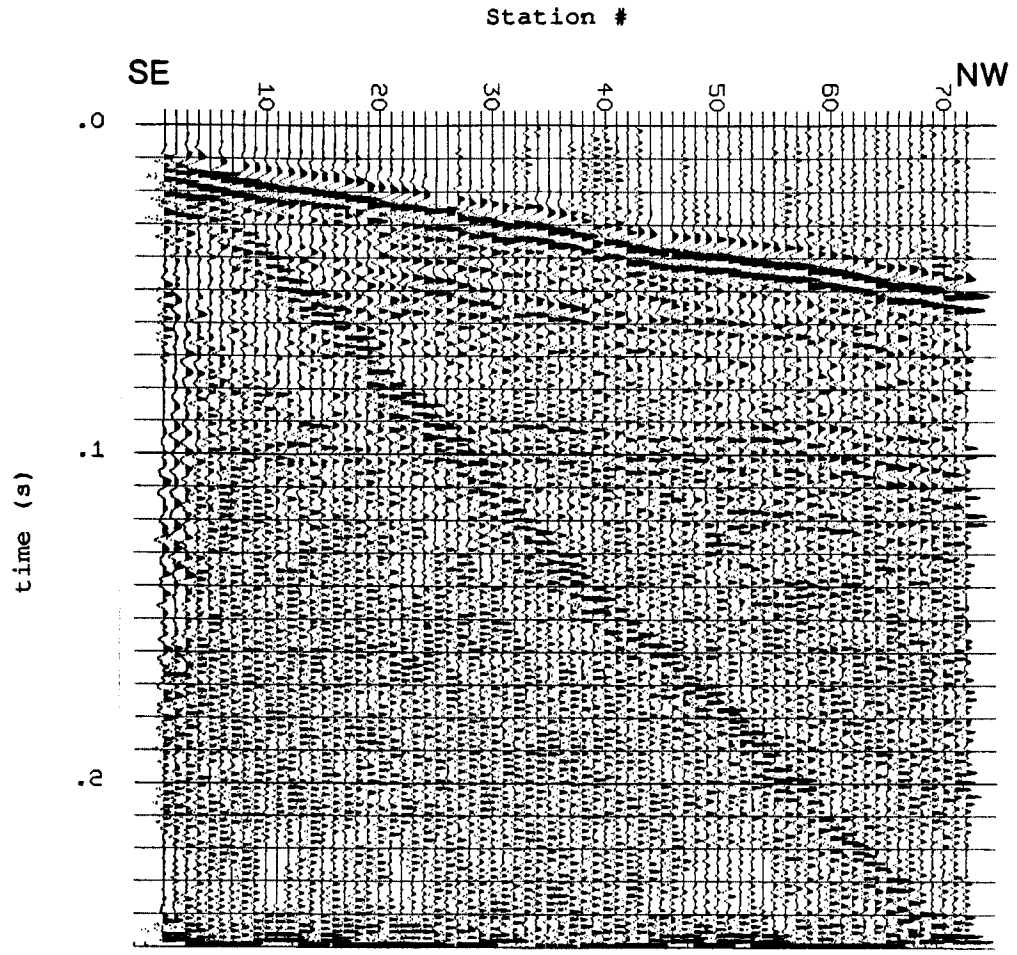

Figure 13. Deconvolved plot of Walkaway 4 from site near Clinton, Kansas. Note the reduced width of the reverberating noise. Acquired with open low-cut filters.

Walkaway 5

Walkaway 5 (Fig. 14) was acquired to determine the effect of firing a second shot into an augured hole with exactly the same acquisition parameters (Table 4). The first shot (Fig. 11) would tend to create a path for the second bullet. This would slightly alter the source energy (Seeber and Steeples, 1986). The resulting data are of a noticeably higher amplitude and slightly higher frequency (Fig. 14).

Walkaway 6

Walkaway 6 (Fig. 15) was acquired to determine the effect of saturating an augured hole with water prior to shooting. This walkaway noise test was recorded after saturating the augured hole which was used for Walkaways 4 and 5. All other acquisition and instrumentation parameters were identical to Walkaways 4 and 5 (Table 4). The raw field data suggest a slight reduction in both amplitude and frequency content relative to Walkaway 5 (Compare Fig's. 11, 14, and 15).

Walkaway 7

Walkaway 7 was acquired to determine the effects of source type on reverberating energy (Fig. 16). A sledge hammer was used as the seismic source, with all other acquisition and instrumentation parameters kept constant (Table 4). Evident on Figure 16 are the air-coupled wave, ground roll, and refraction energy. Much of this

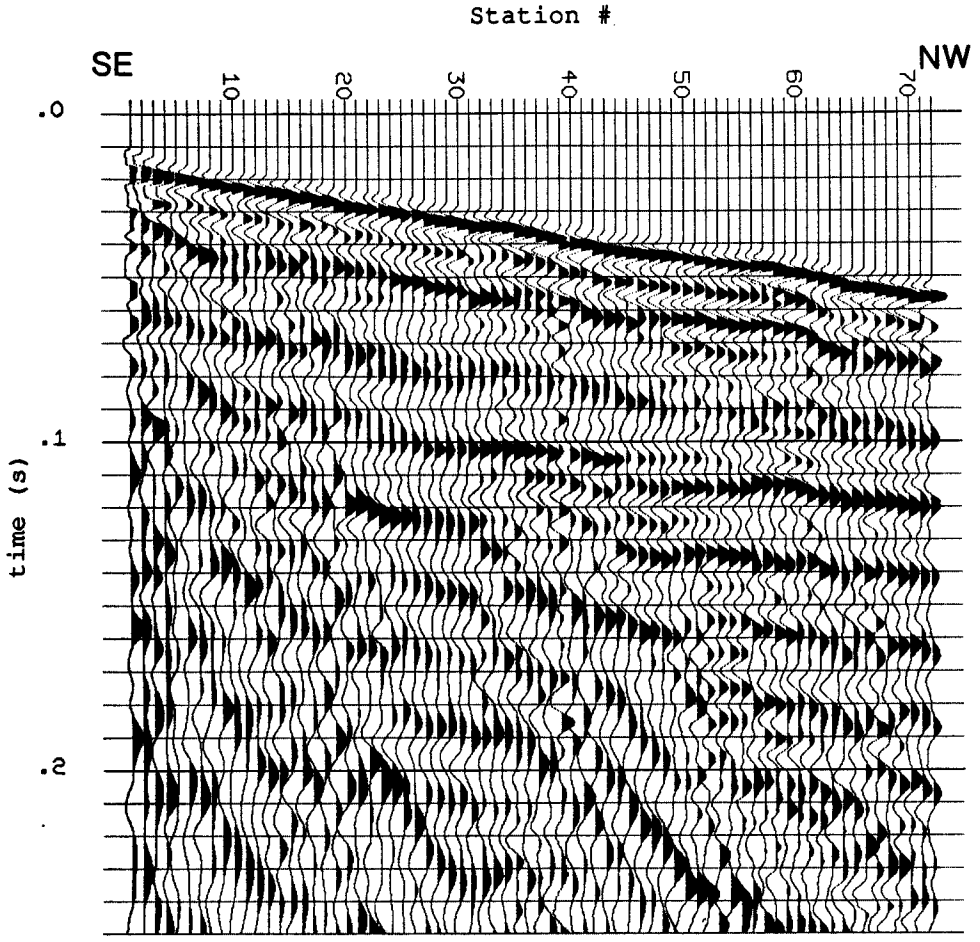

Figure 14. Walkaway 5 from site near Clinton, Kansas. This was recorded after the second shot in the same hole which was used for Walkaway 4. Note the higher amplitudes and frequencies (Station 20 at 38 ms) relative to Figure 11. Acquired with open low-cut filters.

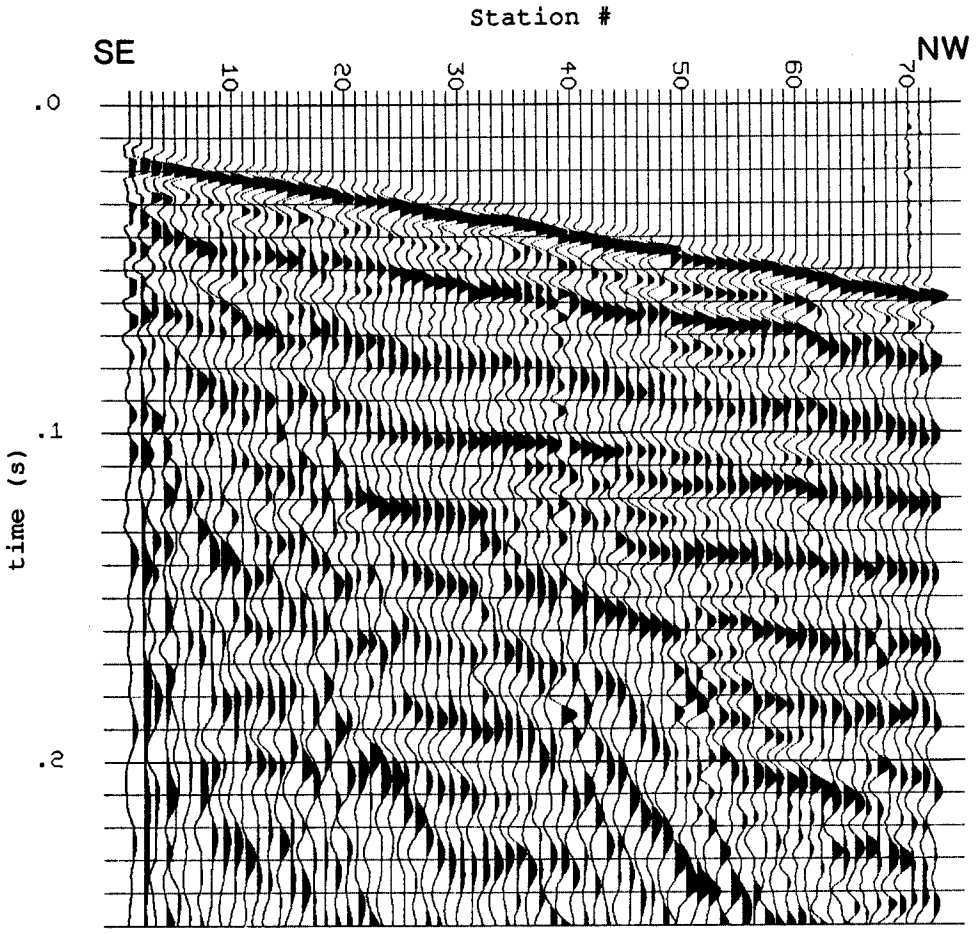

Figure 15. Walkaway 6 from site near Clinton, Kansas. This was recorded after saturating the augured hole which was used for Walkaways 4 and 5. Note the slight reduction in amplitude and frequency relative to Figure 14. Acquired with open low-cut filters.

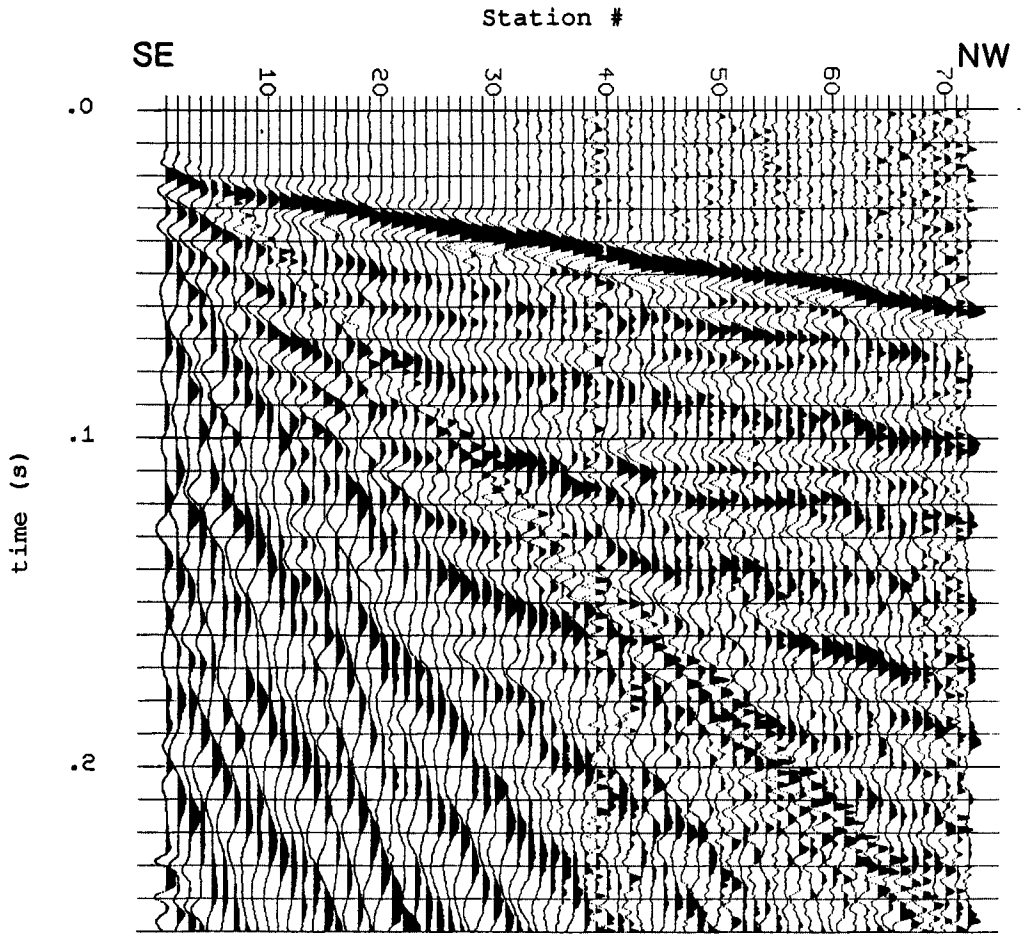

Figure 16. Walkaway 7 from site near Clinton, Kansas. This was recorded with a sledge hammer in place of the .50 caliber rifle used for all the other seismic data in this thesis. Note the appearance of the air-coupled wave and the clarity of the ground roll relative to that on Walkaway 4 (Fig. 11). Acquired with open low-cut filters.

noise is less conspicuous on Figure 11 because the signal-to-noise ratio of the data using a .50 caliber rifle is high relative to that of a sledge hammer. Upon digital filtering, the data quality of Walkaway 7 was improved (Fig. 17). As expected, the signal frequency of the data acquired using a sledge hammer is low relative to that of a .50 caliber rifle (Fig's. 17 and 11, respectively). On Figure 17, the refracted arrival appears as a doublet or triplet occupying less than 30 ms. Once again, digital filtering removed much of the reverberating energy from the walkaway noise test data.

Walkaway 8

Various analog filters were used to test the ability of removing reverberating energy in the field. Walkaway 8 (Fig. 18) was acquired using 220 Hz low-cut filters (Table 4). This walkaway noise test data is directly comparable with the digitally filtered version of Walkaway 4 (Fig. 12). Differences in the two figures are due primarily to the fact that the pre-emphasis, analog filters are logarithmic, while the corresponding digital filter is linear. In both cases, the noise test data contain high-frequency reflection energy.

Walkaway 9

Although reverse profiles were acquired for each noise test, Walkaway 9 is one of the few which exhibits unique information (Fig. 19). The acquisition parameters

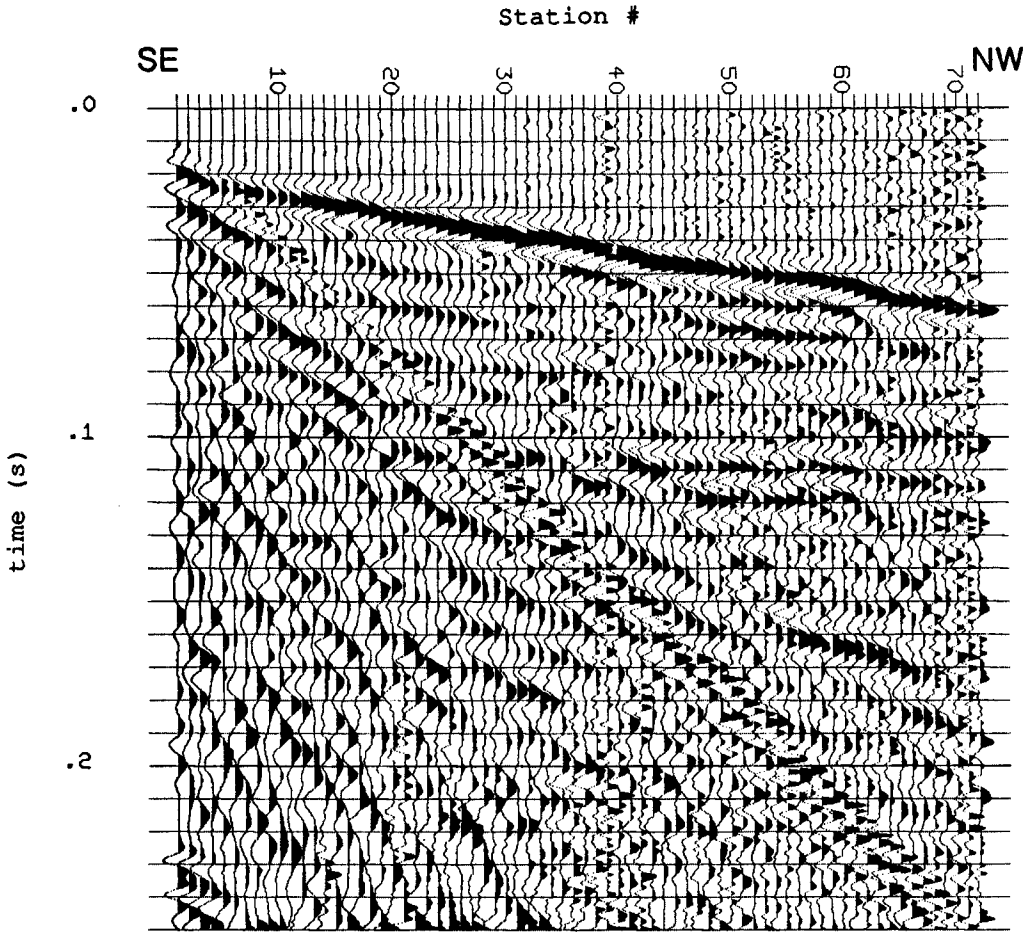

Figure 17. Digitally filtered plot of Walkaway 7 from near Clinton, Kansas. Note the low signal frequency relative to that of Figure 12. Acquired with open low-cut filters.

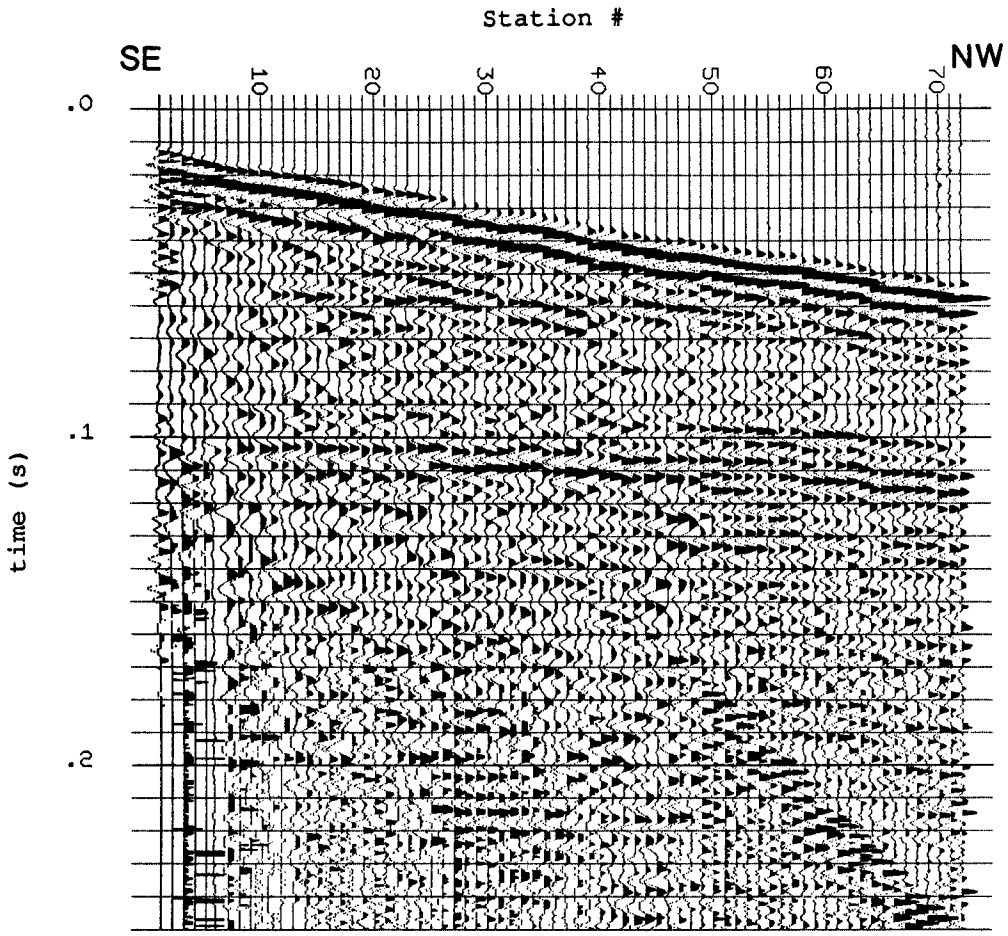

Figure 18. Walkaway 8 from site near Clinton, Kansas. Note the similarity with Figure 12. Acquired with 220 Hz low-cut filters.

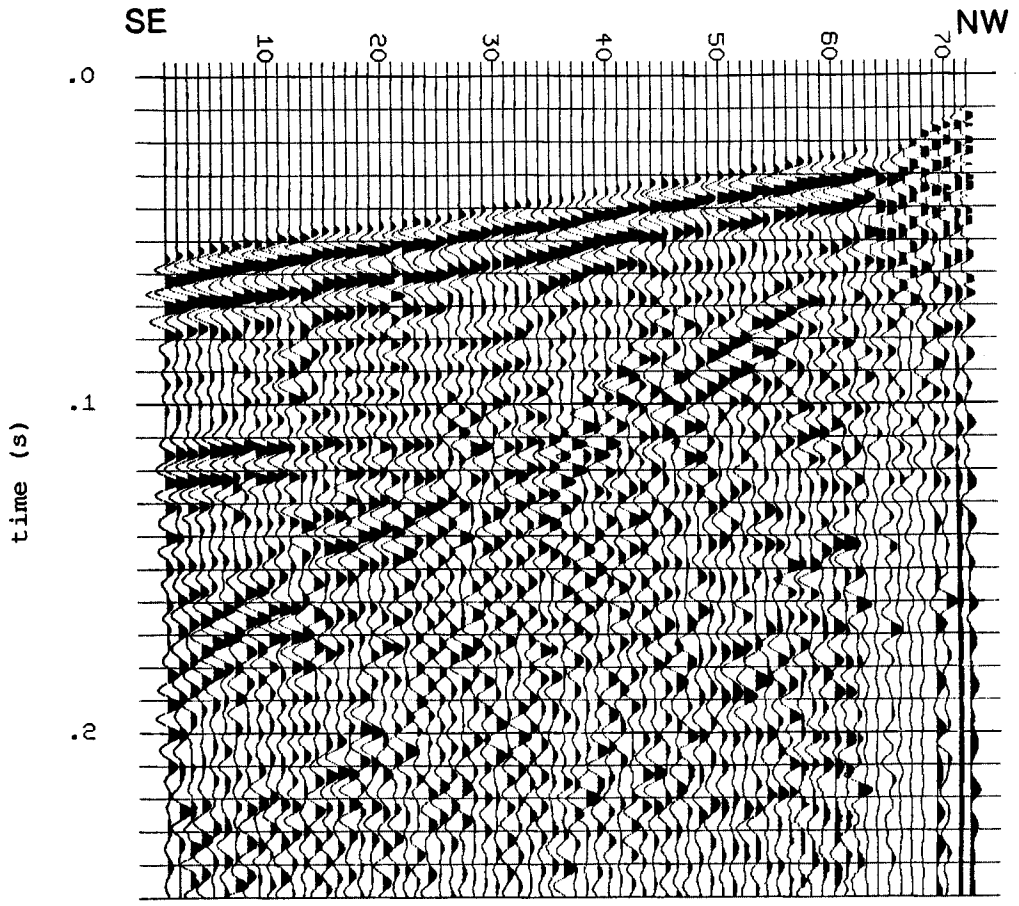

Figure 19. Walkaway 9 from site near Clinton, Kansas. Note the occurrence of direct-wave energy. Also note the multiple peaks and troughs of all the identifiable energy. Acquired with 110 Hz low-cut filters.

used for this walkaway noise test are listed on Table 4. Readily visible on Figure 19 are refraction energy, reflection energy, and the direct wave. All three appear to exhibit multiple peaks and troughs. Since these waves follow different paths, it is unlikely that they would exhibit similar reverberation patterns. Thus, it is possible that the refracted energy on Figure 19 represents the convolved source wavelet, and not reverberating seismic energy.

Common-Depth-Point Data

The first shallow reflection CDP survey (Line 0) at the site near Lyndon, Kansas, was acquired for the proposed SSC facility (Miller, et al, 1988). Line 0 was wholly acquired over Quaternary alluvium. For this thesis, it was desirable to acquire data over varying near-surface materials. Therefore, the majority of the subsequent lines were acquired with approximately half of the stations over Quaternary alluvium and half over Pennsylvanian materials. The first CDP line acquired with this layout (Line 1) was split in half for processing purposes. The acquisition parameters used for this line are listed on Tables 2 and 3.

Line 1

The half of Line 1 (Line 1A) shot over Quaternary alluvium (Fig. 20) exhibits reasonably good data quality. The processing procedure used for this line is given in

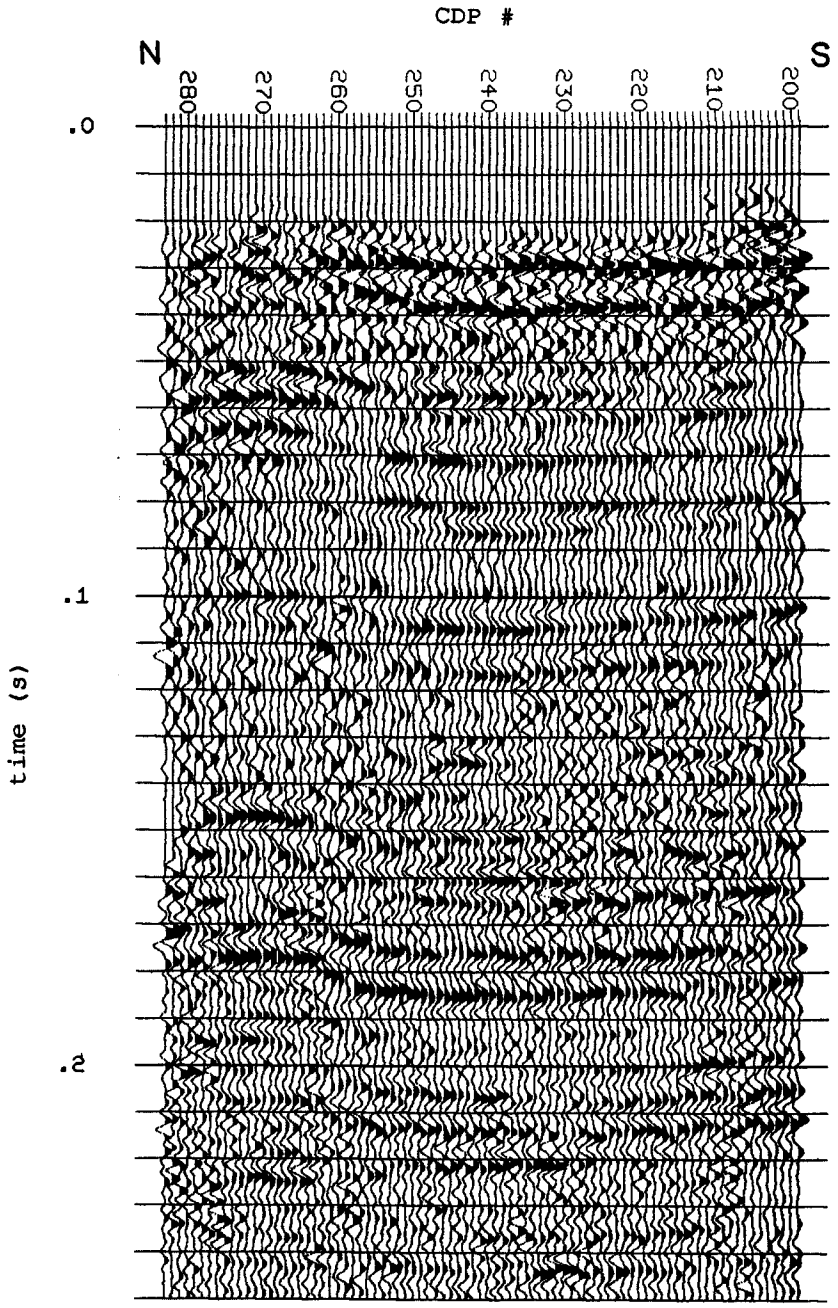

Figure 20. Stacked seismic section of CDP Line 1A from near Lyndon, Kansas. Note the relatively good data quality and the velocity pull-up to the north. Acquired with 220 Hz low-cut filters.

Table 5. The high-amplitude events occurring at 30 ms and 39 ms are remnants of the reverberation noise after normal moveout correction and stacking. Since these events exhibit linear, rather than hyperbolic moveout (Fig. 7b), they should be attenuated upon the application of a velocity function. Only some attenuation is evident because the receiver offsets were low enough that, upon normal moveout correction, there is still some coherence.

Coherent reflection events are visible on the seismic section (Fig. 20) between 52 ms and 244 ms. The represented units are approximately parallel and thus are consistent with the local, flat stratigraphy. Apparent structure to the north, beginning approximately at CDP 259, is a velocity pull-up resulting from local, higher-velocity near-surface materials. If the event which occurs at 80 ms at CDP 220 is followed north, with some difficulty, it can be seen at approximately 72 ms at CDP 270. This relatively small change of 8 ms (two-way traveltime) corresponds to a 40 ft change in computed depth, based on stacking velocities alone. It should also be noted, that there is about a 6 ft increase in elevation between CDPs 199 and 283. Thus, the near-surface geology alone could cause a relative subsurface depth calculation error of 46 ft, in this instance.

CDP numbers correspond exactly to double the

station location. Thus, according to the seismic record (Fig. 20), there is a near-surface velocity contrast beginning somewhere between Stations 129 (CDP 258) and 130 (CDP 260). Since the effective outcrop area of the lowermost limestone unit of the Ozawkie Limestone Member occurs between Stations 134 and 142, there is evidence of Pennsylvanian system limestone subcropping beneath the road surface between Stations 130 and 134.

Static problems can also affect depth calculations. The stacking velocity is that velocity which will best stack in a reflection event. Static problems will cause the actual moveout to be nonhyperbolic. Therefore, the stacking velocity will not necessarily yield reliable depth determinations in areas with significant static problems.

Contrast the clarity of Line 1A (Fig. 20) with that of Line 1B (Fig. 21), the other half of Line 1, shot over Pennsylvanian material. Not only can near-surface geology cause static problems, and velocity pull-up, but it can also cause wholesale destruction of data quality. Ideally, the only difference between these two lines is the near-surface geology. All the shots for Line 1A were in Quaternary alluvium. All the shots for Line 1B were in Pennsylvanian materials. Some events on the south side of Line 1B (Fig. 21) are barely correlatable with events on the north side of Line 1A (Fig. 20). These

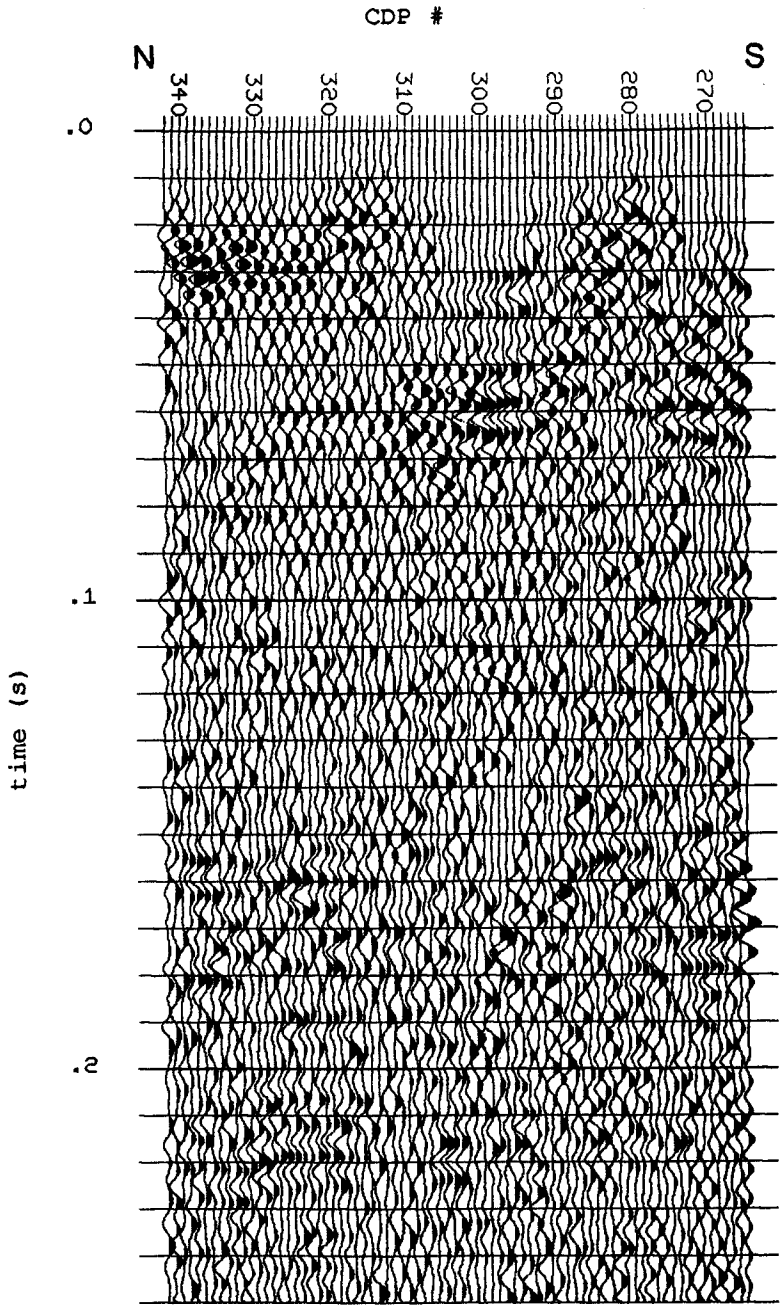

Figure 21. Stacked seismic section of CDP Line 1B from near Lyndon, Kansas. Contrast the quality of this data with that of Figure 20. Acquired with 220 Hz low-cut filters.

include events at 61 ms, 68 ms, 100 ms, 172 ms, and 178 ms. Correlating events across Line 1B is another problem entirely.

The processing procedure for line 1B is shown in Table 5. It differs from that used on Line 1A in only minor respects. No bad traces were deleted primarily because almost all traces were bad. No automatic static corrections were applied because static problems are insignificant compared with the problems inherent in this data set.

In a vain attempt to pry signal from noise, the data from Lines 1A and 1B were deconvolved. In particular, I used autopredictive deconvolution with a second zero-crossing operating wavelet. It was applied pre-stack and pre-normal-moveout. Theoretically, if the reverberations were true multiples they would have been eliminated. Not only were the reverberations not eliminated (< 50 ms), but the data quality on Line 1A was substantially reduced (Fig. 22). Unfortunately, the data from Line 1B fared no better upon deconvolution (Fig. 23).

Field files from Line 1 are shown in Figure 24. Field File 33 was shot over Quaternary alluvium, and all the receivers were in alluvium as well. Field File 42 shows the result of having "live" receivers in near-surface limestone, with the source still in alluvium. Note the deflection of the first arrival (in time)

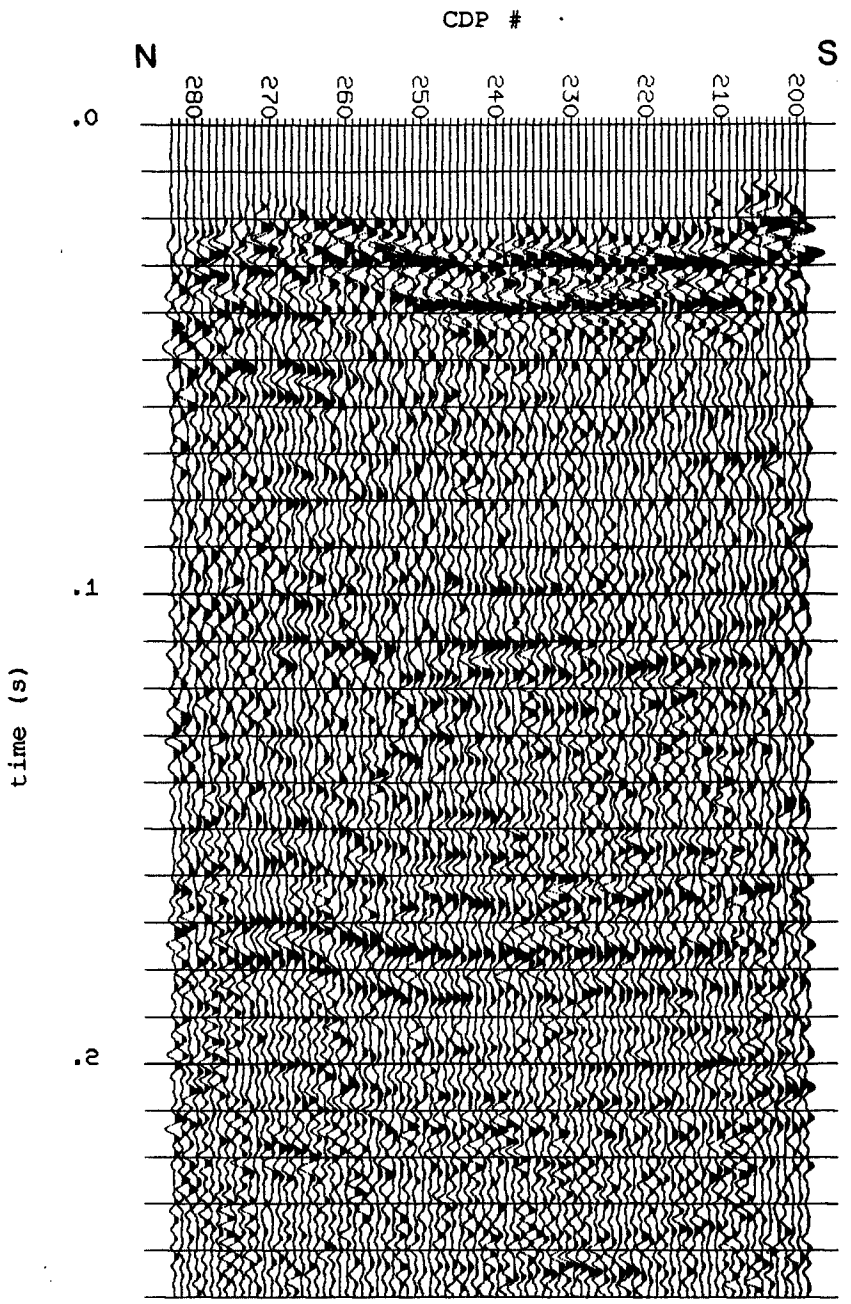

Figure 22. Deconvolved seismic section of CDP Line 1A from near Lyndon, Kansas. Note the reduction in data quality compared to Figure 20.

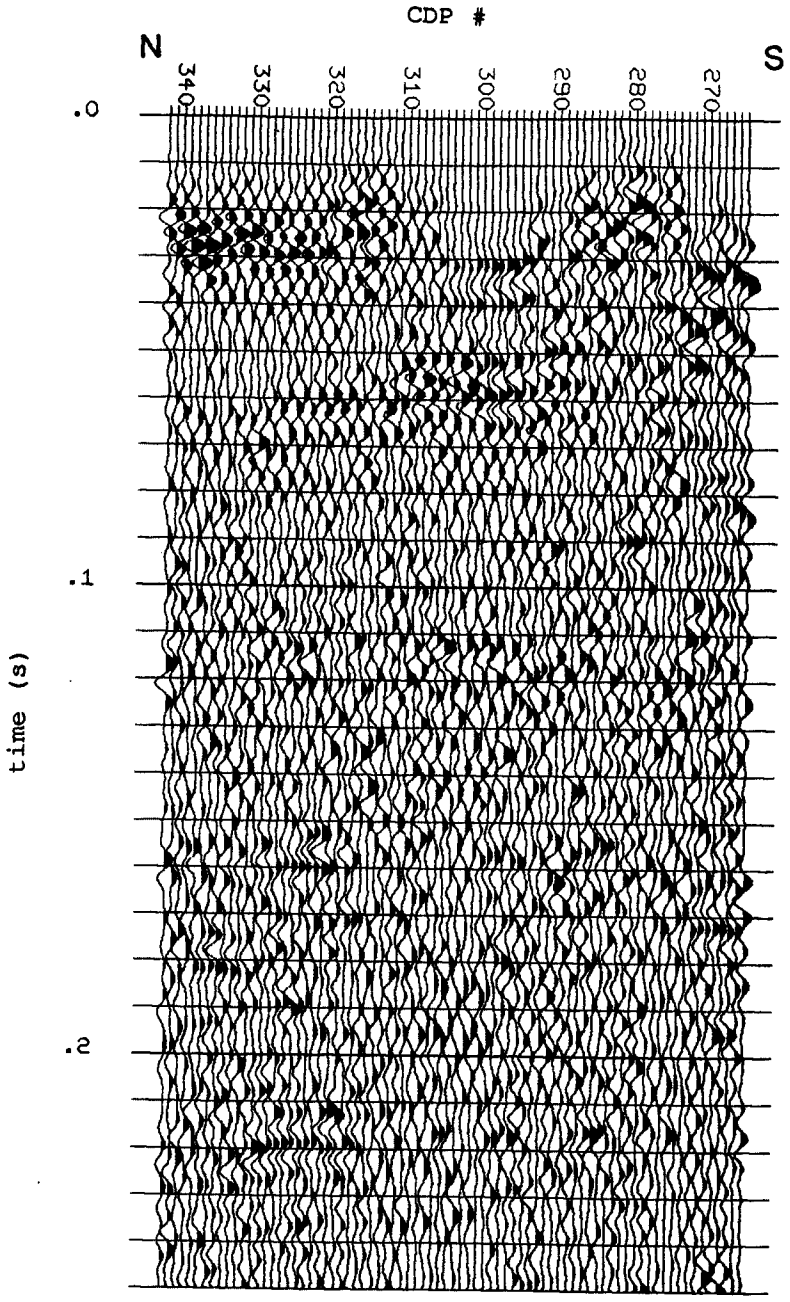

Figure 23. Deconvolved seismic section of CDP Line 1B from near Lyndon, Kansas. Note the near absence of reflection energy.

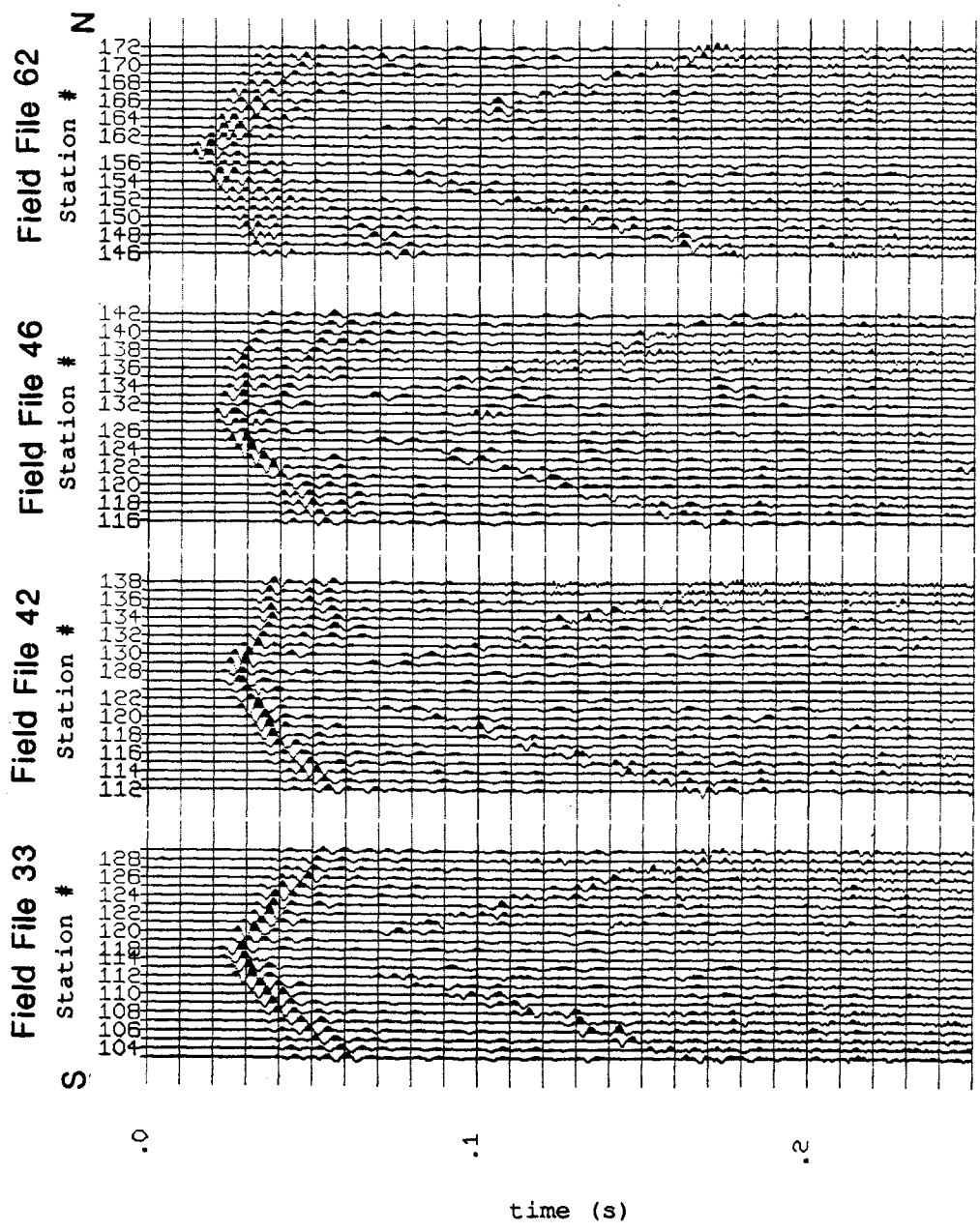

Figure 24. Field files from Line 1 near Lyndon, Kansas. Note the deflection of the first arrival (in time) between Stations 135 and 138 on Field File 42. Also note the near absence of reflection energy between Stations 130 and 138. Acquired with 220 Hz low-cut filters.

between Stations 135 and 138. Also note that reflection events are easily identified on the south side of this field file, while they are largely unidentifiable to the north. Field File 46 (Fig. 24) shows the effect of moving further to the north over the near-surface limestone unit. Static problems are severe on Field File 46 when compared with Field File 33. On Field File 62, the first arrival is anomalously early when compared to the other field files in Figure 24. Reflection events are barely visible at 105 ms and 158 ms on Field File 62, even though both the source and the receivers were in Pennsylvanian materials.

Line 2

The second CDP line (Line 2) acquired for this study is displayed on Figure 25b. The acquisition parameters for Line 2 are listed in Tables 2 and 3. Station locations occupied for Line 2 were identical to those used for Line 1, and therefore the CDP numbers also correspond. For Line 2, however, the data were processed as a unit, regardless of near-surface geology (Table 5).

The overall data quality on Line 2 (Fig. 25b) is superior to that of Line 1 (Fig's. 20 and 21) for several reasons. For Line 2, two geophones per group were used in order to increase the signal-to-noise ratio (Steeples and Miller, 1988). In addition, because the data for

Figure 25. **a.** Near-surface geologic cross-section near Lyndon, Kansas. **b.** Stacked seismic section of CDP Line 2 from near Lyndon, Kansas. Note the area of chaotic energy between CDPs 264 and 337 corresponding fairly well with the near-surface Ozawkie Limestone Member.

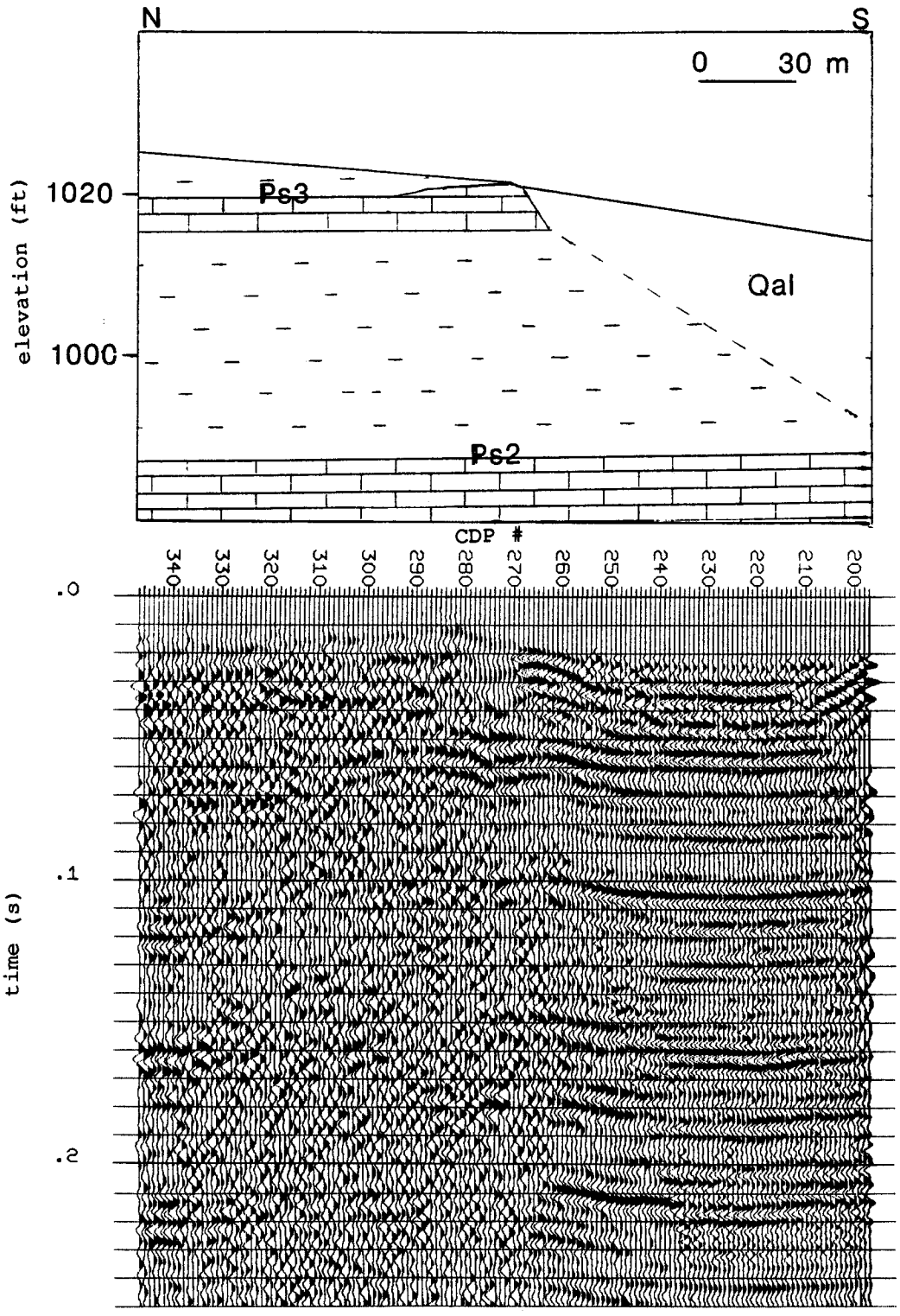
N
S
0 30 m
elevation (ft)
1020
1000
Ps3
Qal
Ps2
CDP #
340
330
320
310
300
290
280
270
260
250
240
230
220
210
200
.0
.1
.2
time (s)

Line 2 were not split in half, there is increased fold over the area where Line 1 was divided. A slightly different processing procedure was also used for Line 2 (Table 5). In particular, a temporally and spatially-varying digital frequency filter was applied to Line 2. Note the change in signal frequency from south to north on Figure 25b. An artifact of this procedure is a "suture zone" running from the beginning of CDP 273 to the end of CDP 235. This type of filter was necessary because the frequency content of the signal varies according to near-surface conditions.

The most apparent feature on the seismic section (Fig. 25b) is the decrease in data quality towards the north. Note, however, that the northernmost part of Line 2 also exhibits fairly good data quality. The area of poor data quality, between CDPs 264 and 337 (Fig. 25b) will be, herein, referred to as the chaotic zone. It is not possible to reliably correlate the reflections from either side of the chaotic zone from this section alone.

Line 3

In an attempt to glean signal from the chaotic zone on Line 2, several acquisition parameters were varied on subsequent CDP lines (Tables 2 and 3). For Line 3 (Fig. 26), 600 Hz low-cut filters and open high-cut filters were used in an attempt to increase the amplitude of high-frequency information relative to low-frequency

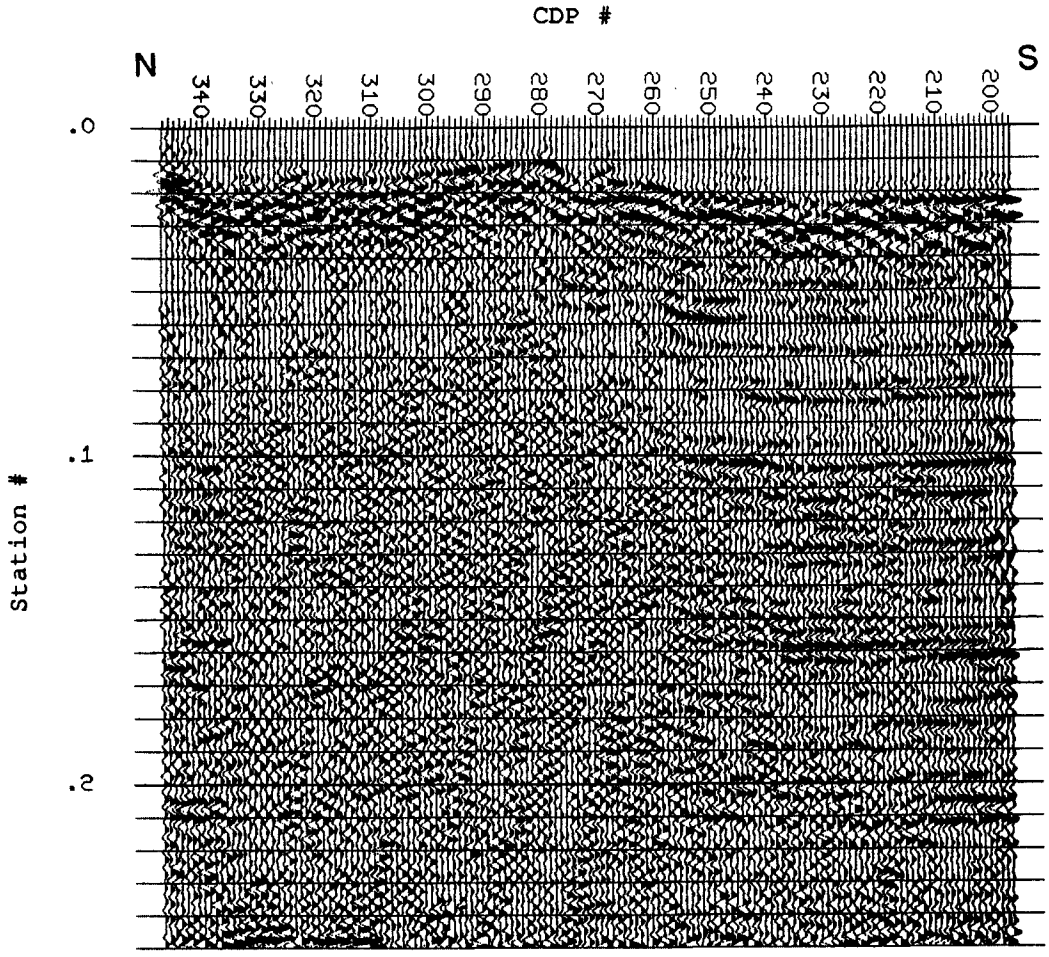

Figure 26. Stacked seismic section of CDP Line 3 from near Lyndon, Kansas. Note the inferior data quality relative to that of Line 2 (Fig. 25b). Acquired with 600 Hz low-cut filters.

information. It was hoped that this would permit the resolution of relatively shallow reflections (< 100 ms). This was also done to determine the likelihood of low-frequency noise obscuring high-frequency signal. The processing procedure used on Line 3 is listed on Table 5. To derive the maximum possible signal clarity from the CDP data, a digital filter with a 100% passband between 150 Hz and 375 Hz was used (Fig. 26). Since the analog filters have a slope of 24 dB per octave, the amplitude of the resulting data was down between 24 dB and 48 dB from that of the original data. Note that the data quality of Line 3 (Fig. 26) is clearly inferior to that of Line 2 (Fig. 25b). This indicates that the pre-emphasis filters were too high. Since the chaotic zone is still apparent, it must not be due to anomalously high-amplitude, low-frequency noise obscuring high frequency signal (in this frequency range).

Line 4

To test the other extreme, that of high-frequency noise obscuring low-frequency signal, Line 4 (Fig. 27) was acquired with 20 Hz low-cut filters and open high-cut filters (Tables 2 and 3). With these filters it was hoped that low-frequency information would not be overshadowed by high-frequency information. The processing procedure for Line 4 is listed in Table 5. The 100% digital passband used for Figure 27 was from 160

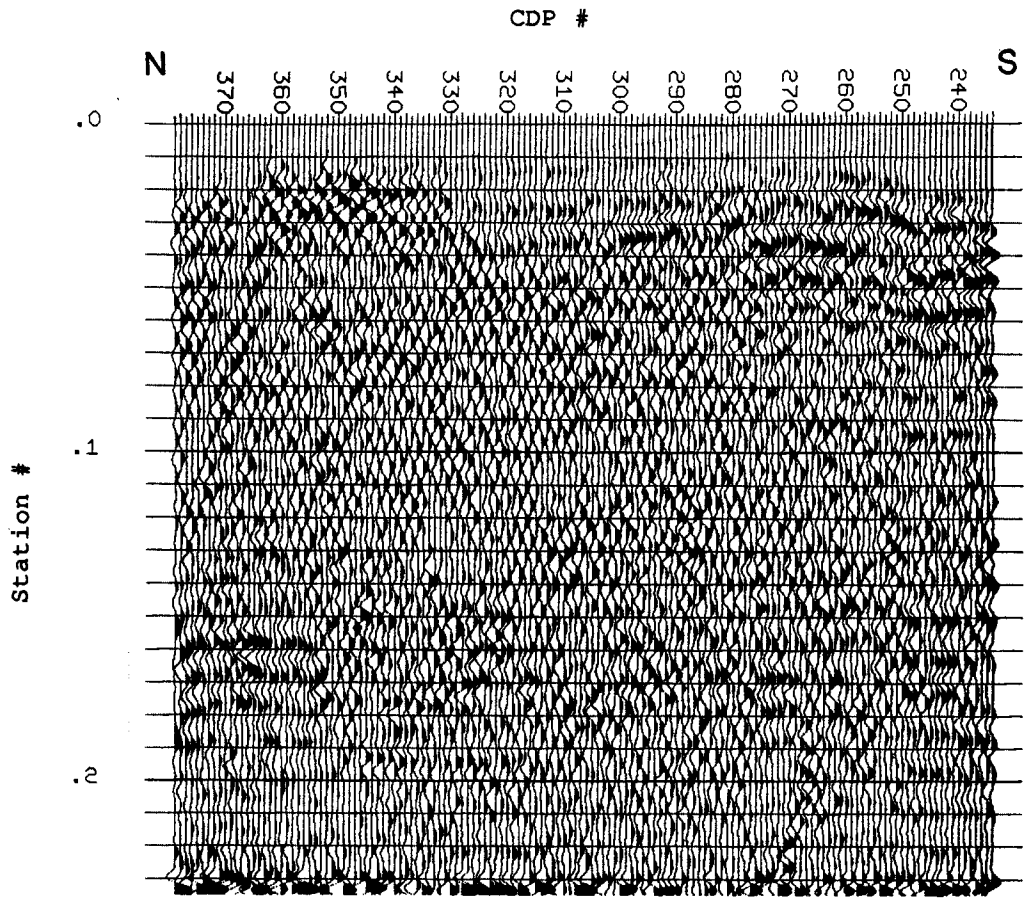

Figure 27. Stacked seismic section of CDP Line 4 from near Lyndon, Kansas. Note that the data quality is inferior to that of Line 2 (Fig. 25b). Acquired with 20 Hz low-cut filters.

Hz to 230 Hz. Line 4 displays subsurface information between CDPs 234 and 379, and thus can only be compared with Lines 1,2, and 3 where they overlap, between CDPs 234 and 347. The data quality on Line 4 is at least as poor as that of Line 3, indicating that the chaotic zone is probably not due to signal being obscured by noise.

To determine if reflection information does indeed exist beneath the noise on Figure 27, an attempt was made to isolate it through use of the tau - p transform (described in the section entitled "General Processing Procedure"). Figure 28 exhibits strong apparent reflection information. It is indeed tempting to refer to all the coherent events as reflections. If they all were reflections, my task would be virtually complete. The problem is that most of the coherent events on Figure 28 do not represent reflection information. This can be shown by returning to Line 2 (Fig. 25). The geology of the area is relatively simple and is represented, at depth, by relatively flat reflections on both sides of the chaotic zone on Figure 25b. Therefore, eliminating the possibility of gross structural disturbance in the area, hidden reflectors should be relatively flat and parallel.

An additional argument opposing the legitimacy of the reflections on Figure 28 is shown in Appendix E. Here, I use an identical velocity filter (tau - p

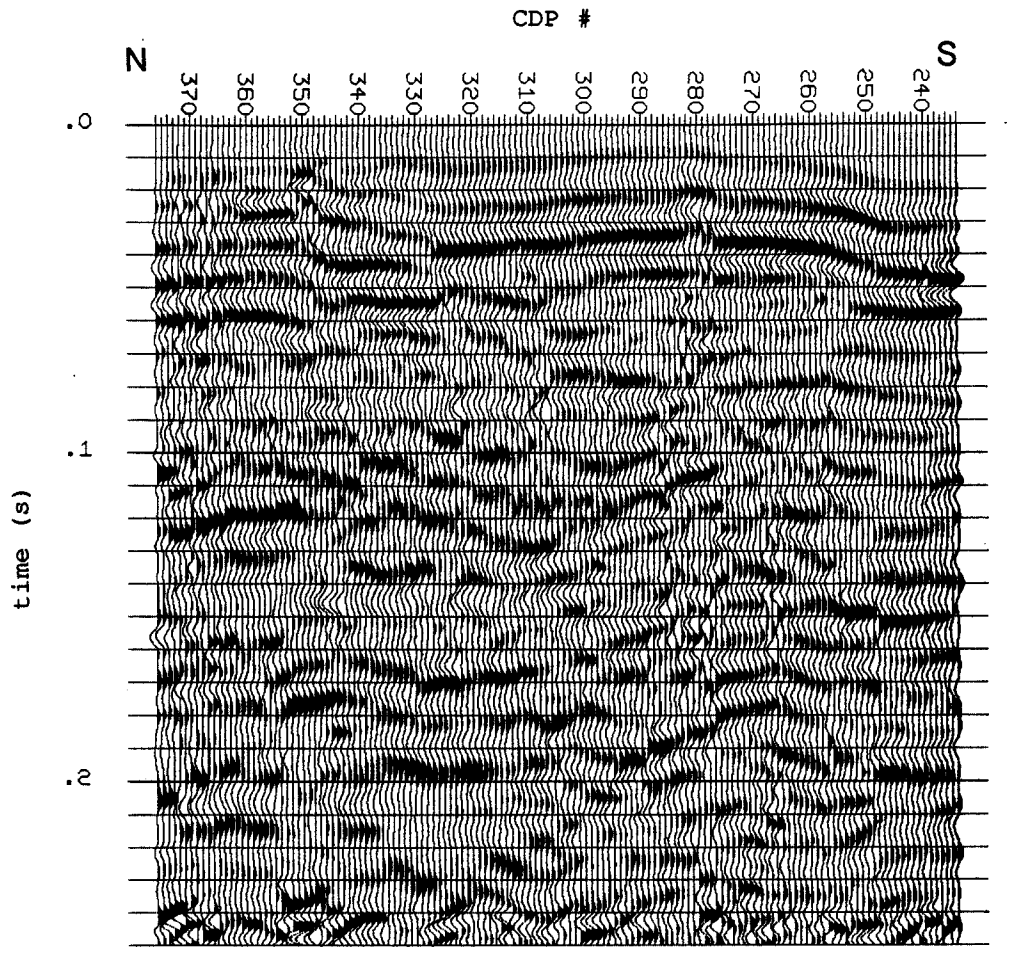

Figure 28. Velocity filtered seismic section of CDP Line 4 from near Lyndon, Kansas. Note the alarming increase in apparent data quality.

transform) on random data with the same geometry as that of Line 4. Coherent events are evident on Figure 62. Thus, there is a certain amount of coherency, at some arbitrary velocity, inherent in random data. This can also be seen on the signal-to-noise plots of random data in Appendix D (Fig. 55). The data sets (Fig's. 28 and 62) look too similar to suggest anything but near-randomness of the information in the chaotic zone.

Line 6

Thus far, Line 2 (Fig. 25b) is clearly the best CDP line in the study area, in terms of signal-to-noise content. This line combined with Line 5 (not included separately) comprises Line 6 (Fig. 29). Line 5 includes the same stations as Line 4, but with nearly the same acquisition parameters as Line 2 (Tables 2 and 3). Line 6 displays subsurface information between Stations 99 and 189 (CDPs 197-379). Obvious on Figure 29, is the return of reflection signal north of the chaotic zone (below 100 ms). However, even with reflection information on both sides of the chaotic zone, correlation is still unreliable. The signal-to-noise ratio for Figure 29 is plotted and contoured on Figures 30 and 31, respectively.

Residual static corrections applied prior to stacking finally permit correlation across the chaotic zone (Fig. 32b). Note the continuity of the relatively flat reflector at 104 ms (at CDP 198). Also note the

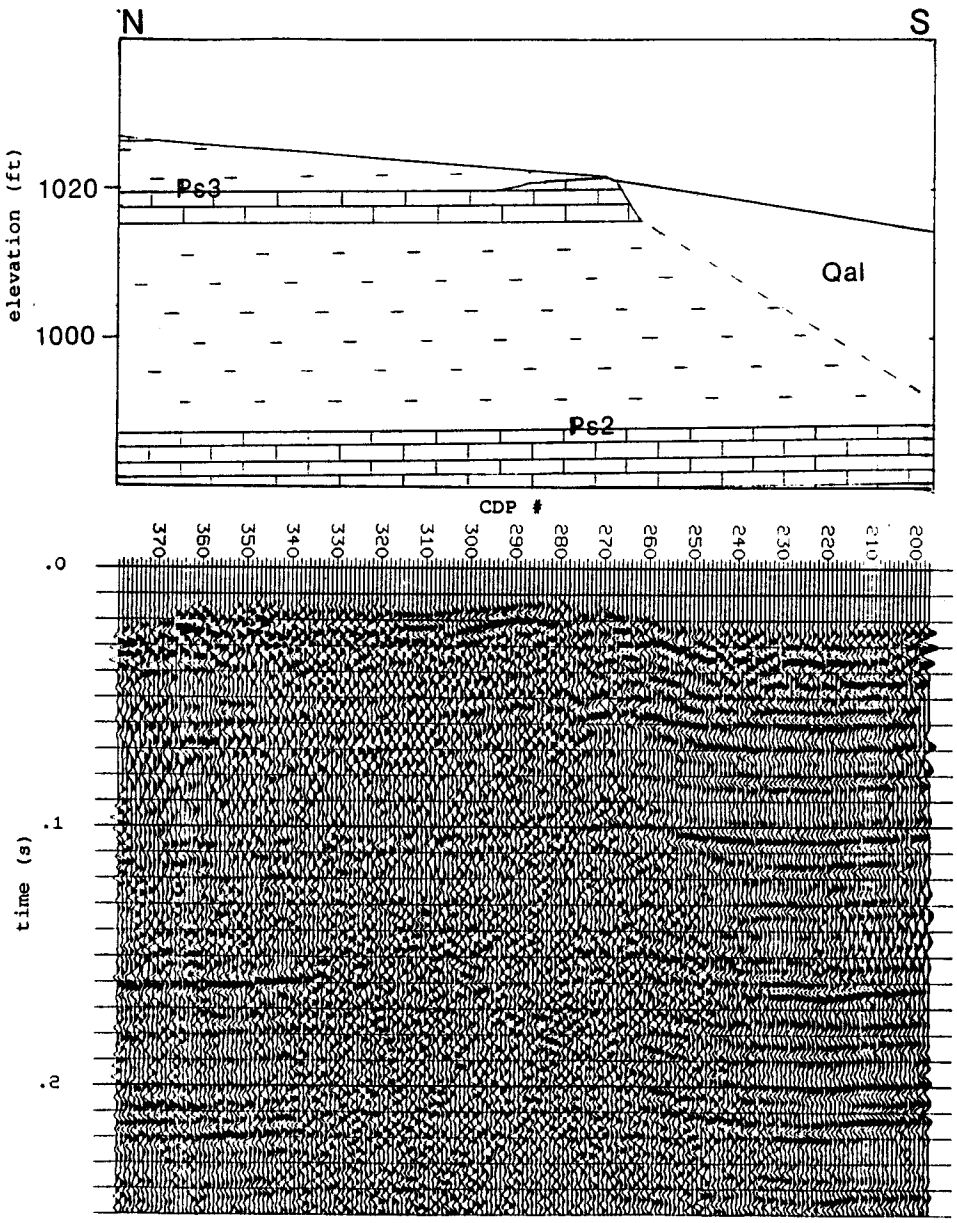

Figure 29. Intermediate stacked seismic section of CDP Line 6 from near Lyndon, Kansas. This is composed of CDP Lines 2 and 5. Note that correlation across the chaotic zone is still difficult and unreliable. Acquired with 220 Hz low-cut filters.

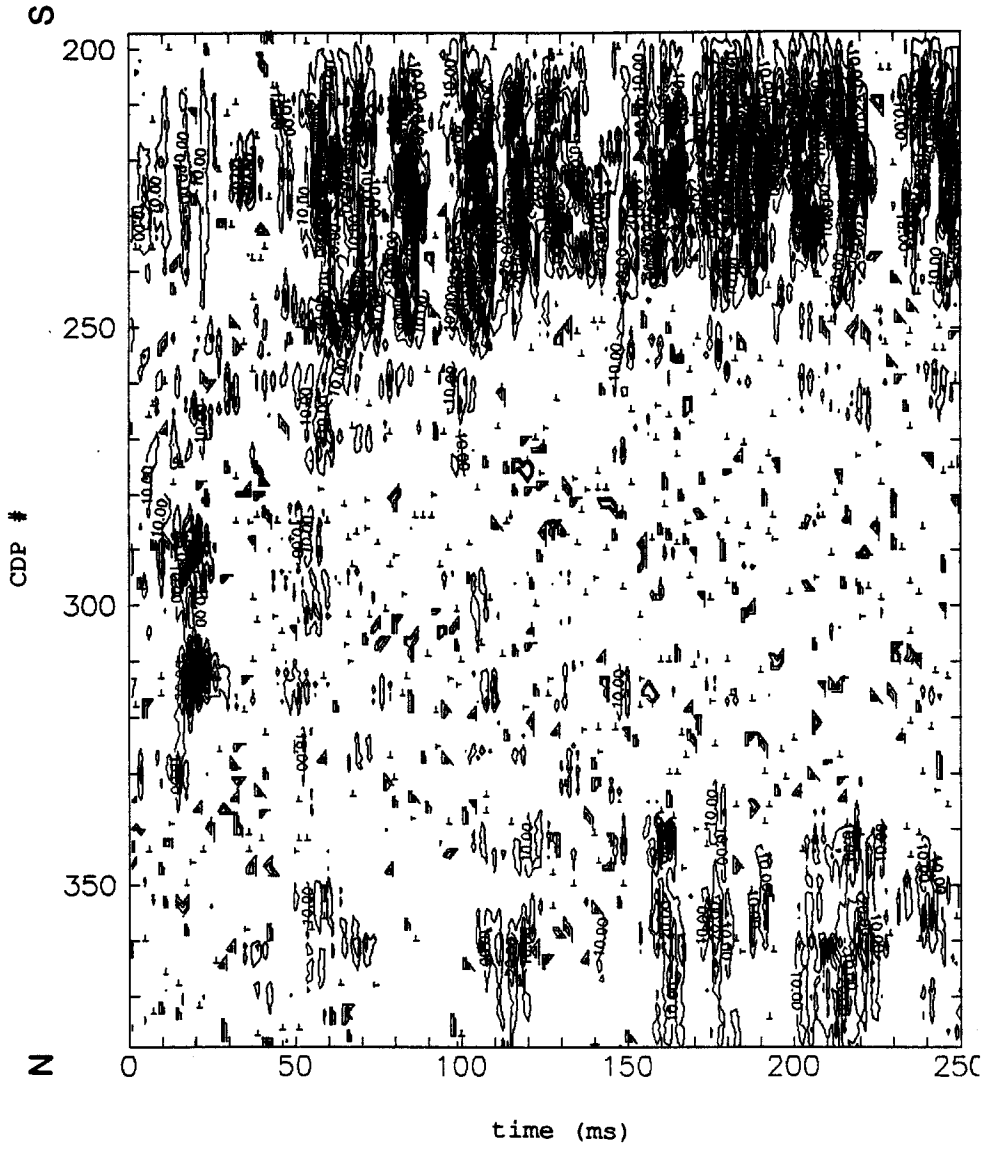

Figure 30. Signal-to-noise contour map of data in Figure 29. Note the near absence of signal in the chaotic zone.

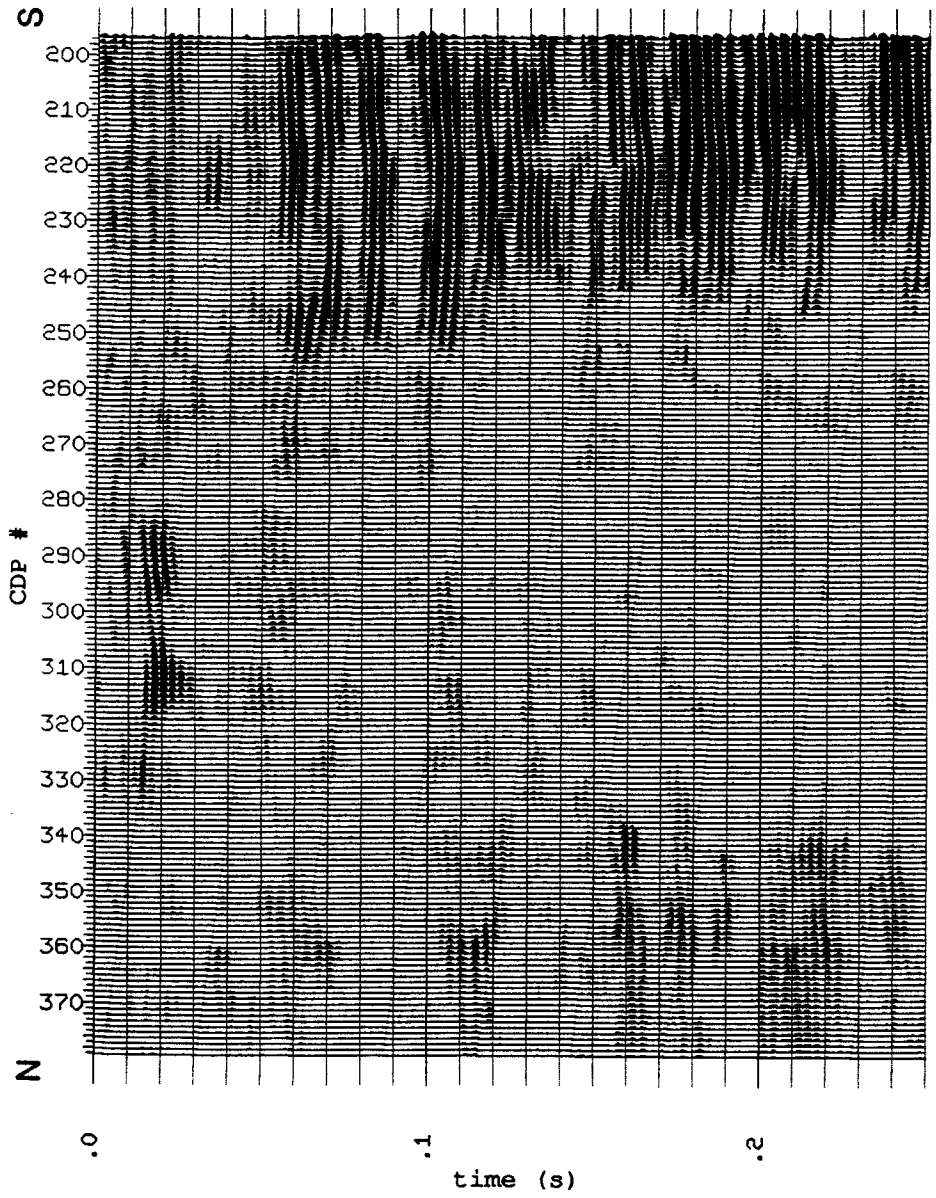

Figure 31. Signal-to-noise plot of data in Figure 29. Note the near absence of signal in the chaotic zone.

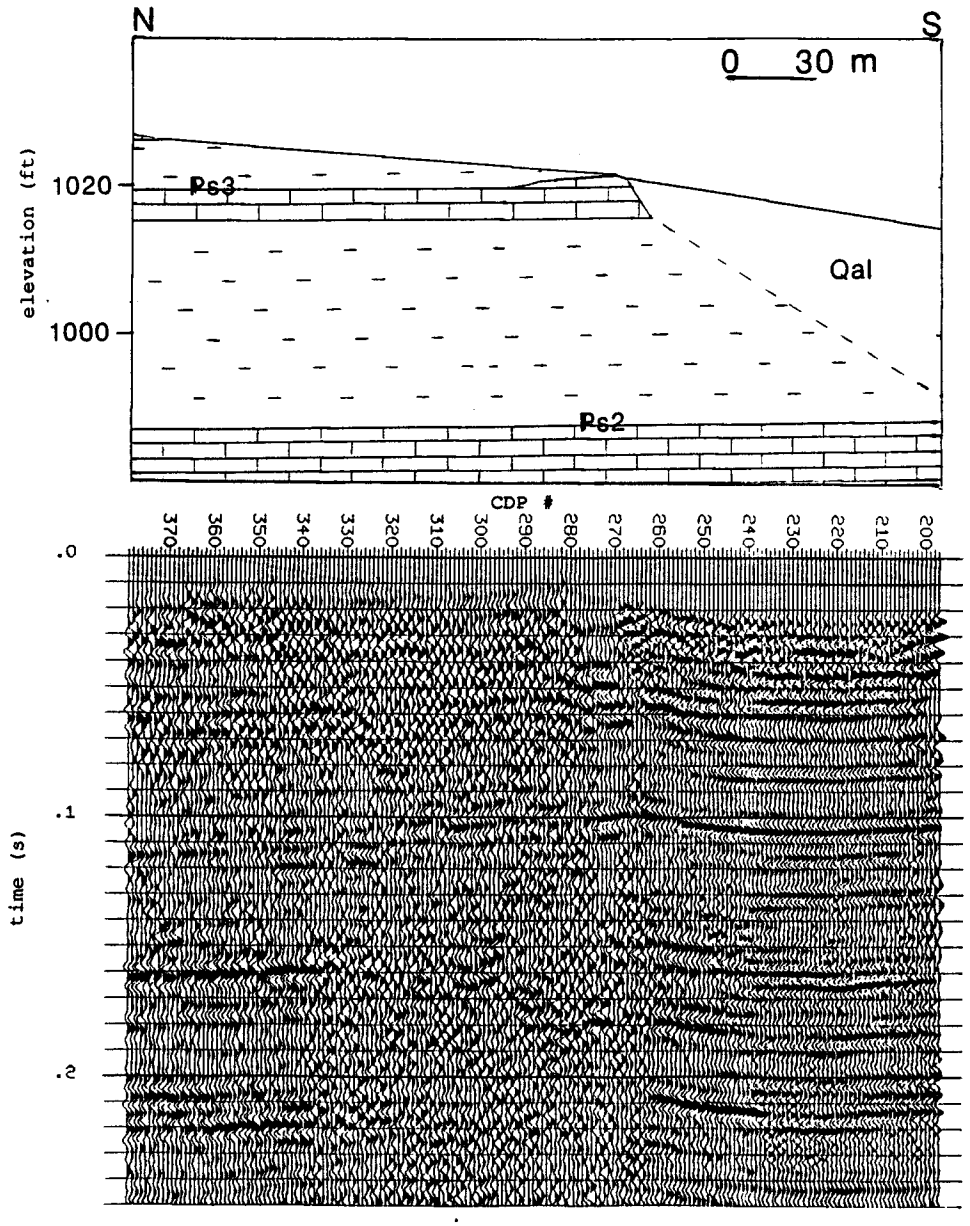

Figure 32. **a.** Near-surface geologic cross-section of site near Lyndon, Kansas. Note the occurrence of near-surface limestone beneath alluvium. **b.** Final stacked seismic section of CDP Line 6 from near Lyndon, Kansas. Note the continuity of the reflector across the chaotic zone (100 ms at CDP 272). Acquired with 220 Hz low-cut filters.

improvement in the reflection event at 54 ms between CDPs 349 and 377 (compare with Fig. 29). The complete processing procedure utilized for Line 6 is listed in Table 5. The temporally and spatially-varying digital frequency filter of Line 2 was applied to the data of Line 6 to produce this final stacked section (Fig. 32b). The improvement of Figure 32b over Figure 29 is shown graphically in Figures 33 and 30, respectively (also see Fig's. 34 and 31).

Data Sorted by Near-surface Geology

In an attempt to determine if the observed signal loss is related to acquisition geometry, the data of Line 2 were sorted by near-surface geology. Traces recorded with both sources and receivers in Pennsylvanian materials comprise Line 2PP (Fig. 35). Traces recorded with sources in Quaternary alluvium and receivers in Pennsylvanian materials are included in Line 2QP (Fig. 38). Traces recorded with sources in Pennsylvanian materials and receivers in Quaternary alluvium are included in Line 2PQ (Fig. 41). Lastly, traces with both sources and receivers in Quaternary alluvium comprise Line 2QQ (Fig. 44). These CDP lines were processed using the same procedure used on Line 2 (Table 5).

As stated above, Line 2PP is composed of traces recorded with both sources and receivers in Pennsylvanian materials. Included on Line 2PP are CDPs 277 through 347

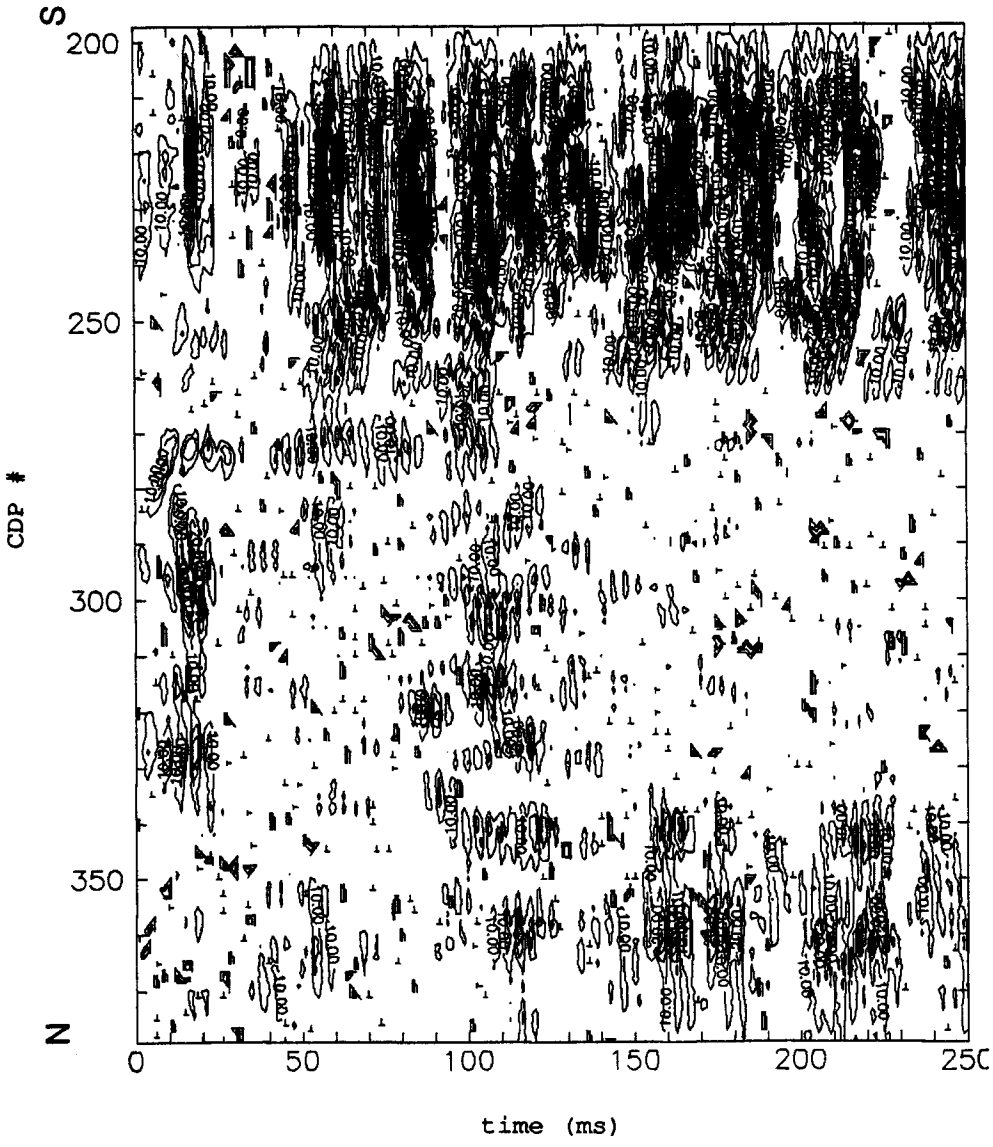

Figure 33. Signal-to-noise contour map of the data in Figure 32b. Note the increased signal in the chaotic zone relative to Figure 30.

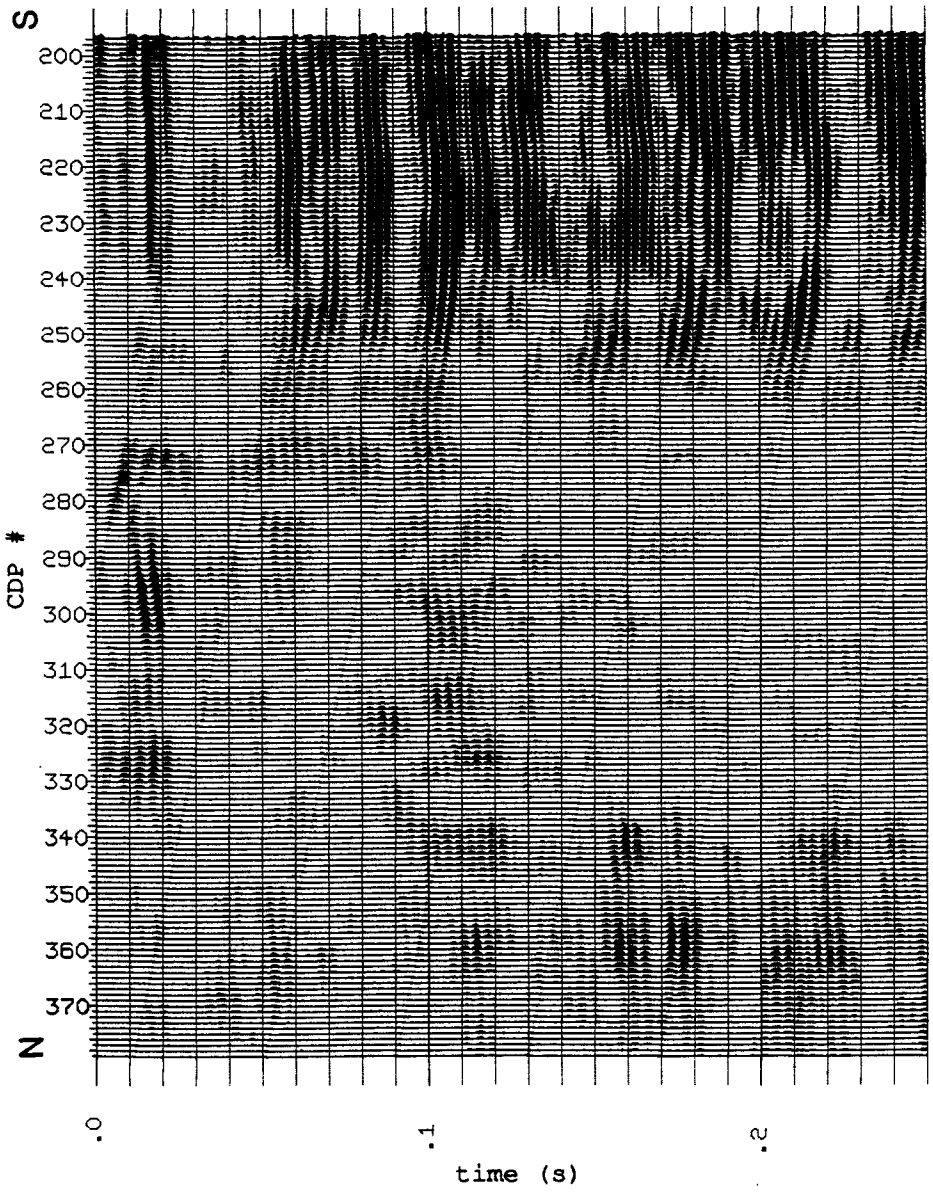

Figure 34. Signal-to-noise plot of the data in Figure 32b. Note the increased signal in the chaotic zone relative to Figure 31.

(Fig. 35). The data quality of this line is the poorest of any CDP line in the study. The signal-to-noise content of the data of Figure 35 exhibits virtually zero coherent signal (Fig's. 36 and 37). A slightly different sampling frequency (in time) accounts for the moderately increased signal-to-noise content displayed in Figure 37 over that in Figure 36 (App. D). Note that the CDPs which correspond to the outcrop area of the lowermost limestone unit of the Ozawkie Limestone Member (CDPs 268-284) are indistinguishable from those north of the outcrop.

With sources in Quaternary alluvium and receivers in Pennsylvanian materials (Line 2QP), the data quality is improved over that of Line 2PP (compare Fig's. 35 and 38). Reflection events are faint but visible from 59 ms (CDP 253) through 220 ms (Fig. 38). The signal-to-noise content of the data of Figure 38 is shown in Figures 39 and 40. Figure 40, especially, shows diminishing signal towards the north.

Line 2PQ, with sources in Pennsylvanian materials and receivers in Quaternary alluvium, exhibits poor data quality (Fig. 41). The signal-to-noise plots for this line (Fig's. 42 and 43) are inaccurate. This can be shown by comparison of the signal-to-noise plots with the seismic section (Fig. 41) and with the coherent events on Figure 40. Many of the coherent events shown in Figures

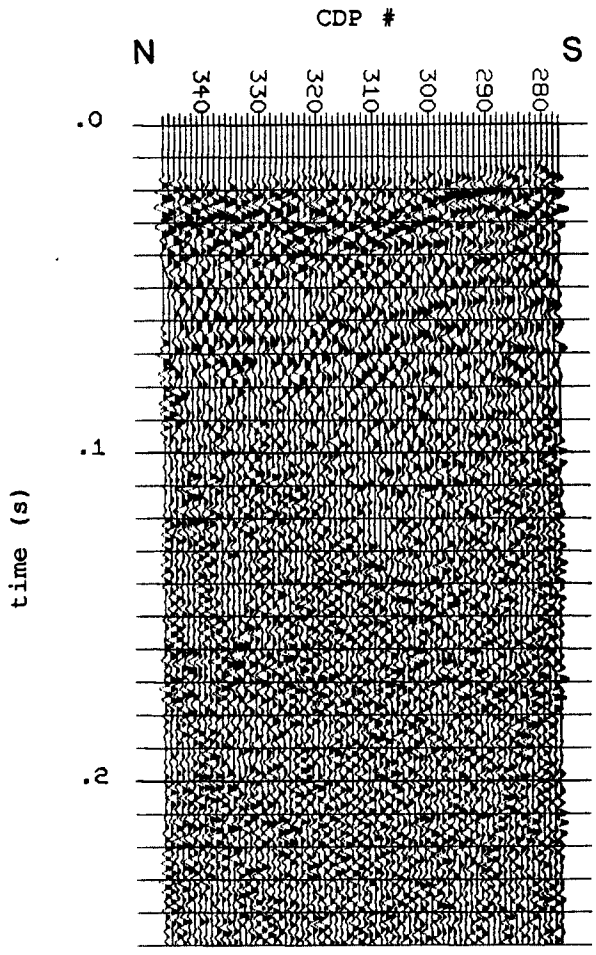

Figure 35. Stacked seismic section of CDP Line 2PP. This includes traces from Line 2 acquired with both the source and the receiver in Pennsylvanian material. The data quality of this line is the poorest of any CDP line in the study.

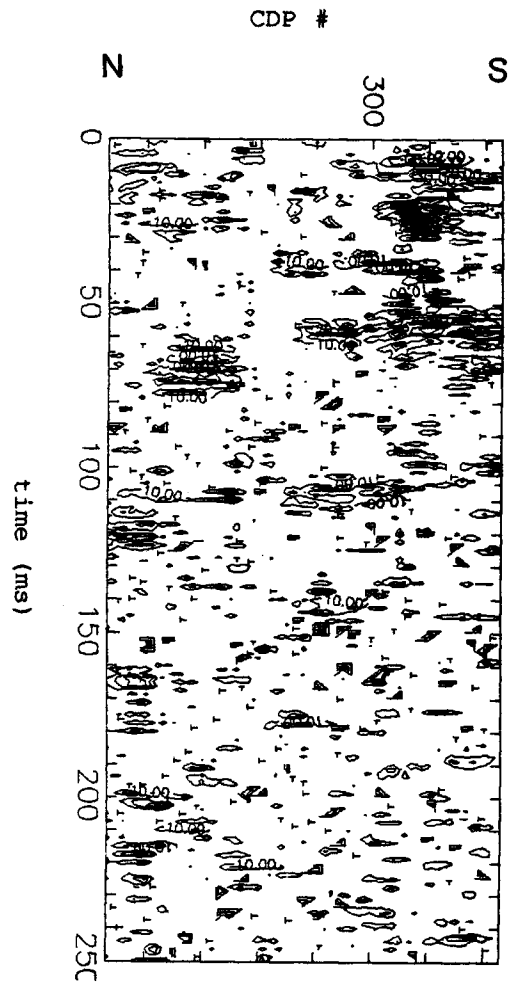

Figure 36. Signal-to-noise contour map of the data in Figure 35. Note the absence of signal.

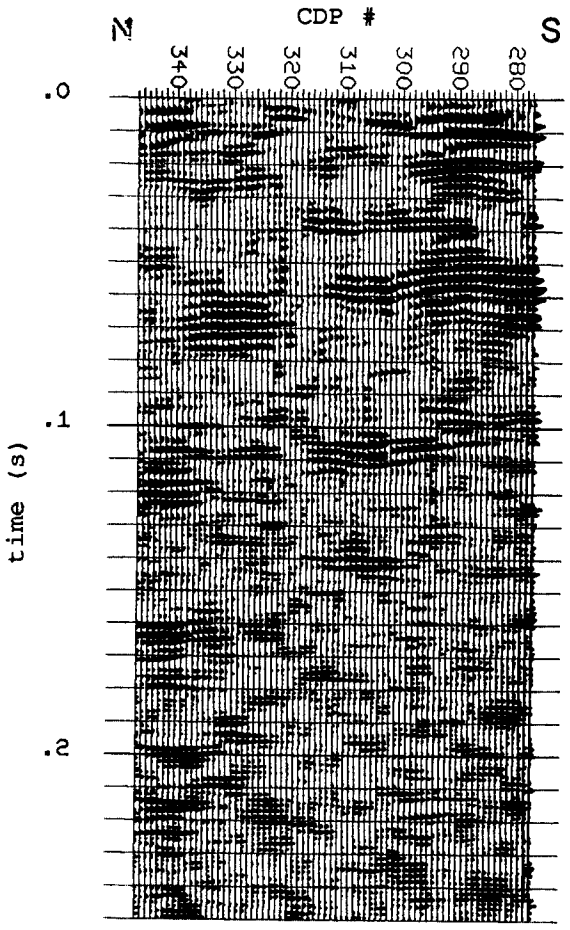

Figure 37. Signal-to-noise plot of the data in Figure 35. Note the near absence of signal.

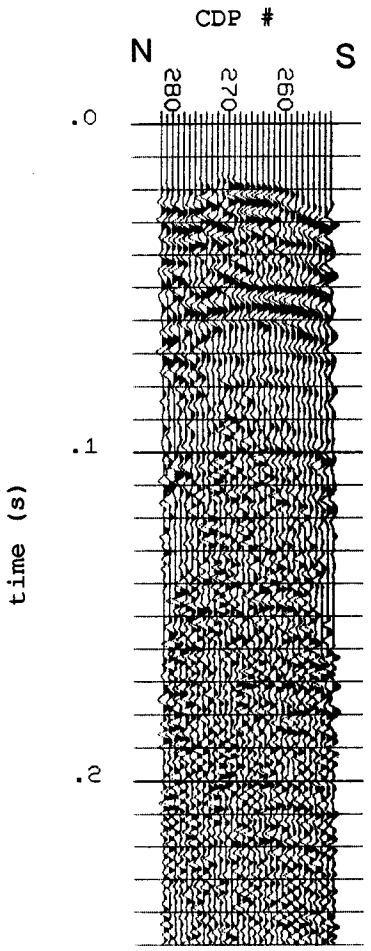

Figure 38. Stacked seismic section of CDP Line 2QP. This includes traces from Line 2 acquired with the source in Quaternary alluvium and the receiver in Pennsylvanian material. Note the faint reflection events between 59 ms and 220 ms.

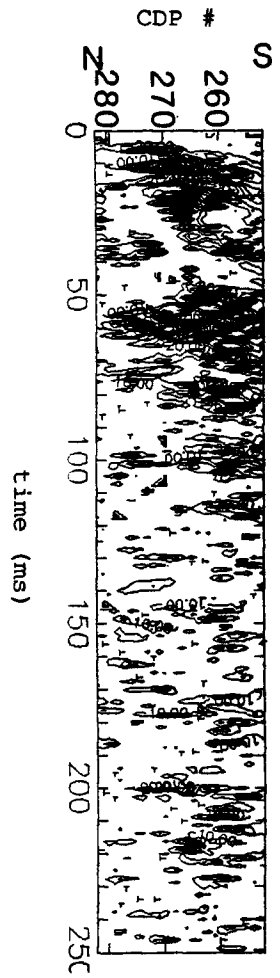

Figure 39. Signal-to-noise contour map of the data in Figure 38. Note the increased signal relative to that of Figure 36.

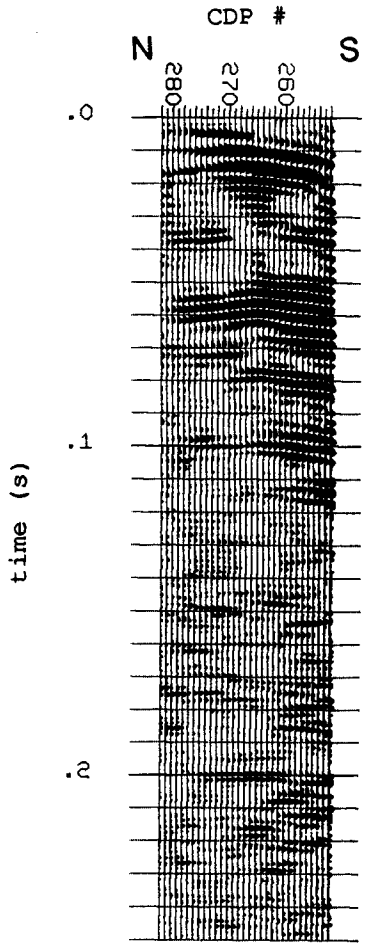

Figure 40. Signal-to-noise plot of the data in Figure 38. Note the increased signal relative to that of Figure 37.

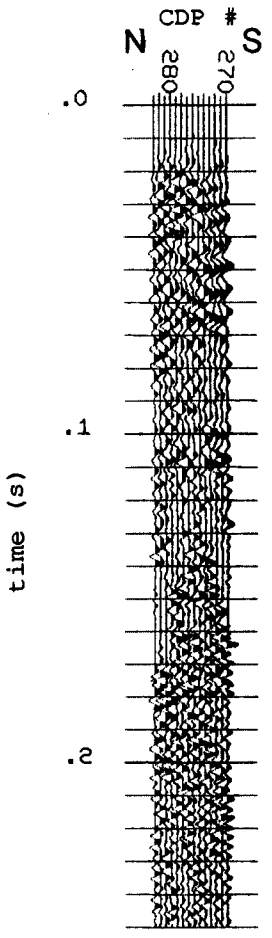

Figure 41. Stacked seismic section of CDP Line 2PQ. This includes traces from Line 2 acquired with the source in Pennsylvanian material and the receiver in Quaternary alluvium. Note the poor data quality relative to that of Figure 38.

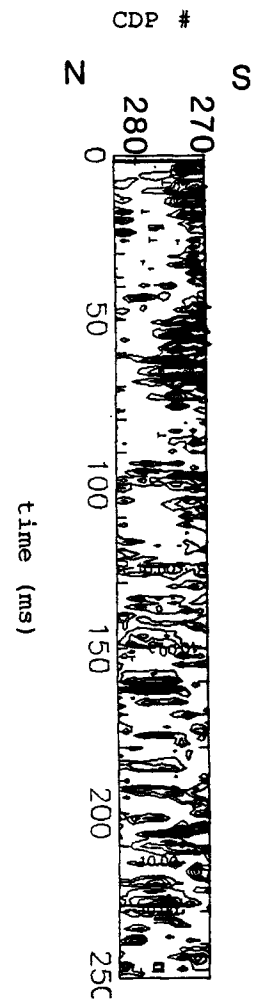

Figure 42. Signal-to-noise contour map of the data in Figure 41. Note the high apparent (but fictitious) signal exhibited on this figure (see text for explanation).

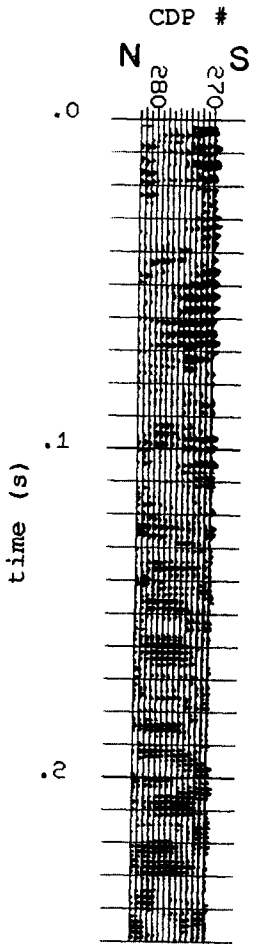

Figure 43. Signal-to-noise plot of the data in Figure 41. Note the high apparent (but fictitious) signal exhibited on this figure (see text for explanation).

42 and 43 have no basis in reality. The reason for the failure of the signal-to-noise program, in this instance, is that the number of CDPs being summed (m+1) is too high relative to the number of CDPs on the line. This smearing effect can also be seen on Figure 60, again resulting from too high a value of m+1. The number of CDPs summed (m+1) was kept constant (7) in this experiment to facilitate comparison. This example indicates that one should be suspicious of any process resulting in anomalously high signal-to-noise content that is not evident on the original seismic section.

For Line 2QQ, both sources and receivers were in alluvium (Fig. 44). This seismic section exhibits a relatively high signal-to-noise ratio (Fig's. 45 and 46). The lowermost limestone unit of the Ozawkie Limestone Member crops out north of Line 2QQ (Fig. 44). The signal quality is, however, diminished towards the outcrop, especially at depth.

Upon elimination of field files nearest the outcrop of the lowermost limestone unit of the Ozawkie Limestone Member, the data quality of Line 2QQ is substantially improved in the area of affected CDPs (Fig. 47). This can be seen even more emphatically on Figures 48 and 49. The utility of the signal-to-noise program can best be seen upon comparison of Figures 46 and 49. Incoherent data yields a signal-to-noise ratio of zero, thus areas

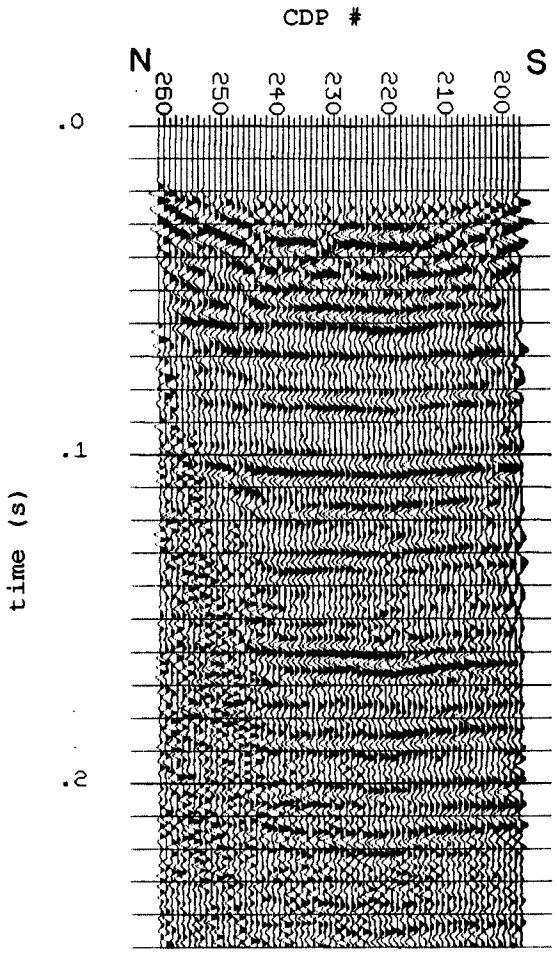

Figure 44. Stacked seismic section of CDP Line 2QQ. This includes traces from Line 2 acquired with both the source and the receiver in Quaternary alluvium. Note the wedge-shaped area of poor data quality.

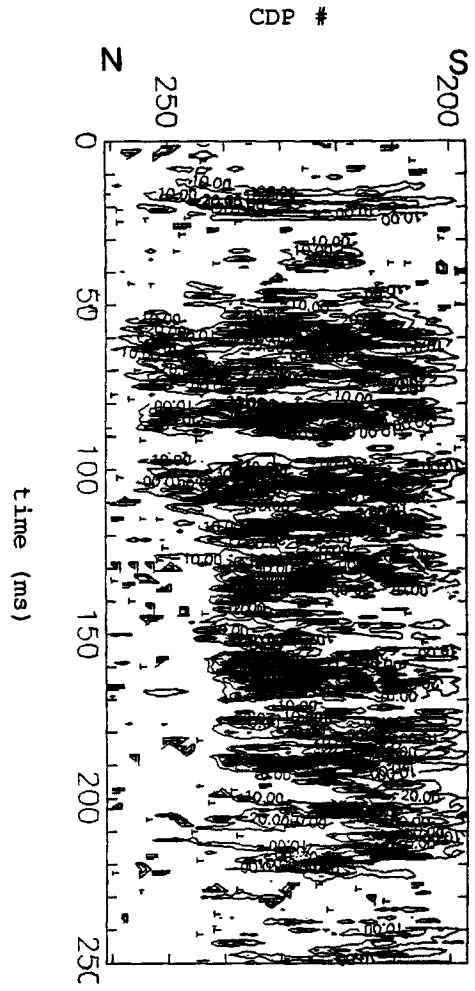

Figure 45. Signal-to-noise contour map of the data in Figure 44. Note the wedge-shaped area of poor data quality.

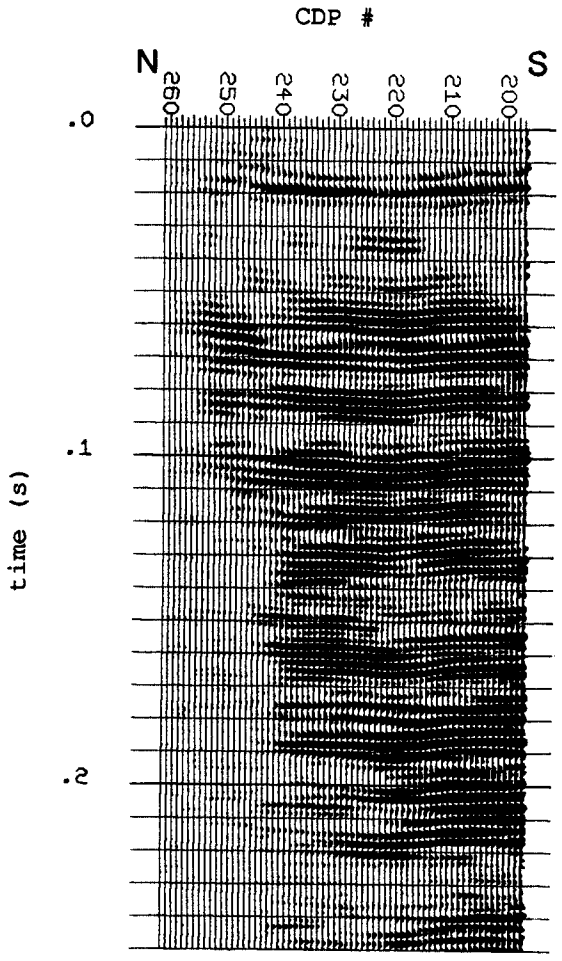

Figure 46. Signal-to-noise plot of the data in Figure 44. Note the wedge-shaped area of poor data quality.

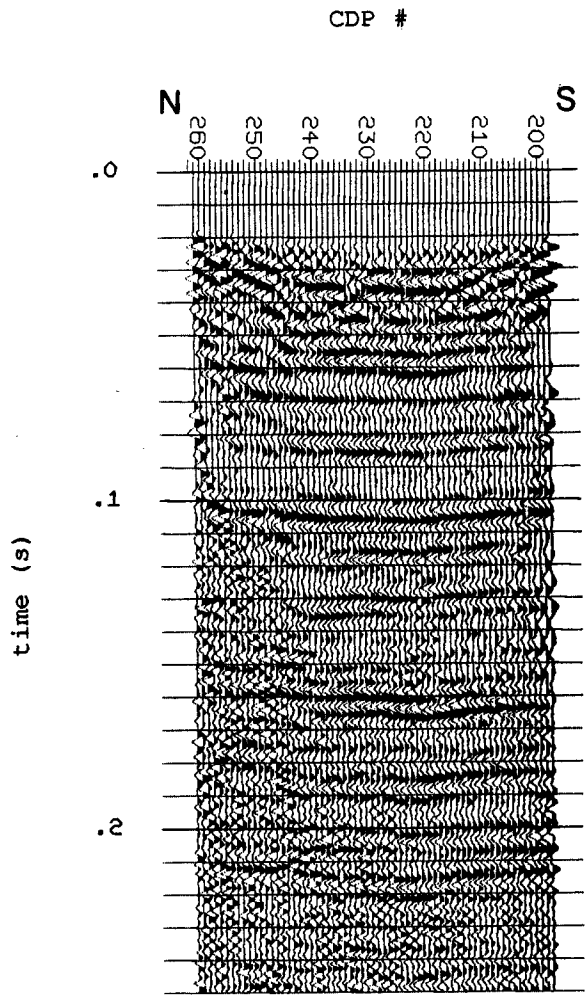

Figure 47. Stacked seismic section of CDP Line 2QQ. This figure is identical to Figure 44 except for the exclusion of data from field files nearest the outcrop of the Ozawkie Limestone Member. Compare the data quality with that of Figure 44.

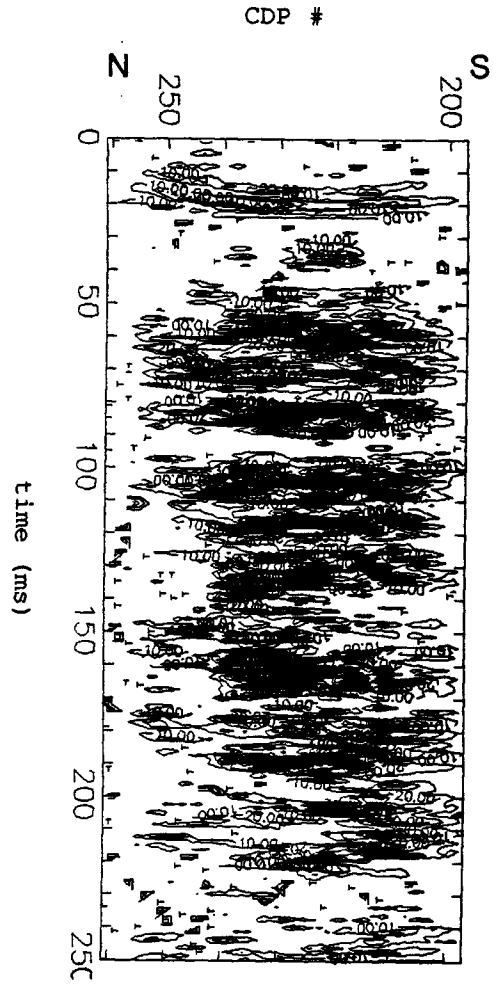

Figure 48. Signal-to-noise contour map of the data in Figure 47. Note the increase in signal between CDPs 248 and 261, relative to that of Figure 45.

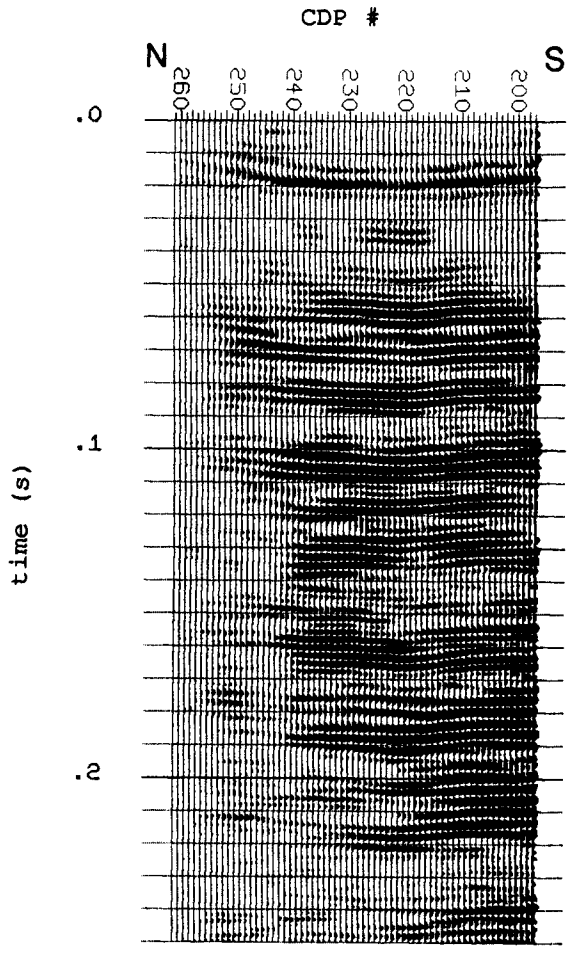

Figure 49. Signal-to-noise plot of the data in Figure 47. Note the increase in signal between CDPs 248 and 261, relative to that of Figure 46.

of no coherency on Figure 44 are essentially blank on Figures 45 and 46. Upon removal of Field Files 40 through 42 (those nearest the outcrop), many of the blank areas of Figure 46 exhibit coherency on Figure 49. This indicates that the traces from Field Files 40 through 42 were poor in data quality. The poor data quality of the removed traces can be seen on CDP 262 (Fig. 50). The last three traces on the right are from Field Files 40 through 42 respectively. Any correlation with other traces (in time) is strictly by chance. Thus, data quality can actually be improved by excluding data, even when this data was acquired with both the sources and the receivers in alluvium. An identical procedure of removing field files approaching the chaotic zone from the north would be impractical due to the gradual nature of the near-surface changes.

Discussion

Limestone Beneath Alluvium

The chaotic zone occurs between CDPs 264 and 337 on Line 6 (Fig. 32b). The effective outcrop area of the lowermost limestone unit of the Ozawkie Limestone Member occurs between Stations 134 and 142, which corresponds to CDPs 268 and 284, respectively. Therefore, the chaotic zone extends beyond the effective outcrop area in both directions. This is additional evidence for limestone subcropping beneath the alluvium, just south of the

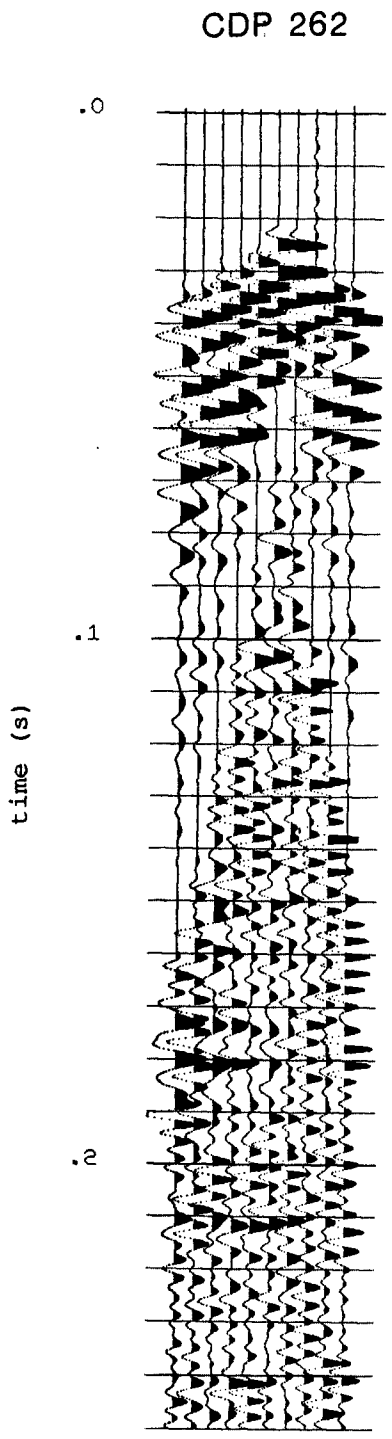

Figure 50. CDP 262 of Line 2 from near Lyndon, Kansas. Note the poor data quality of the last three traces on the right.

outcrop of the lowermost limestone unit of the Ozawkie Limestone Member (Fig. 32a). Confirmation drilling at Station 132 (CDP 264) yielded limestone at a depth of 3.4 ft. Thus, in this instance, subsurface geology can be predicted on the basis of data quality alone.

Returning to Line 2QQ (Fig. 44), note the wedge-shaped form of the area of poor data quality. A possible explanation for this phenomenon may be seen on Figure 32a. Though all shots and receivers were in alluvium for Line 2QQ, as mentioned above, there is evidence on the seismic data that limestone occurs in the subsurface. It is also likely that the limestone unit is buried more deeply towards the south. Thus, CDPs further to the south would be affected by the disrupted energy progressively later in the record. This is exactly what we observe on Line 2QQ (Fig. 44). The increase in data quality upon the removal of field files closest to the outcrop supports the above argument. This is because fewer traces affected by the subcropping limestone are stacked together in Figure 47. The above observations strongly suggest that near-surface limestone disrupts the transmission of seismic energy.

Frequency Content of Signal

There is significant evidence that the chaotic zone is related to the frequency content of the impinging seismic energy. The necessity of temporally and

spatially-varying digital frequency filtering indicates differential signal frequency content across Line 6 (Fig. 32b). The success of conventional seismic methods over near-surface limestone units is due to the low-frequency content of the impinging energy.

From the definition of Widess (1973), a bed may be resolved if it is at least one-eighth wavelength in thickness. Thus in the Lyndon study area, the lowermost limestone unit of the Ozawkie Limestone Member (5 ft, 2,000 m/s) is unresolvable with frequencies smaller than 164 Hz. Conventional methods ordinarily utilize frequencies on the order of 20 Hz to 80 Hz. Thus, the Ozawkie Limestone Member would be effectively invisible in a conventional seismic reflection survey. It must also be emphasized that frequencies somewhat lower than 164 Hz would "sense" the Ozawkie Limestone Member, even though they would be unable to fully resolve it. As this thesis shows, shallow methods have also failed to resolve the Ozawkie Limestone Member at the site near Lyndon, Kansas. Though we have recorded the necessary frequencies, reverberation noise and transmission losses prohibit the resolution of near-surface strata.

Transmission Losses in Relation to Sources and Receivers

Not only are transmission losses related to signal frequency, but they seem to be related more to the source than to the receiver. Evidence implicating the source

includes the superior data quality of Line 2QP (Fig. 38) over that of Line 2PQ (Fig. 41). In addition, Line 1A (Fig. 20) is vastly superior to Line 1B (Fig. 21). Thus CDP lines with sources in Quaternary alluvium are superior to CDP lines with sources in Pennsylvanian materials. The occurrence of poor data quality associated with sources over thin Quaternary alluvium may also be attributed to subcropping limestone.

The failure of Line 4 (Fig. 27) to successfully image the chaotic zone is an additional bit of evidence implicating the source. Regardless of the pre-emphasis filters on a seismograph, a source will create a certain spectrum of energy. In this case, unwanted high-frequency noise was received by the geophones. With open high-cut filters, this high-frequency noise could easily overshadow any recorded low-frequency signal. For Line 4 (Fig. 27), it was hoped that relatively low-frequency geophones (40 Hz) would have abated this problem, because the frequency characteristics of such receivers favor lower frequencies. Lower high-cut pre-emphasis analog filters, along with low-frequency geophones, may have been able to attenuate the high-frequency noise. Thus, it is possible, in this geologic situation, to have a source with a signature that is too high in frequency content.

Effect of Overburden Thickness

Though there is strong evidence linking poor data quality to near-surface limestone, the northernmost part of Line 6 (Fig. 32b) exhibits the return of reflection signal. This is in spite of the subcropping Ozawkie Limestone Member (Fig. 32a). The only obvious difference between the area of the chaotic zone and the area to the north exhibiting the return of reflection energy, is the depth to the limestone unit. The reoccurrence of reflection energy in the northernmost part of Line 6 (beyond CDP 337) must therefore be indicative of sufficient overburden for the transmission of seismic energy. Drilling at Station 169 (CDP 338) yielded limestone at a depth of 4.9 ft. Possible mechanisms for the occurrence of the chaotic zone are given below.

A Possible Transmission Loss Mechanism

A possible mechanism for transmission losses involves wide-angle reflection. Wide-angle reflection occurs when the angle of incidence is greater than the critical angle, where the critical angle (i) is given by: $i = \arcsin(v1/v2)$, v1 is the seismic velocity of the upper layer, and v2 is the seismic velocity of the lower layer (Fig. 63). Energy approaching an interface at an angle greater than the critical angle (from the vertical) will be totally reflected.

At the site near Lyndon, Kansas, the very near-

surface geology of the area producing the chaotic zone includes road-fill, soil, and shale overlying limestone. Here, road-fill, soil, and shale will be referred to as overburden. As the thickness of the overburden decreases, there is a decreasing amount of transmitted energy available to any given receiver (Fig. 63; Table 6). The amount of energy actually transmitted from the source does not change, but the amount received by a given geophone decreases according to the Zoeppritz equations (App. F). In contrast, the percentage of wide-angle reflection energy impinging on a given receiver increases. Thus, it is possible that transmission losses result entirely from an abundance of wide-angle reflection energy.

At a given offset, a significant amount of wide-angle reflection energy would be received at points near a shallow interface of high acoustic impedance contrast. With increasing depth of the interface, a smaller percentage of the received energy would be from wide-angle reflections (Fig. 63). From seismic and drill data at the site near Lyndon, Kansas, the necessary overburden thickness for energy transmission appears to be approximately 4.9 ft. Unfortunately, the results of modeling the Zoeppritz equations using computed and estimated parameters, failed to conclusively support or contradict this hypothesis (App. F).

Other Possible Causes of the Chaotic Zone

There are many other possible causes for the chaotic zone observed on data acquired above near-surface limestone units. If limestone were opaque to certain frequencies under certain conditions, transmission losses would result. This is unlikely since opacity is normally a material property, and there is no known material change which occurs in the lowermost limestone unit of the Ozawkie Limestone Member. It is also possible that the chaotic zone could be due entirely to phenomena actually occurring outside the plane of the survey. This would require a fairly large effective Fresnel zone (Sheriff, 1984). Migrating the data of Line 6 (Fig. 32b) would test this possibility. In addition, the overburden layer above the limestone may act as a waveguide for channel waves if its velocity is below the velocity of sound in air. Besides attenuation, however, the thickness of the waveguide should not affect its ability to conduct energy. In addition, this would fail to explain the occurrence of poor data quality directly beneath the outcrop.

There is the possibility that structural disturbance is the cause of the chaotic zone (on Lines 1 through 6). However, from known local geology, a fault zone of 110 m is unlikely. The regional dip of the area is approximately 20 ft per mile, to the northeast

(O'Connor, 1955). Between CDPs 379 and 347 (Fig. 32), there is approximately a 2.3 ft difference in elevation. The higher elevation at CDP 379 is due to subcropping and outcropping Pennsylvanian materials. After accounting for the difference in elevation and the resulting difference in traveltime, I conclude that the dip on the seismic section is consistent with the regional dip. Thus, any structural disturbance that may be present is insignificant relative to the effects of the near-surface geology.

Reverberating Refractions as a Function of Near-surface Geology

The walkaway noise test data acquired near Lyndon, Kansas exhibit approximately 50 ms of reverberation energy on both the forward (Fig. 7b) and reverse profiles (Fig. 8). The reverberating energy travels at a velocity of approximately 2,700 m/s in both directions. Since the reverberating energy exhibits linear moveout and the velocity is the same in both directions, despite differing near-surface geology, the reverberations must be refraction energy (ringing refractions). The refracting layer is probably the Oread Limestone, although this is not certain since the direct wave is not evident. And since frequency filtering was unsuccessful at the site near Lyndon, Kansas, the frequency of the reverberating energy must be nearly the same as that of

the reflection energy.

The unfiltered walkaway noise test data acquired at the site near Clinton, Kansas exhibits about 130 ms of reverberating refraction energy. Both the .50 caliber rifle and the sledge hammer yield approximately the same amount of reverberating energy (Fig's. 11 and 16). Thus, the reverberating energy is not a phenomenon unique to impulsive projectile sources.

Both analog and digital frequency filtering proved successful in eliminating much of the reverberating energy from the data acquired near Clinton, Kansas. Frequency filtering was unsuccessful on the data acquired near Lyndon, Kansas. Since many of the acquisition and instrumentation parameters were the same at both sites, I conclude that reverberating energy is a function of an unknown feature of local geology. This is because local geology is the only pertinent difference between the two sites. Additional evidence is the higher-frequency reverberations acquired over the outcrop of the lowermost limestone unit of the Ozawkie Limestone Member. Here again there is a change in reverberation character due solely to local geology. Besides this higher frequency phenomenon associated with outcropping limestone, the character of the reverberations must be a function of the first refracting interface. This is evident because of the occurrence of nearly identical

reverberation energy over distinctly different geology in the upper 30 ft on the data acquired near Lyndon, Kansas.

Upon frequency filtering there remain about 20 ms of apparently reverberating energy on the data acquired near Clinton, Kansas (Fig. 12). This could be due to the convolved source wavelet, and thus not represent reverberations at all. Spiking deconvolution is designed to compress such a wavelet to more of an impulse. However, the failure of this procedure does not necessarily indicate that the remaining apparent reverberations are not part of a convolved source wavelet. In fact, the occurrence of "reverberating" reflection and direct wave energy on Figure 19 suggests that the remaining apparent reverberations are simply a function of the convolved source wavelet.

Recommendations for Future Study

There are several possible ways to acquire high-quality data in areas exhibiting transmission losses. If the approximate thickness of the near-surface limestone unit is known, researchers could attempt to undershoot the limestone. This is a technique often used to acquire data beneath rivers and roads. Also, if the wide-angle hypothesis (presented earlier) is accurate, then extremely small offsets should result in improved data quality. Another possibility would be to use a source

with a lower frequency spectrum than that of the .50 caliber rifle, along with low natural frequency geophones, open low-cut filters, and relatively low high-cut filters. A varying-frequency source, such as vibroseis, may also prove useful. Field tests, such as velocity determinations, may prove fruitful for modeling purposes. Some impractical possibilities include: backfilling to a desired overburden thickness, and countersinking the sources and the receivers. To determine the actual cause of the transmission losses, experimental arrays of receivers could be deployed at various elevations above a subcropping limestone unit. Ideally, the source could also be set at various elevations.

Since reverberating noise appears to be a function of relatively near-surface geology (first refractor), attention should be focused upon the source wavelet. Initially, it would be necessary to determine the shape of the source wavelet. Since it is the convolved source wavelet which appears to result in reverberating energy, it is desirable to determine the effects of altering the source wavelet. Advanced wavelet processing techniques could then be employed to minimize the reverberating noise.

Conclusions

1. Near-surface geology may cause static problems, velocity pull-up, and even wholesale destruction of seismic reflection data quality. This is seen on data acquired near Lyndon, Kansas, where there is a chaotic zone resulting from transmission losses on data occurring beneath a subcropping and outcropping limestone unit.

2. Near-surface geology can be predicted on the basis of data quality. This is evident on the data acquired near Lyndon, Kansas, where the zone of transmission loss extends beyond the effective outcrop area of the lowermost limestone unit of the Ozawkie Limestone Member in two directions. From the occurrence of velocity pull-up and chaotic data from beneath the alluvium, I successfully predicted that limestone subcrops beneath the alluvium. Due to the wedge-shaped noise pattern, I also conclude that the limestone unit is buried more deeply towards the south.

3. Temporally and spatially-varying digital frequency filtering proves useful in improving the signal-to-noise ratio, primarily on the margin of the zone of transmission loss. Thus, the frequency content of the signal varies according to near-surface conditions. However, since various pre-emphasis and digital filters could not reveal signal in the zone of transmission loss,

it must not be due solely to signal being obscured by noise. In the unlikely event of both signal and noise having the same frequency content, the noise must have a markedly higher amplitude. Comparison of the velocity filtered data of the chaotic zone with random data suggests near-randomness of the information in the chaotic zone.

4. The occurrence of the chaotic zone is related to the frequency content of the impinging seismic energy. Because it is most pronounced at high frequencies, it would not occur on a conventional seismic survey performed over the area. The occurrence of the chaotic zone is also related more to geologic conditions near the source than to geologic conditions near the receiver.

5. The only obvious difference between the area of the chaotic zone and the area to the north (which exhibits reflection signal) is the depth to the limestone unit. The difficulty of correlating across the chaotic zone is due, exclusively, to varying near-surface geology. The chaotic zone is apparently due to transmission losses. A profusion of wide-angle reflection energy is a possible mechanism for transmission losses over near-surface limestone units. This would result in a chaotic zone on seismic sections. Other possible causes of the chaotic zone include opacity, Fresnel effects, channel waves, and structure. The dip on the seismic section at Lyndon is

consistent with regional dip. Therefore, any existing structural disturbance is insignificant relative to the effects of the near-surface geology.

6. Reverberation energy severely limits the effective use of the shallow reflection method on depths shallower than that corresponding to 50 ms, at the site near Lyndon, Kansas. Since the reverberating energy exhibits linear moveout and the velocity is the same in both directions, despite differing near-surface geology, the reverberations must be refraction energy.

7. Frequency filtering was successful at the site near Clinton, Kansas, but unsuccessful at the site near Lyndon, Kansas. Thus, the frequency of the reverberating energy on the data from the site near Lyndon, Kansas, must be nearly the same as that of the reflection energy. On the data acquired near Clinton, Kansas, the apparent reverberating energy which remains after frequency filtering is evidently a function of the convolved source wavelet.

8. Regardless of shot location or pre-emphasis filters, walkaway noise test data exhibits disruption of the reverberating wave train directly beneath the outcrop of the lowermost limestone unit of the Ozawkie Limestone Member near Lyndon, Kansas. Thus, the character of the reverberating energy is a function of local geology, and in particular, the first refracting interface.

References

Bally, A.W., ed., Seismic expression of structural styles, AAPG Studies in Geology Series #15, Vol. 1, p. 1.2.1-36, 1983.

Clinton Lake, Engineer record drawings, U.S. Army Corps of Engineers, 1976.

Douze, E.J., and Laster, S.J., Statistics of semblance, Geophysics, Vol. 44, No. 12, p. 1999-2003, 1979.

Halliday, D., and Resnick, R., Physics, Parts I and II, 3rd ed., Wiley, p. 941, 1978.

Hunter, J.A., Pullen, S.E., Burns, R.A., Gagne, R.M., and Good, R.S., Shallow seismic reflection mapping of the overburden-bedrock interface with the engineering seismograph - some simple techniques, Geophysics, v. 49, 1984, p. 1381 - 1385.

Kalik, A,J., Signal-to-noise through use of the semblance coherency statistic, Kansas Geological Survey, Open-file Report #88-27, 1988.

Knapp, R.W., Properties of the air-coupled wave, Society of Exploration Geophysicists 40th Annual Midwest Meeting expanded abstracts, 1987.

Knapp, R.W., Miller, R.D., Steeples, D.W., Kalik, A.J., and Song, Y.Y., Seismic reflection profiling of the near-surface, Geophysical Society of Tulsa, 1988.

Knapp, R.W., and Steeples, D.W., High- resolution common-depth-point seismic reflection profiling: Instrumentation, Geophysics, v. 51, p. 276-282, 1986a.

Knapp, R.W., and Steeples, D.W., High-resolution common-depth-point seismic reflection profiling: Field acquisition parameter design, Geophysics, v. 51, p. 283-294, 1986b.

McClain, T.J., Geologic Map, Lawrence West, Kansas, University of Kansas, Kansas Geological Survey, Map M-14, 1979.

Miller, R.D., Steeples, D.W., Treadway, J.A., Birkelo, B.A., Myers, P.B., and Kalik, A.J., Shallow high-resolution seismic reflection program around the proposed superconducting super-collider facility in Kansas, Kansas Geological Survey, Open-file Report #87-33, p. 5, 1988.

Mitchum, R.M., Jr., Vail, P.R., and Thompson, S., III, Seismic stratigraphy and global changes of sea level, Part two: The depositional sequence as a basic unit for stratigraphic analysis, AAPG Memoir 26, p. 56, 1977a.

Mitchum. R.M., Jr., Vail, P.R., and Sangree, J.B., Seismic stratigraphy and global changes of sea level, Part six: Stratigraphic interpretation of seismic reflection patterns in depositional sequences, AAPG Memoir 26, p. 128, 1977b.

O'Connor, Howard G., Geology, mineral resources, and ground-water resources of Osage County, Kansas, University of Kansas Publication, v. 13, p. 5-16, 1955.

O'Connor, Howard G., Geology and ground-water resources of Douglas County, Kansas, University of Kansas Publication, Bulletin 148, p. 33-42, 1960.

Pullen, S.E., and Hunter, J.A., Seismic model studies of the overburden-bedrock reflection, Geophysics, v. 50, p. 1684-1688, 1985.

Seeber, M.D., and Steeples, D.W., Seismic data obtained using a .50-caliber machine gun as high-resolution seismic source, AAPG Bulletin, Vol. 70, No. 8, August, 1986.

Sheriff, R.E., ed., Encyclopedic dictionary of exploration geophysics, Society of Exploration Geophysicists, 1984.

Sheriff, R.E., and Geldart, L.P., Exploration seismology, Vol. 1 - 2, Cambridge University Press, 1982.

Steeples, D.W., and Knapp, R.W., Reflections from 25 feet or less, Society of Exploration Geophysicists 52nd Annual Meeting expanded abstracts, p. 469-471, 1982.

Steeples, D.W., and Miller, R.D., Seismic reflection methods applied to engineering, environmental, and ground-water problems, Kansas Geological Survey, 1988.

Tatham, R.H., Keeney J.W., and Noponen I., Application of the tau-p transform in processing seismic reflection data, Society of Exploration Geophysics, Las Vegas, 1983.

Widess, M.B., How thin is a thin bed, Geophysics, v. 38, p. 1176-1180, 1973.

Zeller, Doris E., The stratigraphic succession in Kansas, Kansas Geological Survey Bulletin 189, University of Kansas Publication, 1968.

Appendix A

Figures 51 through 53 are copies of engineering records of the Clinton Spillway, near Clinton, Kansas. Figure 51 shows the location of the Spillway, as well as, the location of borings and cores. Figure 52 exhibits cross-sections of the Spillway based on the borings. Figure 53 defines the symbols, abbreviations, and some of the terms used on Figures 6, 51, 52, and 53.

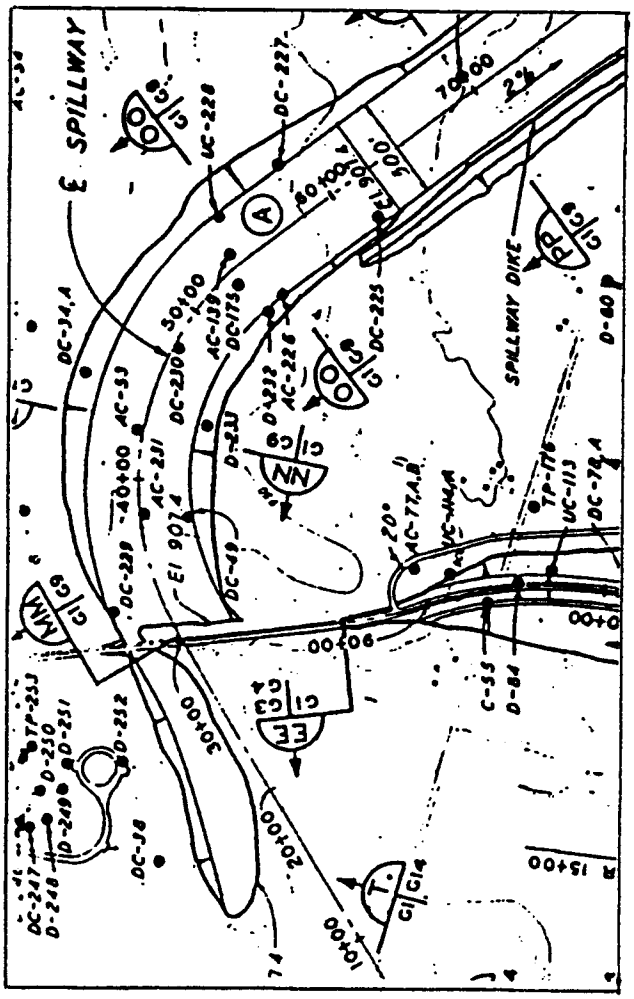

Figure 51. Engineering record drawing of Clinton spillway near Clinton, Kansas, showing boring and core locations.

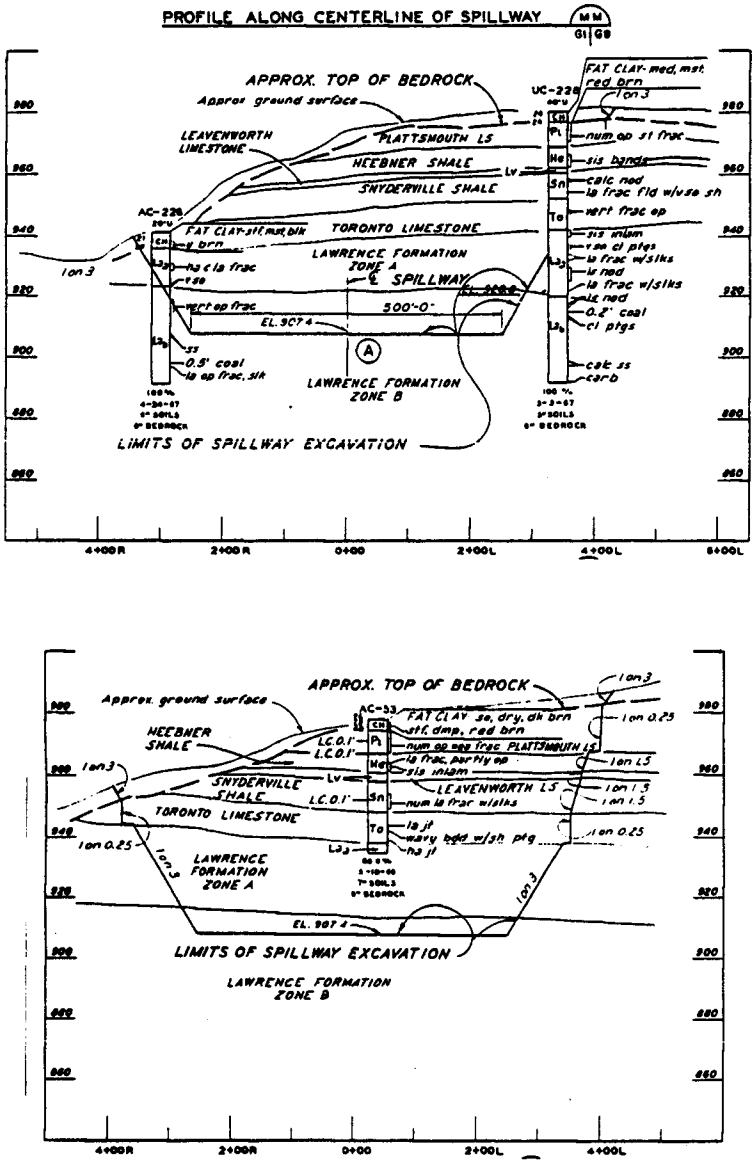

Figure 52. Referenced borings and cross-sections from the Clinton Lake area, near Clinton, Kansas.

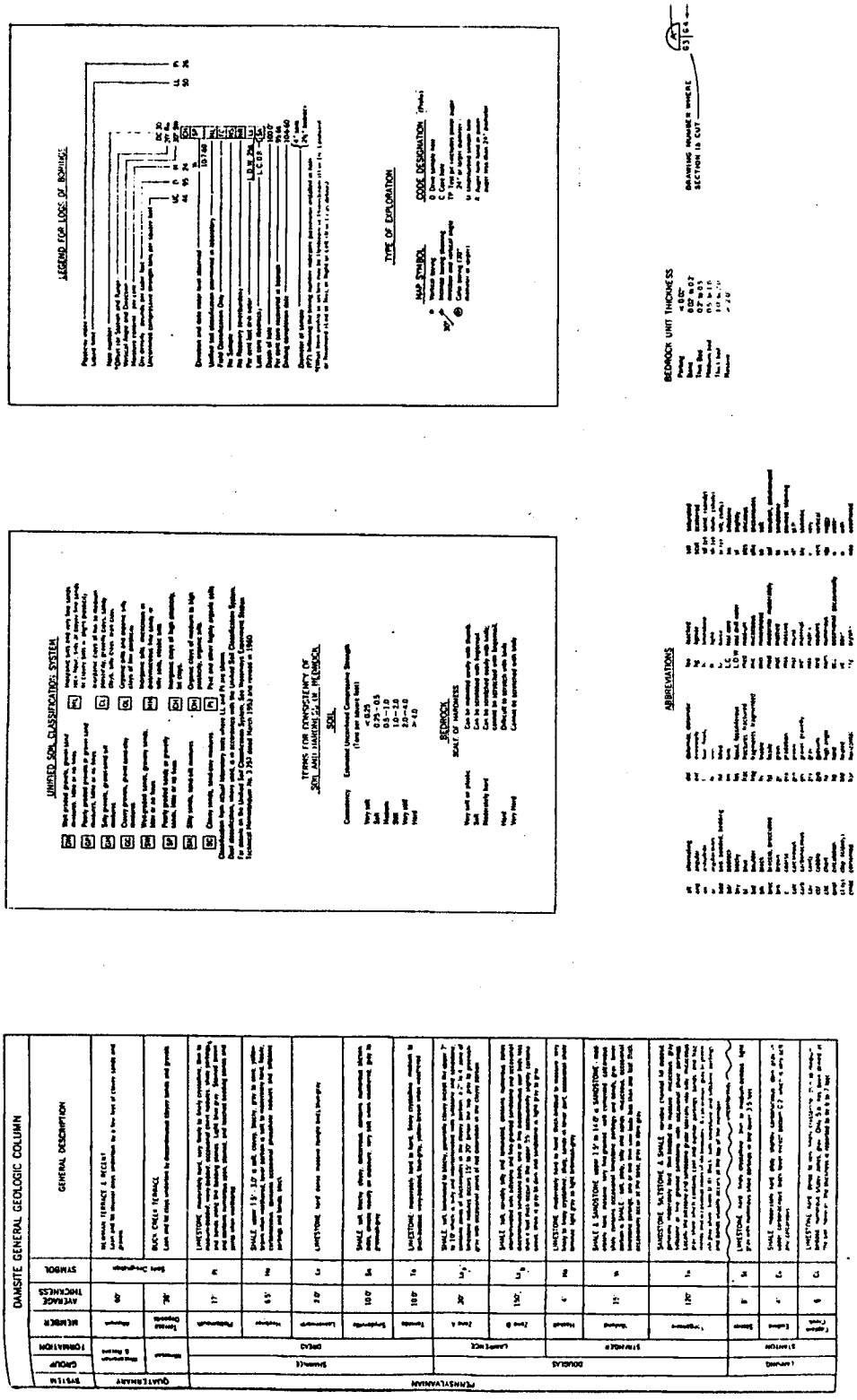

Figure 53. Explanation of symbols and abbreviations used on Figures 6, 51, and 52.

Appendix B

```
      program sn
*************************************************************
c     sn.f77  version: 1.0
c     written by Andrew J. Kalik 4/21/88
c
c     This program computes trace coherency based upon
c     the semblance statistic within a CDP window m and
c     sample interval n.  The output file given by the
c     user must be plotted using SPEX software.  The
c     output file beginning with "C" must be run through
c     SURFACE 2 for contour plots.
c
c     link with :udd:geophysics:tread.ob
c     link using MTOP > 15
c
c     Necessary parameters provided by the user:
c
c     n      = Window Length
c     m      = Number of CDP's to Sum Over
c     time1  = Start Time
c     time2  = End Time
c     dt     = Sampling frequency for contour plots
c     beg    = Beginning CDP
c     end    = Ending CDP
c     st     = Sampling rate of original data
c
c     Computed parameters:
c
c     fileout = Output file for contour maps
c     nsamp   = Number of samples per trace
c     incre   = Sample interval
c     len     = Record length
c     t1      = first sample
c     t2      = last sample
c
c     Unstacked data is preferable!
c
*************************************************************
c
c    Dimension and Initialize Variables
c
      parameter (is=150,if=400)
      real*4 amp(1000,is:if),den(1000,is:if)
      real*4 ss(1000,is:if),s(1000,is:if)
      real*4 hin(1000),hamp(1000,1800)
      real xmax,c
      integer*2 j,reel1(1600),k,reel2(200),trh(120)
      integer*2 nsamp,itype,incre
      integer n,t1,t2,dt,size(is:if),time1,time2,st
```

```
      integer cdp,top,bot,a,b,len,mid,m,mm,kount,count
      integer beg,end
      character*30 datain,dataout,fileout
c
c     Call Subroutine IO
c
      call io(n,m,time1,time2,dt,beg,end,datain,dataout)
      fileout=dataout//"C"
c
c     Open Data Files
c
      open(15,file=fileout,status='fresh',recfm='ds',
     +iointent="output",maxrecl=9900)
      open(1,file=datain,iointent='input',mode='binary',
     +recfm='dynamic',form='unformatted')
      open(2,file=dataout,iointent='output',
     +mode='binary',recfm='dynamic',form='unformatted')
c
c     Read and Write Reel Header
c
      read(1) j,(reel1(i),i=1,j),k,(reel2(i),i=1,k)
      write(2) j,(reel1(i),i=1,j),k,(reel2(i),i=1,k)
c
c     Determine the Number of Samples, Sample Inteval,
c     Record Length, and Sampling Extremes
c
      nsamp=reel2(11)
      incre=reel2(9)
      itype=reel2(13)
      a=nsamp
      b=incre
      c=float(b)/1000.
      len=int(a*c)
      if (time2 .eq. 0) time2=len
      t1=n/2+1+(time1/c)
      t2=(time2/c)-n/2
      st=1
      cdp=1+end-beg
      j=120+2*nsamp
c
c     Set Matrices and Array Values to Zero
c
      do 10 ii=beg-m,end+m
        size(ii)=0
        do 20 kk=t1,t2
          den(kk,ii)=0.
          amp(kk,ii)=0.
          s(kk,ii)=0.
          ss(kk,ii)=0.
20      continue
10    continue
```

```
      do 22 jj=1,1800
        do 25 kk=t1,t2
          hamp(kk,jj)=0.
25      continue
22    continue
c
c     Read Traces and Accumulate Matrices
c
      count=0
30    call tread(trh,hin,nsamp,itype,1,ierr)
        if (ierr .ne. 0)  goto 80
        if (trh(12) .lt. beg .or. trh(12) .gt. end)
     +goto 70
        cdp=trh(12)
c
c     Keep Track of the Fold (size) of each CDP
c
        size(cdp)=size(cdp)+1
        count=count+1
        do 35 kk=t1,t2,st
          hamp(kk,count)=hin(kk)
          if (st .ne. 1) hamp(kk-1,count)=(hin(kk)+
     +hin(kk-2))/2.
35      continue
70    goto 30
c
c     Last Trace has been Read, HAMP Matrix is Complete
c
80    continue
c
c     Compute Moving Pointers for First and Last Trace
c     within the Window (m) for each CDP
c
      do 40 ii=beg,end
        mid=0
        do 41 mm=beg,ii
          mid=mid+size(mm)
41      continue
        top=mid
        do 42 mm=ii-m/2,ii
          top=top-size(mm)
42      continue
        bot=mid
        do 43 mm=ii,ii+m/2
          bot=bot+size(mm)
43      continue
c
c       Compute Effective Numerator and Denominator of
c       Semblance Statistic within the Sample and CDP
c       Trace Windows
c
```

```
        do 50 kk=t1,t2
          do 60 jj=kk-n/2,kk+n/2
            do 65 ll=top,bot
              amp(kk,ii)=amp(kk,ii)+hamp(kk,ll)
              den(kk,ii)=den(kk,ii)+hamp(kk,ll)**2
65          continue
60        continue
50      continue
40    continue
c
c     Compute Semblance Matrix and Largest Value for
c     Normalization
c
      xmax=0.
      do 90 ii=beg,end
        do 100 kk=t1,t2
          if (den(kk,ii) .eq. 0.) then
           s(kk,ii)=0.
           goto 100
          endif
          s(kk,ii)=amp(kk,ii)**2/(den(kk,ii)*count)
          xmax=amax1(xmax,s(kk,ii))
100     continue
90    continue
c
c     Normalize Semblance Matrix for Wiggle Plots
c
      do 115 ii=beg,end
        do 120 kk=t1,t2
          ss(kk,ii)=100.*s(kk,ii)/xmax
120     continue
        trh(6)=ii
        trh(88)=1
        write(2) j,trh,(ss(kk,ii),kk=1,nsamp)
115   continue
c
c     Compute Normalized Matrix for Contour Plots
c
      do 105 ii=end,beg,-1
        kount=0
        do 95 ik=t1,t2,dt
          kount=kount+1
          ss(kount,ii)=100.*s(ik,ii)/xmax
95      continue
        write(15,110) (ss(nn,ii),nn=1,kount)
110     format(1x,200f5.1)
105   continue
c
      stop
      end
**********************************************************
```

```
      subroutine io(n,m,time1,time2,dt,beg,end,datain,
     +dataout)
      integer n,beg,end,m,mm,time1,time2,dt
      real res
      character*30 datain,dataout
c
c     Retrieve Required Parameters Interactively
c
      write(*,1)
1     format(/,10x,"Enter input pathname: ",/)
      read(*,2) datain
2     format(a30)
      write(*,5)
5     format(/,10x,"Enter output pathname: ",/)
      read(*,2) dataout
9     write(*,10)
10    format(/,10x,"Enter window length (n): ")
      write(*,15)
15    format(10x,"(Default = 1)",/)
      read(*,20) n
20    format(i10)
      if (n .gt. 9) then
       write(*,25)
25     format(/,10x,"WINDOW IS TOO LARGE",/)
       goto 9
      endif
      if (n .eq. 0) n=1
      write(*,30)
30    format(/,10x,"Enter number of CDP's (m): ",/)
      read(*,20) mm
      res=float(mm)/2.
      if (frac(res) .ne. 0.) then
       m=mm-1
      else
       m=mm
      endif
      write(*,40)
40    format(/,10x,"Enter start time (time1): ",/)
      write(*,45)
45    format(10x,"(Default = 0)",/)
      read(*,20) time1
      if (time1 .eq. 0) time1=0
      write(*,50)
50    format(/,10x,"Enter end time (time2): ",/)
      write(*,55)
55    format(10x,"(Default = End of Record)",/)
      read(*,20) time2
      write(*,65)
65    format(/,10x,"Enter sample interval (dt): ",/)
      write(*,75)
75    format(10x,"(Default = 1)",/)
```

```
      read(*,20) dt
      if (dt .eq. 0) dt=1
      write(*,60)
60    format(/,10x,"Enter beginning CDP (beg): ",/)
      read(*,20) beg
      write(*,70)
70    format(/,10x,"Enter ending CDP (end): ",/)
      read(*,20) end
      return
      end
```

Appendix C

The four files below are necessary in order to plot the output of program SN.F77 (App. B) on the Data General MV 20000. The first three files are used to create signal-to-noise contour maps. The last file on this page is required for wiggle-trace plots.

```
*****SURFACE2 DATA*****************************************
TITL    Semblance Coherency Contour Map
DEVI    6,'ANDREW'
MATR    15,200,183,1,0,0,'(1X,200F5.1)'
EXTR    1,250,197,379
CONT    1,0,    ,0,0, ,
CINT    0,0,10,0,1,.05,2, ,5
BOX     10,5,10,5,0,0,200,2,.1
BXEX    0,250,197,379
SIZC    1,6,7
PERF
STOP
END


*****SURFACE2 EXECUTION STATEMENT************************
SURF2 CONT.RAS CCREP CCEXC MAP.AK/FC=09 C.SN.AK/FC=15


*****RASTER FILE CREATION FOR SURFACE2 CONTOUR PLOTTING*
RASTER/V=CONPLOT.AK MAP.AK




*****SPEX PLOT ROUTINE FOR WIGGLE TRACE PLOTTING********
I DATAIN :UDD:GGSEIS:W.SN.AK
V :UDD:GGSEIS:PLOT.AK
D :UDD:GGSEIS:SPACE.AK
* SPEX
*C3FIELD1111112222223333334444445555556666667777778888888
* PLOT  610   1600  0           23
*F
```

Appendix D

Random unstacked data are shown in Figure 54. This data was used in order to test program SN.F77 (App. B). On Figures 55 through 60 only three parameters were varied: the number of samples (n), the number of CDPs (m+1), and the sampling frequency (st). All the random values are between -100 and 100. There are 1000 values per trace; four values each millisecond. Barely noticeable on Figure 54, are inserted spikes at 62 ms and 187 ms. The spike at 62 ms was given a value of 50 on each trace. The spike at 187 ms was given a value of 25 from traces 1 to 32. The value at 187 ms on traces 33 through 64 is random. Note how obvious the spikes are on the signal-to-noise plots of Figures 55 through 60. The negligible effect on random data of varying the number of samples (in time) for which the semblance statistic is summed over (n), is shown in Figures 55 and 56. Note that with random data, there is no noticeable change in coherency by summing over additional samples. The effect of varying the number of traces for which the semblance statistic is summed over (m+1), is shown in Figures 56, 57, 59, and 60. Figure 57 is noticeably noisier (more blank area) than Figure 56. This indicates less random correlation upon averaging. Figures 59 and 60 show the effect of summing over too many traces. This smearing effect is indicative of instability, and causes random noise to appear coherent. This effect can also be seen on Figures 42 and 43.

Please note that unlike the data used in Figures 42 and 43, the random data is single fold. The effect of lower frequency random data can be seen on Figure 58. For this figure, every other value of Figure 54 was linearly interpolated. This process yielded a lower effective frequency. Comparison of Figure 58 with Figure 57 indicates that higher frequency data (Fig. 57) is more prone to random correlation.

Within the body of this thesis, two presentation formats of the signal-to-noise content are displayed (refer to Fig's. 36 and 37). Besides presentation format, Figures 36 and 37 differ only in sampling frequency. After the coherency matrix is computed, all contour plots are made up of data sampled one-fifth as often as that of the corresponding wiggle-trace plots. This is due to a limitation inherent in the contouring software.

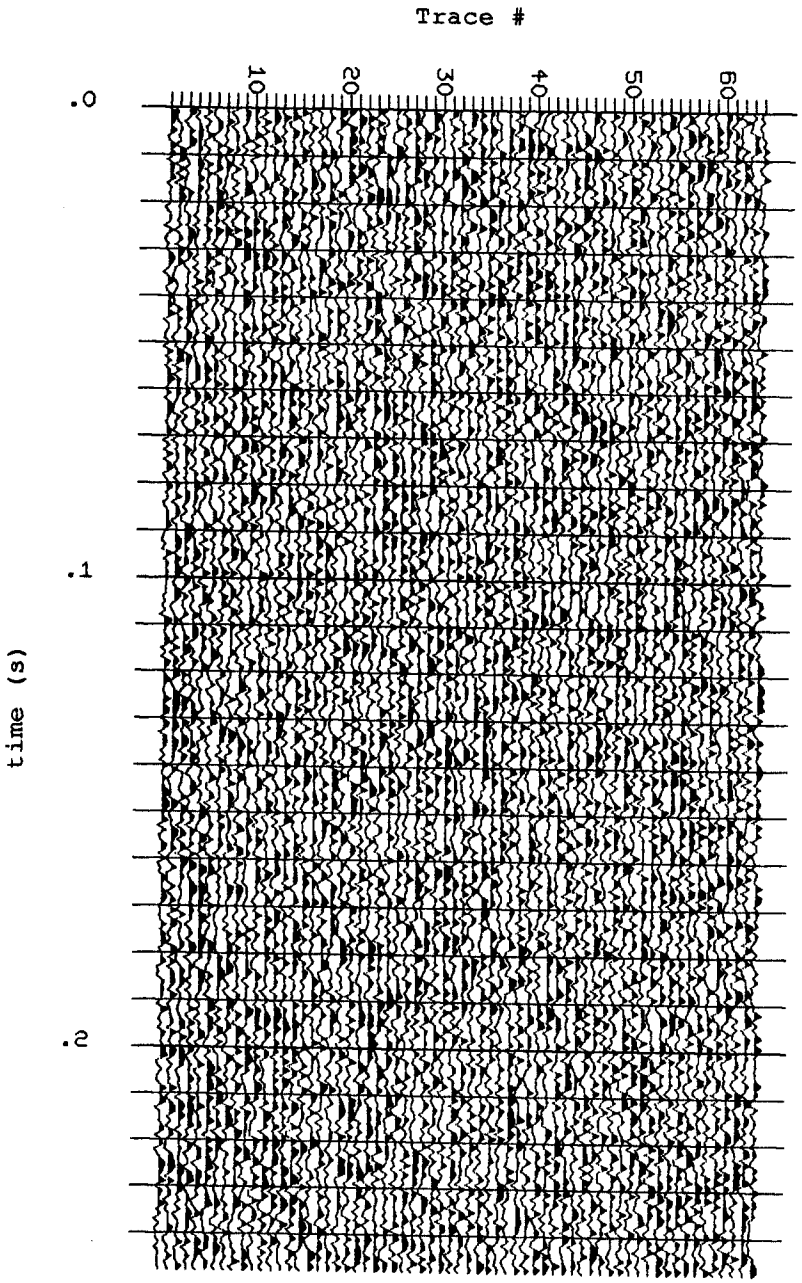

Figure 54. Unstacked random seismic data. Barely noticeable are embedded spikes at 62 ms and 187 ms (see text for explanation).

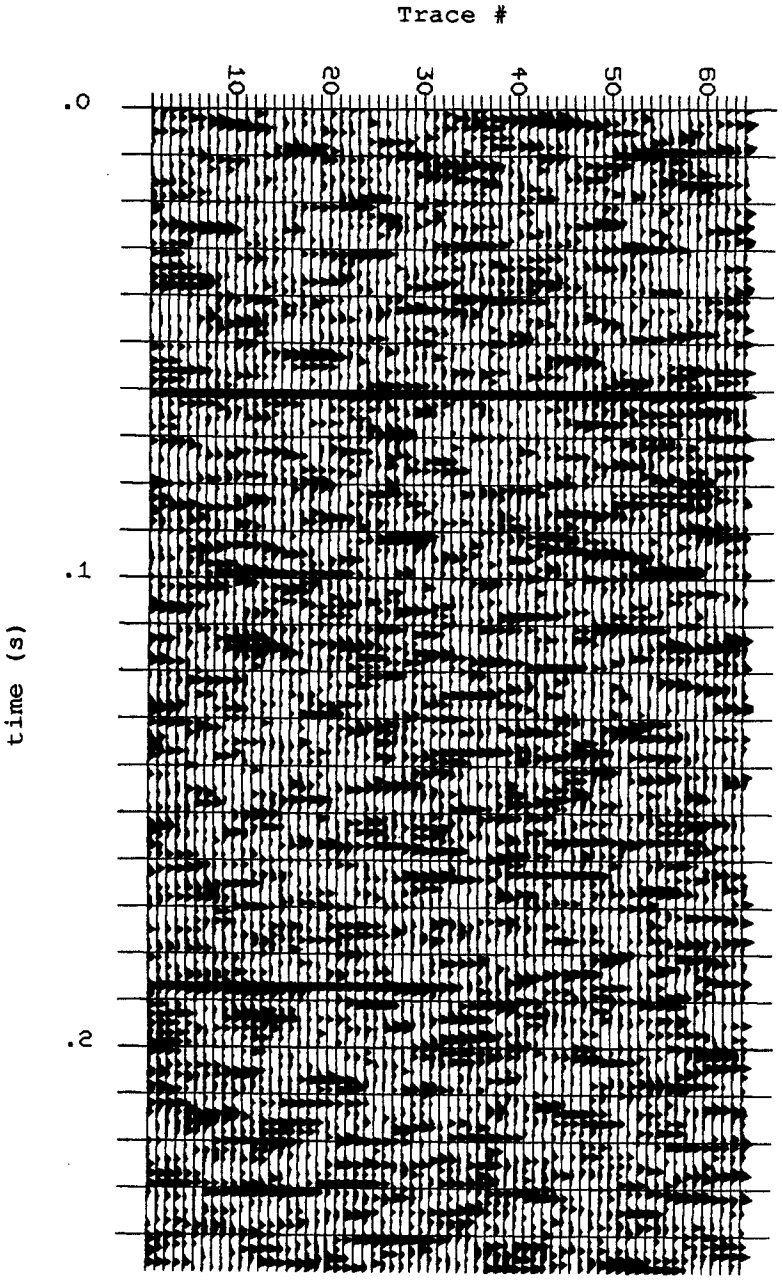

Figure 55. Signal-to-noise plot of the random data in Figure 54, summing over m+1=5 traces and n=1 sample. Note the almost startling appearance of the embedded spikes.

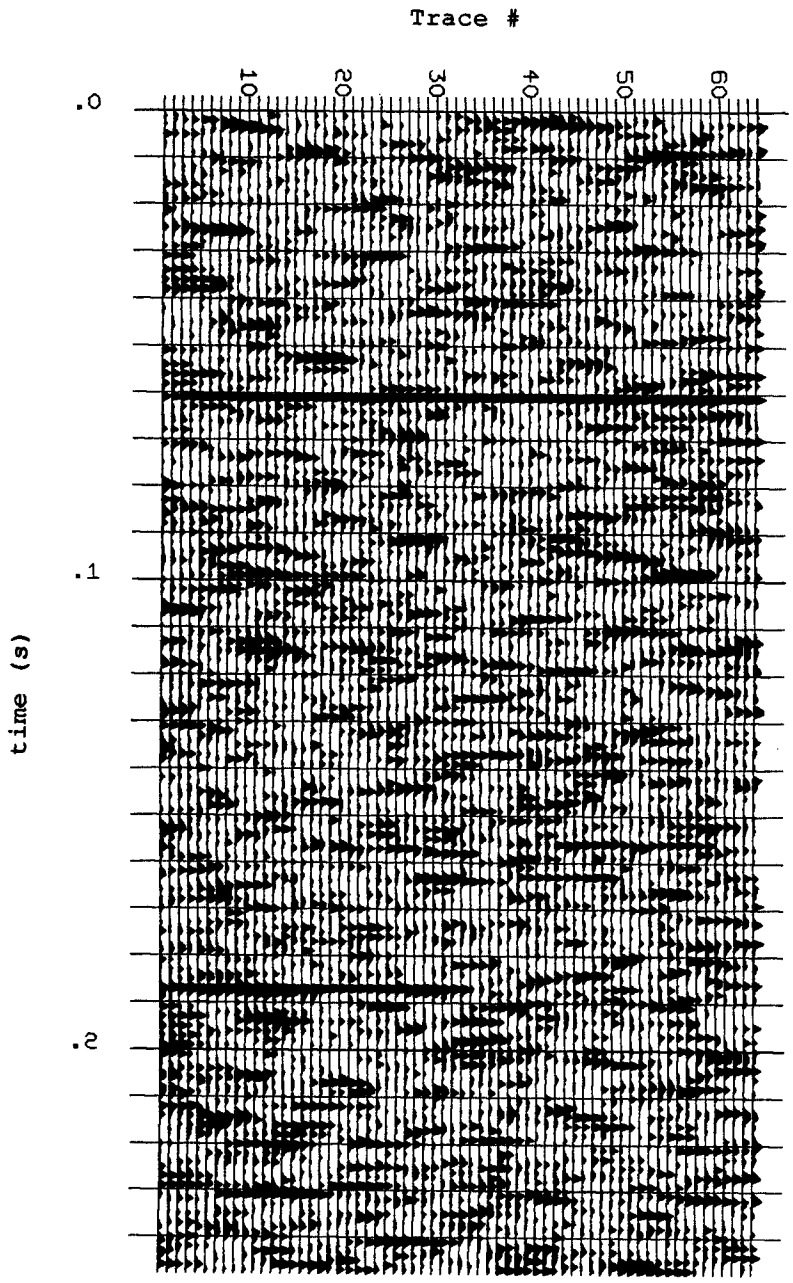

Figure 56. Signal-to-noise plot of the random data in Figure 54. Here the semblance statistic was summed over m+1=5 traces and n=3 samples. Note that with random data, there is no noticeable change in coherency by summing over additional samples.

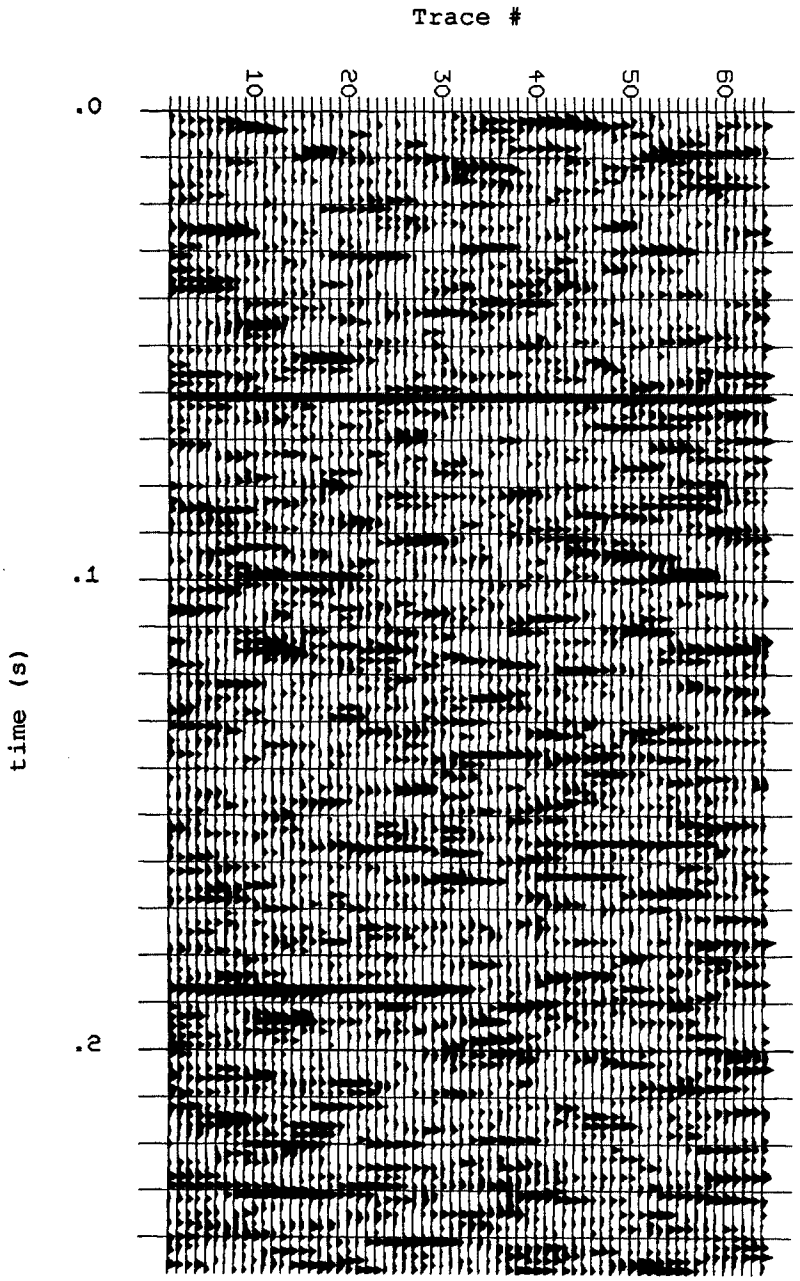

Figure 57. Signal-to-noise plot of the random data in Figure 54, summing over m+1=7 traces and n=3 samples. Note the decrease in coherency relative to Figure 56.

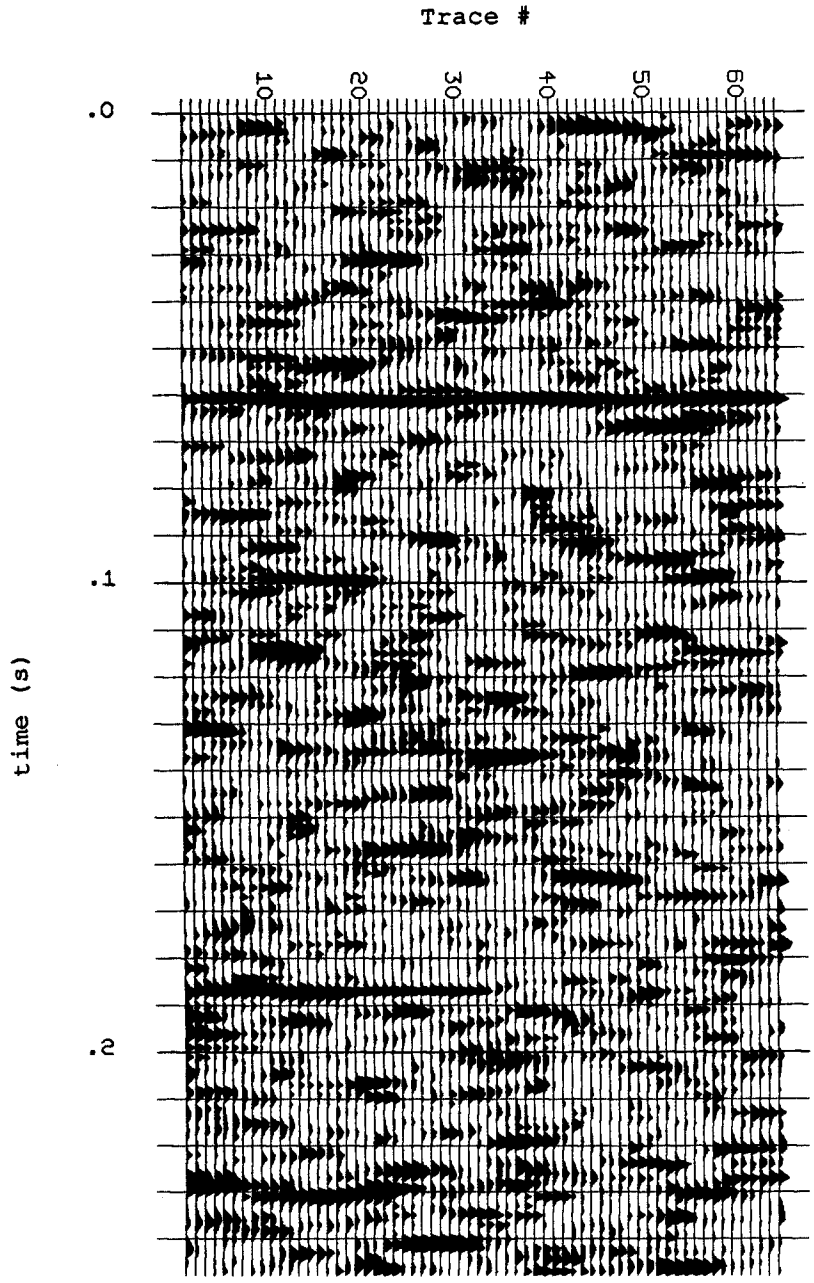

Figure 58. Signal-to-noise plot of the random data in Figure 54, again summing over m+1=7 traces and n=3 samples, but at an effective frequency of one-half that used for Figure 57. Note the substantial decrease in random coherency relative to Figure 57.

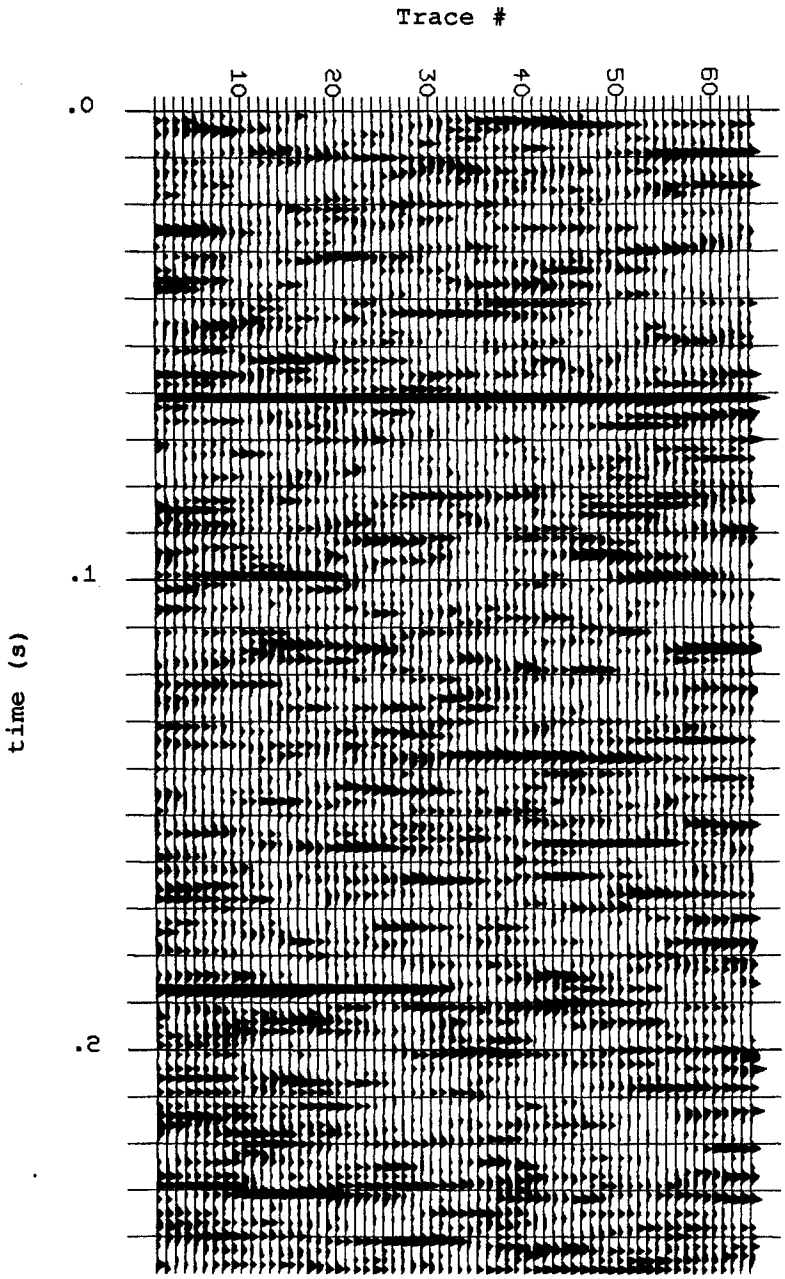

Figure 59. Signal-to-noise plot of the random data in Figure 54, summing over m+1=13 traces and n=3 samples. Note the incipient "smearing" of apparent coherency.

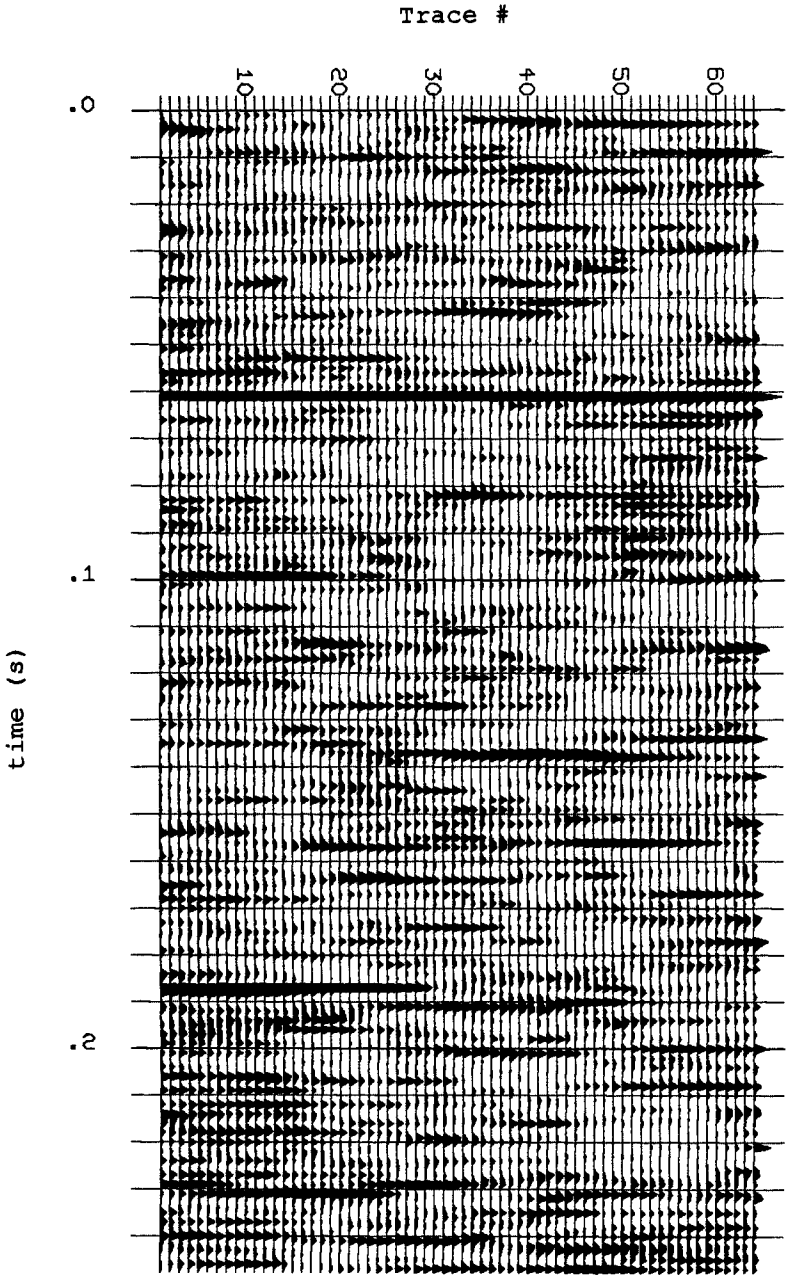

Figure 60. Signal-to-noise plot of the random data in Figure 54, summing over m+1=21 traces and n=3 samples. Note the smearing effect resulting from summing over too many traces relative to the number of traces in the original data set.

Appendix E

Random stacked data are shown in Figure 61. This data was used to test the velocity filter used on Line 4. The random data was created with the same fold and offset information as that of Line 4 (Fig. 27). Upon application of the same velocity and frequency filters used on Line 4, the data appears exceptionally coherent (Fig. 62). Comparison with Figure 28 gives rise to a certain amount of skepticism towards the validity of the observed coherent events. Obviously, the level of coherency exhibited on Figure 62 is far higher than that of the original random data. In conclusion, it seems that the tau - p, velocity filter is capable of creating coherency, at random, under certain circumstances.

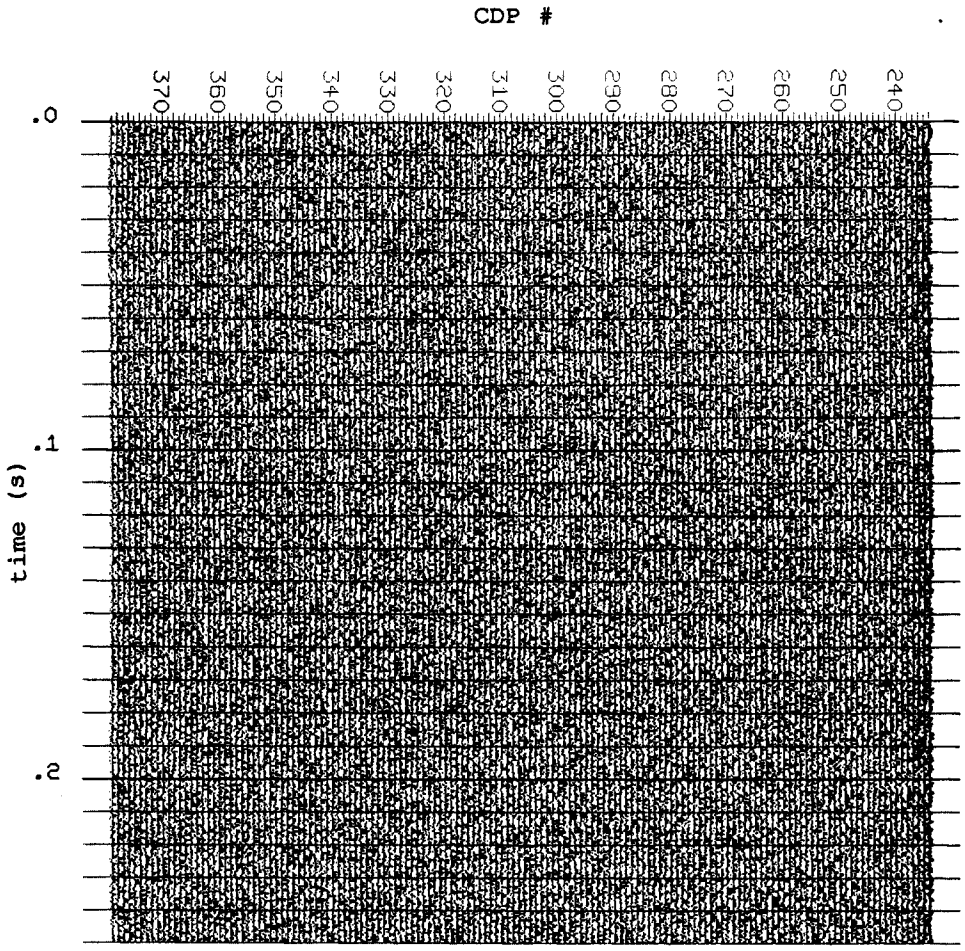

Figure 61. Stacked, totally random seismic data. The geometry of this pseudo-line is identical to that of CDP Line 4 (Fig. 27).

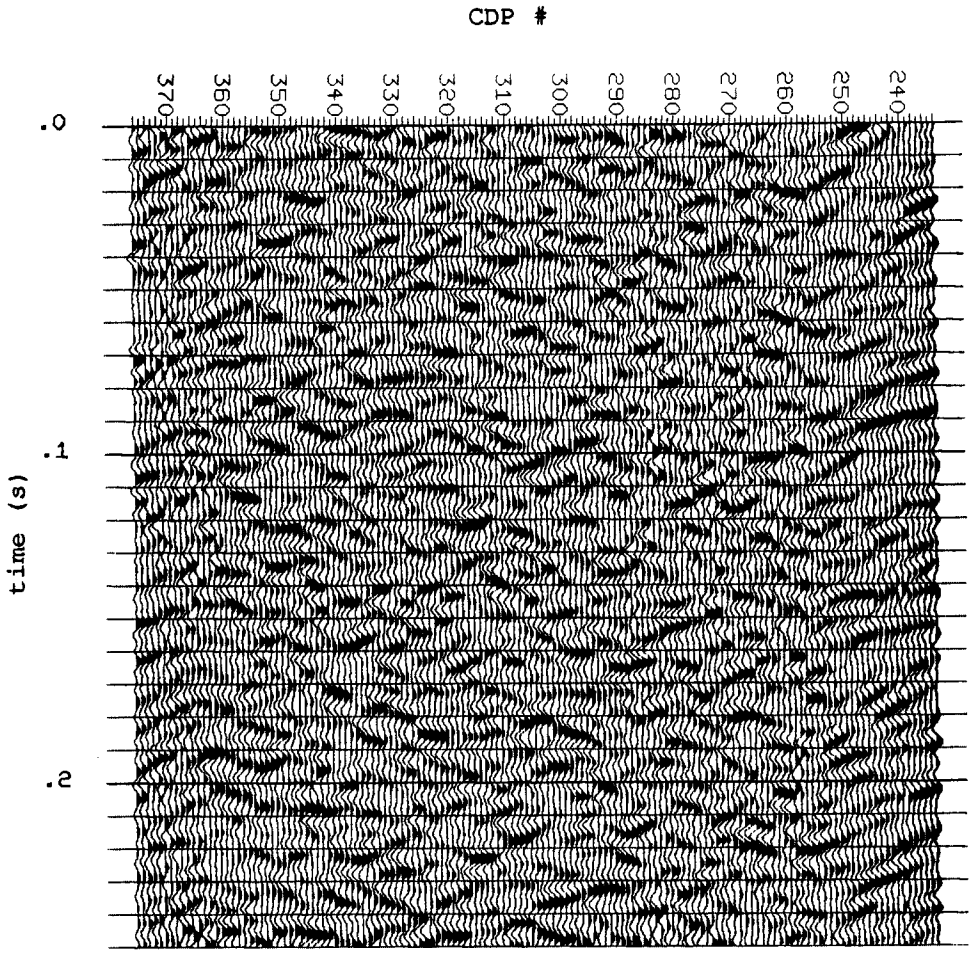

Figure 62. Velocity filtered seismic section of the random data in Figure 61. Note the remarkable coherence inherent in random data upon application of the identical velocity and frequency filters used on Line 4 (Fig. 28).

Appendix F

The following table includes the results of modeling the Zoeppritz equations using computed and realistically estimated parameters, approximating the conditions at the site near Lyndon, Kansas. No energy is transmitted when incident at an angle greater than the critical angle. As expected, the table shows that past the critical angle, the amplitude of the reflected energy rises dramatically. It also shows that as layer 1 increases in thickness, the critically reflected energy is received at further offsets. However, the data do not show the abrupt change necessary to confirm the wide-angle reflection hypothesis (Fig. 63; Table 6).

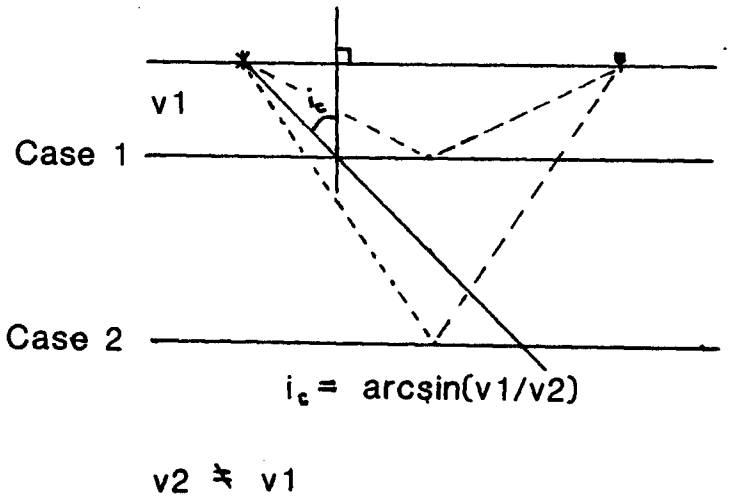

Figure 63. Wide-angle reflection mechanism. Note the increase in transmitted energy available to the geophone upon thickening of the overburden.

Table 6

	Layer 1	Layer 2
Thickness (ft)	2.0	5.0
Density (g/cc)	2.40	2.68
P wave velocity (m/s)	1075.	2000.
S wave velocity (m/s)	621.	1155.
Poisson's Ratio	.25	.25
Critical Angle	32.51	

Station #	Offset (m)	Incident Angle	Reflection Amplitude
1	.0	.0	.3501
2	3.0	67.9	.8445
3	6.0	78.5	.9965
4	9.0	82.3	.9921
5	12.0	84.2	.9921
6	15.0	85.4	.9928
7	18.0	86.1	.9936
8	21.0	86.7	.9943
9	24.0	87.1	.9949
10	27.0	87.4	.9954
11	30.0	87.7	.9958
12	33.0	87.9	.9961
13	36.0	88.1	.9964
14	39.0	88.2	.9967
15	42.0	88.3	.9969
16	45.0	88.4	.9971
17	48.0	88.5	.9973
18	51.0	88.6	.9974
19	54.0	88.7	.9976
20	57.0	88.8	.9977
21	60.0	88.8	.9978
22	63.0	88.9	.9979
23	66.0	88.9	.9980
24	69.0	89.0	.9981

	Layer 1	Layer 2
Thickness (ft)	4.0	5.0
Density (g/cc)	2.40	2.68
P wave velocity (m/s)	1075.	2000.
S wave velocity (m/s)	621.	1155.
Poisson's Ratio	.25	.25
Critical Angle	32.51	

Station #	Offset (m)	Incident Angle	Reflection Amplitude
1	.0	.0	.3501
2	3.0	50.9	.5524
3	6.0	67.9	.8445
4	9.0	74.8	.9999
5	12.0	78.5	.9965
6	15.0	80.8	.9934
7	18.0	82.3	.9921
8	21.0	83.4	.9919
9	24.0	84.2	.9921
10	27.0	84.8	.9924
11	30.0	85.4	.9928
12	33.0	85.8	.9932
13	36.0	86.1	.9936
14	39.0	86.4	.9939
15	42.0	86.7	.9943
16	45.0	86.9	.9946
17	48.0	87.1	.9949
18	51.0	87.3	.9951
19	54.0	87.4	.9954
20	57.0	87.6	.9956
21	60.0	87.7	.9958
22	63.0	87.8	.9960
23	66.0	87.9	.9961
24	69.0	88.0	.9963

	Layer 1	Layer 2
Thickness (ft)	6.0	5.0
Density (g/cc)	2.40	2.68
P wave velocity (m/s)	1075.	2000.
S wave velocity (m/s)	621.	1155.
Poisson's Ratio	.25	.25
Critical Angle	32.51	

Station #	Offset (m)	Incident Angle	Reflection Amplitude
1	.0	.0	.3501
2	3.0	39.4	.5431
3	6.0	58.6	.6549
4	9.0	67.9	.8445
5	12.0	73.0	.9964
6	15.0	76.3	.9995
7	18.0	78.5	.9965
8	21.0	80.1	.9941
9	24.0	81.3	.9928
10	27.0	82.3	.9921
11	30.0	83.0	.9919
12	33.0	83.7	.9919
13	36.0	84.2	.9921
14	39.0	84.6	.9923
15	42.0	85.0	.9925
16	45.0	85.4	.9928
17	48.0	85.6	.9931
18	51.0	85.9	.9933
19	54.0	86.1	.9936
20	57.0	86.3	.9938
21	60.0	86.5	.9941
22	63.0	86.7	.9943
23	66.0	86.8	.9945
24	69.0	87.0	.9947

	Layer 1	Layer 2
Thickness (ft)	8.0	5.0
Density (g/cc)	2.40	2.68
P wave velocity (m/s)	1075.	2000.
S wave velocity (m/s)	621.	1155.
Poisson's Ratio	.25	.25
Critical Angle	32.51	

Station #	Offset (m)	Incident Angle	Reflection Amplitude
1	.0	.0	.3501
2	3.0	31.6	.4760
3	6.0	50.9	.5524
4	9.0	61.5	.7029
5	12.0	67.9	.8445
6	15.0	72.0	.9905
7	18.0	74.8	.9999
8	21.0	76.9	.9988
9	24.0	78.5	.9965
10	27.0	79.8	.9946
11	30.0	80.8	.9934
12	33.0	81.6	.9926
13	36.0	82.3	.9921
14	39.0	82.9	.9919
15	42.0	83.4	.9919
16	45.0	83.8	.9919
17	48.0	84.2	.9921
18	51.0	84.5	.9922
19	54.0	84.8	.9924
20	57.0	85.1	.9926
21	60.0	85.4	.9928
22	63.0	85.6	.9930
23	66.0	85.8	.9932
24	69.0	86.0	.9934

	Layer 1	Layer 2
Thickness (ft)	10.0	5.0
Density (g/cc)	2.40	2.68
P wave velocity (m/s)	1075.	2000.
S wave velocity (m/s)	621.	1155.
Poisson's Ratio	.25	.25
Critical Angle	32.51	

Station #	Offset (m)	Incident Angle	Reflection Amplitude
1	.0	.0	.3501
2	3.0	26.2	.2895
3	6.0	44.5	.5074
4	9.0	55.9	.6144
5	12.0	63.1	.7303
6	15.0	67.9	.8445
7	18.0	71.3	.9843
8	21.0	73.8	.9986
9	24.0	75.7	.9999
10	27.0	77.3	.9983
11	30.0	78.5	.9965
12	33.0	79.5	.9949
13	36.0	80.4	.9938
14	39.0	81.1	.9930
15	42.0	81.7	.9925
16	45.0	82.3	.9921
17	48.0	82.8	.9920
18	51.0	83.2	.9919
19	54.0	83.6	.9919
20	57.0	83.9	.9920
21	60.0	84.2	.9921
22	63.0	84.5	.9922
23	66.0	84.7	.9923
24	69.0	85.0	.9925

	Layer 1	Layer 2
Thickness (ft)	20.0	5.0
Density (g/cc)	2.40	2.68
P wave velocity (m/s)	1075.	2000.
S wave velocity (m/s)	621.	1155.
Poisson's Ratio	.25	.25
Critical Angle	32.51	

Station #	Offset (m)	Incident Angle	Reflection Amplitude
1	.0	.0	.3501
2	3.0	13.8	.3188
3	6.0	26.2	.2895
4	9.0	36.4	.6351
5	12.0	44.5	.5074
6	15.0	50.9	.5524
7	18.0	55.9	.6144
8	21.0	59.9	.6745
9	24.0	63.1	.7303
10	27.0	65.7	.7839
11	30.0	67.9	.8445
12	33.0	69.7	.9584
13	36.0	71.3	.9843
14	39.0	72.6	.9945
15	42.0	73.8	.9986
16	45.0	74.8	.9999
17	48.0	75.7	.9999
18	51.0	76.6	.9992
19	54.0	77.3	.9983
20	57.0	77.9	.9974
21	60.0	78.5	.9965
22	63.0	79.0	.9956
23	66.0	79.5	.9949
24	69.0	80.0	.9943

	Layer 1	Layer 2
Thickness (ft)	40.0	5.0
Density (g/cc)	2.40	2.68
P wave velocity (m/s)	1075.	2000.
S wave velocity (m/s)	621.	1155.
Poisson's Ratio	.25	.25
Critical Angle	32.51	

Station #	Offset (m)	Incident Angle	Reflection Amplitude
1	.0	.0	.3501
2	3.0	7.0	.3415
3	6.0	13.8	.3188
4	9.0	20.3	.2927
5	12.0	26.2	.2895
6	15.0	31.6	.4760
7	18.0	36.4	.6351
8	21.0	40.7	.5221
9	24.0	44.5	.5074
10	27.0	47.9	.5247
11	30.0	50.9	.5524
12	33.0	53.5	.5832
13	36.0	55.9	.6144
14	39.0	58.0	.6450
15	42.0	59.9	.6745
16	45.0	61.5	.7029
17	48.0	63.1	.7303
18	51.0	64.4	.7571
19	54.0	65.7	.7839
20	57.0	66.8	.8119
21	60.0	67.9	.8445
22	63.0	68.8	.9258
23	66.0	69.7	.9584
24	69.0	70.5	.9745

	Layer 1	Layer 2
Thickness (ft)	60.0	5.0
Density (g/cc)	2.40	2.68
P wave velocity (m/s)	1075.	2000.
S wave velocity (m/s)	621.	1155.
Poisson's Ratio	.25	.25
Critical Angle	32.51	

Station #	Offset (m)	Incident Angle	Reflection Amplitude
1	.0	.0	.3501
2	3.0	4.7	.3462
3	6.0	9.3	.3351
4	9.0	13.8	.3188
5	12.0	18.2	.3007
6	15.0	22.3	.2868
7	18.0	26.2	.2895
8	21.0	29.9	.3504
9	24.0	33.3	.8411
10	27.0	36.4	.6351
11	30.0	39.4	.5431
12	33.0	42.1	.5110
13	36.0	44.5	.5074
14	39.0	46.8	.5172
15	42.0	48.9	.5333
16	45.0	50.9	.5524
17	48.0	52.7	.5728
18	51.0	54.4	.5936
19	54.0	55.9	.6144
20	57.0	57.3	.6349
21	60.0	58.6	.6549
22	63.0	59.9	.6745
23	66.0	61.0	.6935
24	69.0	62.1	.7121

	Layer 1	Layer 2
Thickness (ft)	80.0	5.0
Density (g/cc)	2.40	2.68
P wave velocity (m/s)	1075.	2000.
S wave velocity (m/s)	621.	1155.
Poisson's Ratio	.25	.25
Critical Angle	32.51	

Station #	Offset (m)	Incident Angle	Reflection Amplitude
1	.0	.0	.3501
2	3.0	3.5	.3479
3	6.0	7.0	.3415
4	9.0	10.5	.3314
5	12.0	13.8	.3188
6	15.0	17.1	.3051
7	18.0	20.3	.2927
8	21.0	23.3	.2851
9	24.0	26.2	.2895
10	27.0	29.0	.3237
11	30.0	31.6	.4760
12	33.0	34.1	.7756
13	36.0	36.4	.6351
14	39.0	38.6	.5588
15	42.0	40.7	.5221
16	45.0	42.7	.5082
17	48.0	44.5	.5074
18	51.0	46.3	.5139
19	54.0	47.9	.5247
20	57.0	49.5	.5378
21	60.0	50.9	.5524
22	63.0	52.3	.5676
23	66.0	53.5	.5832
24	69.0	54.7	.5988

	Layer 1	Layer 2
Thickness (ft)	100.0	5.0
Density (g/cc)	2.40	2.68
P wave velocity (m/s)	1075.	2000.
S wave velocity (m/s)	621.	1155.
Poisson's Ratio	.25	.25
Critical Angle	32.51	

Station #	Offset (m)	Incident Angle	Reflection Amplitude
1	.0	.0	.3501
2	3.0	2.8	.3487
3	6.0	5.6	.3445
4	9.0	8.4	.3379
5	12.0	11.1	.3291
6	15.0	13.8	.3188
7	18.0	16.5	.3078
8	21.0	19.0	.2973
9	24.0	21.5	.2888
10	27.0	23.9	.2847
11	30.0	26.2	.2895
12	33.0	28.4	.3126
13	36.0	30.6	.3835
14	39.0	32.6	.9007
15	42.0	34.6	.7410
16	45.0	36.4	.6351
17	48.0	38.2	.5702
18	51.0	39.9	.5332
19	54.0	41.5	.5145
20	57.0	43.1	.5073
21	60.0	44.5	.5074
22	63.0	45.9	.5122
23	66.0	47.3	.5200
24	69.0	48.5	.5297